Performance Analysis of Dense Small Cell Networks

Tian Ding

Doctor Degree

University of Technology Sydney

Faculty of Engineering and Information Technology

2019

CERTIFICATE OF ORIGINAL AUTHORSHIP

I, Tian Ding declare that this thesis, is submitted in fulfilment of the requirements for the award of Doctor degree, in the School of Electrical and Data Engineering at the University of Technology Sydney.

This thesis is wholly my own work unless otherwise reference or acknowledged. In addition, I certify that all information sources and literature used are indicated in the thesis.

This document has not been submitted for qualifications at any other academic institution.

This research is supported by the Australian Government Research Training Program.

Signature: Production Note:
Signature removed prior to publication.

Date: June 04, 2019

ACKNOWLEDGMENT

First I would like to express my sincerest gratitude to my principal supervisor Prof. Guoqiang Mao, for his encouragement and support. I would like to thank Dr. Ming Ding for his help in my research work. I would like to thank my parents for their love. I would like to thank the Graduate Research School and the School of Electrical and Data Engineering at the University of Technology Sydney for providing a favorable environment. Finally, I would like to thank the Faculty of Engineering and Information Technology at the University of Technology Sydney and the Australian Government for the financial support.

THESIS FORMAT STATEMENT

This thesis is in the format of the Conventional thesis.

PUBLICATIONS

[J2] T. Ding, M. Ding, G. Mao, Z. Lin, A. Y. Zomaya and D. López-Pérez, "Performance Analysis of Dense Small Cell Networks With Dynamic TDD," in IEEE Transactions on Vehicular Technology, vol. 67, no. 10, pp. 9816-9830, Oct. 2018.

[J1] T. Ding, M. Ding, G. Mao, Z. Lin, D. López-Pérez and A. Y. Zomaya, "Uplink Performance Analysis of Dense Cellular Networks With LoS and NLoS Transmissions," in IEEE Transactions on Wireless Communications, vol. 16, no. 4, pp. 2601-2613, April 2017.

[C2] T. Ding, M. Ding and G. Mao, “MAC Layer Performance Analysis of Dense Small Cell Networks with Full Duplex”, in 2018 24th Asia-Pacific Conference on Communications (APCC), pp. 1–5, November 2018, Invited Paper.

[C1] T. Ding, M. Ding, G. Mao, Z. Lin, and D. López-Pérez, “Uplink Performance Analysis of Dense Cellular Networks With LoS and NLoS Transmissions,” in 2016 IEEE International Conference on Communications (ICC), pp. 1–6, May 2016.

Abstract

It is envisaged that 5G wireless communications will embrace dense small cell networks (SCNs), which can achieve a high spatial reuse gain, further leading to a high network capacity. In this Thesis, I firstly analyse the coverage probability and the area spectral efficiency (ASE) for the uplink (UL) of dense SCNs considering a practical path loss model incorporating both line-of-sight (LoS) and non-line-of-sight (NLoS) transmissions. Compared with the existing work, I adopt the following novel approaches in my study: (i) I assume a practical user association strategy (UAS) based on the smallest path loss, or equivalently the strongest received signal strength; (ii) I model the positions of both base stations (BSs) and the user equipments (UEs) as two independent Homogeneous Poisson point processes (HPPPs); and (iii) the correlation of BSs' and UEs' positions is considered, thus making my analytical results more accurate. The performance impact of LoS and NLoS transmissions on the ASE for the UL of dense SCNs is shown to be significant, both quantitatively and qualitatively, compared with existing work that does not differentiate LoS and NLoS transmissions. Moreover, SCNs are envisioned to embrace dynamic time division duplexing (TDD) in order to tailor downlink (DL)/UL subframe resources to quick variations and burstiness of DL/UL traffic. The study of dynamic TDD is particularly important because it serves as the predecessor of the full duplex (FD) transmission technology. In this Thesis, I secondly study the performance of the dense SCNs with synchronous dynamic TDD, which has been widely adopted in the existing 4th-generation (4G) systems. I analyse the coverage probability and the ASE in the DL and UL of dense SCNs considering the synchronous dynamic TDD transmissions, and the performance impact of dynamic TDD transmissions on the ASE in the DL and UL of dense SCNs is discussed. Moreover, the performance impact of interference cancellation (IC) is also explored. Furthermore, SCNs are envisaged to embrace the FD transmission technology in order to increase the spectral efficiency of wireless systems. In this Thesis, I thirdly consider the FD communications in a practical SCN scenario, where BSs can select FD or half-duplex (HD) mode according to the real-time DL/UL traffic. I present analytical results on the probabilities of BS mode selection, which match the simulation results well. The analytical results in this Thesis shed new light on the performance of future 5th-generation (5G) dense SCNs.

CONTENTS

LIST OF FIGURES

LIST OF TABLES

I. Introduction

In this Chapter, the research background and motivation of the Thesis are introduced. The main contributions of the Thesis are also clarified.

In recent years, the increase in mobile data traffic has been shown to project an exponential trajectory, and this trend is expected to continue through the next decade. To meet this formidable traffic demand, telecommunication networks have marched beyond the fourth-generation (4G) realm and begun to explore new advanced technologies [1]. By means of network densification, small cell networks (SCNs) can achieve a high spatial reuse gain, which further leads to a high network capacity [1]. Particularly, the orthogonal deployment of SCNs within the existing macrocell network, i.e., small cells and macrocells operating on different frequency spectrum (Small Cell Scenario #2a defined in [2]), is prioritized in the design of the 4th generation (4G) Long Term Evolution (LTE) networks by the 3rd Generation Partnership Project (3GPP). Furthermore, dense SCNs are envisaged to be the workhorse for capacity enhancement in the 5th generation (5G) networks due to its large performance gains and easy deployment [1], [3], [4], [5]. Thus, this research focuses on studying the performance of these orthogonal deployments of dense SCNs.

In our previous work [6], we conducted a study on the downlink (DL) of dense SCNs considering a sophisticated path loss model that differentiates line-of-sight (LoS) and non-line-of-sight (NLoS) transmissions. LoS transmission may occur when the distance between a transmitter and a receiver is small, and NLoS transmission is more common in office environments and in central business districts. Moreover, the probability that there exists a LoS path between the transmitter and the receiver increases as their distance decreases. It is observed in [6] that the reduction of the distance between the transmitter and the receiver as the density of small cell base stations (BSs) increases will cause a transition from NLoS transmission to LoS transmission, which has a significant impact, both quantitatively and qualitatively, on the performance of DL dense SCNs. Motivated by this finding [6], in this research, we continue to query whether such NLoS-to-LoS transitions may significantly affect the performance of uplink (UL) dense SCNs.

Our work distinguishes from existing work [4], [6], [7] on the performance analysis of UL dense SCNs in three major aspects. First, we assume a user association strategy (UAS) that each UE is associated with the BS with the smallest path loss to the UE, or equivalently each UE is associated with the BS that delivers the strongest received signal strength [6]. Note that in our previous work [7] and existing work in the literature [4] , the authors assumed that each UE should be associated with the closest BS. Such assumption is not appropriate for the realistic path loss model with LoS and NLoS transmissions, because in practice it is possible for a UE to associate with a BS that is not the closest one but with a LoS path, instead of the nearest BS with a NLoS path. Second, we assume that the BSs and the UEs are deployed according to two independent Homogeneous Poisson point processes (HPPPs), which is more practical and realistic compared with the previous work [4], [7]. Third, we consider the correlation of BS and UE positions explained later in the Thesis, thus making our numerical results more accurate than the previous work [4], which ignored such correlation. The main contributions of this research are as follows:

- Numerically tractable results are obtained for the UL coverage probability and the UL area spectral efficiency (ASE) performance using a piecewise path loss model, incorporating both LoS and NLoS transmissions.
- Our theoretical analysis of the UL of dense SCNs shows a similar performance trend that was found for the DL of dense SCNs in our previous work [6], i.e., when the density of UEs is larger than a threshold, the ASE may suffer from a slow growth or even a decrease. Then, the ASE will grow almost linearly as the UE density increases above another larger threshold. This finding is in stark contrast with previous results using a simplistic path loss model that does not differentiate LoS and NLoS transmissions [4].
- Our theoretical analysis also indicates that the performance impact of LoS and NLoS transmissions on the UL of SCNs with *UL power compensation* is significant both quantitatively and qualitatively compared with existing work in the literature that does not differentiate LoS and NLoS transmissions. The details of the UL power

compensation scheme will be introduced in Subchapter III-A. In particular, the previous work [4] showed that a larger UL power compensation factor should always deliver a better ASE performance in the practical range of BS density, i.e., $10^1 \sim 10^3$ BSs/km^2. However, our results show that a smaller UL power compensation factor can greatly boost the ASE performance in dense SCNs, i.e., $10^2 \sim 10^3$ BSs/km^2, while a larger UL power compensation factor is more suitable for sparse SCNs, i.e., $10^1 \sim 10^2$ BSs/km^2. Our new finding indicates that it is possible to save UE battery and meanwhile obtain a high ASE in the UL of dense SCNs in 5G, if the UL power compensation factor is optimized.

Besides SCNs, it is also envisaged that 4G/5G wireless communication networks, e.g., LTE Release 12~14 networks, will embrace time division duplexing (TDD), which does not require a pair of frequency carriers and holds the possibility of tailoring the amount of downlink (DL)/uplink (UL) radio resources to the traffic conditions. In the LTE Release 8~11 networks, seven TDD configurations, each associated with a DL-to-UL subframe ratio in a 10-milisecond transmission frame, are available for semi-static selection at the network side [8]. However, the adopted semi-static selection of TDD configuration in LTE Release 8~11 networks is not able to adapt DL/UL subframe resources to the fast fluctuations in DL/UL traffic loads. These fluctuations are exacerbated in small cells due to the low number of connected UEs per small cell and the burstiness of their DL and UL traffic demands.

In order to allow a more *dynamic* and independent adaptation of TDD SCNs to the quick variation of DL/UL traffic demands, a new technology, referred to as dynamic TDD, has drawn much attention recently [9]. With dynamic TDD, the configuration of the TDD DL/UL subframe number in each cell or a cluster of cells can be dynamically changed on a per-frame basis, i.e., once every 10 milliseconds. Dynamic TDD can thus provide a tailored configuration of DL/UL subframe resources for each cell or a cluster of cells at the expense of allowing *inter-cell inter-link interference*, e.g., DL transmissions of a cell may interfere with UL ones of a neighboring cell and vice versa. In more detail, dynamic TDD allows each base station (BS) to decide its own UL and DL split. However,

this creates two additional sources of interference. First, DL transmissions interfering with UL receivers causing interference on BS to BS links. Second, UL transmissions interfering with DL receivers causing interference on user equipment (UE) to UE links. Characterizing the rate distribution in such networks is important for understanding the trade-off between these new types of interference versus a more flexible resource allocation. The study of dynamic TDD is particularly important because it serves as the predecessor of the full duplex (FD) transmission technology, which has been identified as one of the candidate 5G technologies [10].

From the practical views of realistic network deployment, dynamic TDD exploits synchronous frame structures instead of asynchronous ones. More specifically, in an asynchronous network, e.g., Wireless Fidelity (Wi-Fi), the TDD transmission frames are not aligned in time and frequency among cells, i.e., the frame structure is not fixed and each subframe can be DL/UL based on the data requested. Thus the inter-cell inter-link interference is statistically uniform in the time domain and only depends on the DL/UL transmission probability. However, in a synchronous network, such as LTE, the TDD transmission frames from different cells are aligned in time and frequency to simplify the protocol design of radio networks [11]. As a result, the inter-cell inter-link interference becomes a function of the LTE TDD configuration structure.

Thus, this research assumes a scenario of orthogonal deployments of dense SCNs with dynamic TDD, and focuses on studying the system performance. In this research, we first conduct a theoretical study on the media access control (MAC) layer performance of synchronous dynamic TDD, which has not been investigated from a theoretical viewpoint in the literature. Then we carefully investigate the physical (PHY) layer performance of synchronous dynamic TDD combined with our results on the MAC layer time resource utilization (TRU), with emphasis on the analysis of inter-link interference and UL interference cancellation (IC). Our theoretical study sheds a new light in the interesting question: what is the true value of dynamic TDD?

Compared with existing work, the main contributions of this research are as follows:

- We derive closed-form expressions of *the DL/UL time resource utilization* (TRU) for dynamic TDD, which has been widely adopted in the existing LTE systems.
- We derive closed-form expressions for the coverage probability and the area spectral efficiency (ASE) of both the DL and UL, considering dynamic TDD in the synchronous case.
- Based on the above analytical results, the performance of synchronous dynamic TDD is quantified as SCNs evolve into dense ones.

Note that preliminary results of this work has been presented as a conference paper [11]. Compared with [11], the additional contributions of this research are:

- The probability of inter-cell inter-link interference of dynamic TDD is presented in this work.
- The physical (PHY) layer performance analysis of dynamic TDD is thoroughly studied in this work, which was not touched in [11].
- We have combined our results on the MAC layer TRU with the PHY layer SINR results to derive the total area spectral efficiency for synchronous dynamic TDD.

In addition, it is also envisaged that dense SCNs will embrace full duplex (FD), which is the successor of the existing half-duplex (HD), e.g., dynamic TDD. Moreover, the FD communications has been identified as one of the candidate 5G technologies.

With FD, both DL and UL can operate simultaneously in each BS. Compared with HD, the implementation of FD introduces additional interference to the networks, i.e., the intra-cell interference and the inter-cell interference. From the aspect of intra-cell interference, the UL of FD BSs and/or UEs suffer from self-interference (SI) due to the DL signal leakage resulting from the imperfect isolation between transmit and receive antennas. Moreover, the HD UEs in a FD cell are affected by the intra-cell inter-link interference. From the aspect of inter-cell interference, the inter-cell inter-link interference increases because the number of interfering links increase. Besides this challenge in the PHY layer of FD, it is important to investigate the MAC layer performance of FD. To the best our knowledge, the MAC layer analysis of FD has not been investigated from a theoretical viewpoint in

the literature.

In this research, for the first time, we conduct a theoretical study on the MAC layer performance of FD transmission technology for a realistic SCN scenario, where BSs can select FD/HD mode according to the real-time DL/UL traffic. More specifically, we focus on a fundamental question: how will the network densification and the process of replacing HD UE with FD UE affect the MAC layer performance of SCN with FD? To answer this question, we present a single contribution in this research as follows:

- We derive closed-form expressions for the probabilities of BS mode selection, considering a realistic SCN scenario with a hybrid of FD BSs and FD/HD UEs.

TABLE I
NOTATION SUMMARY

Notation	Items
λ, $\widetilde{\lambda}$	Density of BSs and active BSs
$\mathrm{Pr}^{\mathrm{L}}(r)$	LoS probability
A_n^{L}, A_n^{NL}	LoS and NLoS reference path loss
α_n^{L}, α_n^{NL}	LoS and NLoS path loss exponents
ϵ	Fractional path loss compensation (FPC) factor
P^{cov}, A^{ASE}	Coverage probability and area spectral efficiency (ASE)

The symbols used in the Thesis are defined in Table I. The remainder of this Thesis is structured as follows. Chapter II compares the closest related work to our work. Chapter III presents the performance analysis for the UL of dense SCNs. Chapter IV presents the performance analysis of dense SCNs with dynamic TDD. Chapter V presents the performance analysis of dense SCNs with full duplex. Finally, the conclusions are drawn in Chapter VI.

II. Literature Review

In this Chapter, the closest related works are discussed and compared to the Thesis.

A. UL of Dense SCNs

In the DL performance analysis of cellular networks based on stochastic geometry, BS positions are typically modeled as a Homogeneous Poisson point process (HPPP) on the plane [12], and in this case, the coverage probability can be expressed in a closed-form. Furthermore, an important and novel capacity model was proposed for HPPP random cellular networks, where the impact of random interference on the cooperative communications is analyzed by a closed-form expression [13]. In the UL performance analysis of cellular networks based on stochastic geometry, UE positions are typically modeled as a HPPP on the plane [4], and BS positions are assumed to be uniformly and randomly deployed in the Voronoi cell of each UE. The difficulty of modeling both BSs and UEs as a HPPP is that the BS and UE positions are coupled [4], [14], and the dependence of UE positions is therefore hard to analyse [15], [16], [17]. Such dependence occurs because if a UE is associated with a BS that delivers the strongest received signal (or is closest to the UE), it implies that there are no other BSs that can be located in positions that deliver the strongest received signal (or in a closer distance than the aforementioned BS). To derive tractable and closed-form results, previous work ignored this dependence and modeled the distance between a UE and its associated BS as an independent identical distributed (i.i.d.) random variable.

In greater detail, in [4], the authors assumed that the UEs are randomly distributed following a HPPP, and exactly one BS is randomly and uniformly located in each UE's Voronoi cell, i.e., each BS associates with its nearest UE. It is also assumed that the distance between each BS and its serving UE is i.i.d. Rayleigh distributed. The system model of only deploying UEs as a HPPP [4] makes it difficult to conduct network performance analysis for UL of SCNs. Furthermore, the association strategy that each BS associates with its nearest UE [4] is impractical, and the assumption that all of the BS-UE association distances are i.i.d. Rayleigh distributed [4] is unrealistic.

In [18], the authors considered UE spatial blocking, which is referred to as the outage caused by limited number of usable channels, and derived approximate expressions for the UL blocking probability and the UL coverage probability. In [19], the authors proposed a tractable model to characterize the UL rate distribution in a K-tier heterogeneous cellular networks (HCNs) considering power control and load balancing. In [20], the authors considered the maximum power limitation for UEs and obtained approximate expressions for the UL outage probability and UL spectral efficiency. However, none of the aforementioned UL related work considered a realistic path loss model with line-of-sight (LoS) and non-line-of-sight (NLoS) transmissions. In contrast, in this research, we consider a sophisticated path loss model incorporating both LoS and NLoS transmissions to study their performance impact on dense SCNs and show that LoS and NLoS transmissions have a significant impact on the performance of UL dense SCNs.

LoS and NLoS transmissions have been previously investigated in the DL performance analysis of dense SCNs [6], [21]. One major conclusion of [6] is that the ASE performance will slowly increase or even decrease in certain BS density regions. It is interesting to see whether this conclusion holds for UL dense SCNs. In our previous work on the UL performance analysis of dense SCNs [7], we assume that each UE is associated with its nearest BS, which may not be a practical assumption when considering LoS and NLoS transmissions. Compared with [7], in this work we consider a more realistic user association strategy, in which a UE associates with the BS that has the smallest path loss, or equivalently delivers the strongest received signal strength. This user association strategy is more realistic and is particularly important when considering both LoS and NLoS transmissions that are present in realistic radio environment, because the closest BS may possibly have only a NLoS path to the UE and therefore may offer a weaker signal than a BS that is further away but has a LoS path to the UE.

The performance analysis of the dense SCNs has gained increasing interest in the literature in the past number of years. In [22], the authors investigated the effect of idle small cells on the signal to interference and noise ratio (SINR) of the cell-specific

reference signal (CRS) and the data signals. In [23], the authors proposed the diversity pulse shaped transmission technique to enhance the throughput over the correlated multiple-input multiple-output (MIMO) channels in an ultra-dense SCN. In [24], the authors studied the transitional behaviors from noise-limited regime to dense interference-limited regime of dense SCNs considering both NLoS and LoS transmissions. In [25], the authors advocated to use device-to-device (D2D) communication to facilitate load balancing of dense SCNs without extra spectrum. In [26], the authors proposed a centralized joint cell association and scheduling mechanism based on dynamic cell switching to achieve more balanced loads and increased performance. In [27], the authors studied the performance of cache-enabled dense SCNs with multi-antenna. In [28], the authors analyzed the amount of harvested energy and throughput of wireless powered 5G dense SCNs. In [29], the authors designed efficient interference management strategies to overcome the limitation of multi-user MIMO in dense SCNs. In [30], the authors investigated the application of FD communications to dense SCNs to increase the spectral efficiency of wireless systems. In [31], the authors presented the impact of the absolute height difference between BS antenna and UE antenna on the network performance of dense SCNs.

B. Dense SCNs with Dynamic TDD

From the media access control (MAC) layer viewpoint, most of the previous works [14], [32], [33], [34], [35] only investigated the dynamic TDD operating in an asynchronous network, and did not study the performance of the dynamic TDD operating in a synchronous one.

From the physical (PHY) layer viewpoint, the signal-to-interference-plus-noise ratio (SINR) performance of dynamic TDD has been analyzed assuming deterministic positions of BSs and UEs in [36], and considering stochastic positions of BSs and UEs in [14], [32] with the homogeneous poisson point process (HPPP) model. However, it is difficult to directly perform analysis of the inter-cell inter-link interference using the HPPP model. For example, in [14], the authors scaled the BS density in their analysis based on the simulation results of coverage probability, to make them match well. Similar tricks were

adopted in [10] to address the complex problem of inter-cell inter-link interference. In [33], the energy efficiency of pico BSs equipped with multi-antenna with dynamic TDD was analyzed based on simulation and analytical results. In [37], the packet throughput of dynamic TDD with random traffic arrivals was analyzed based on simulation and analytical results. In [38], the coverage probability and throughput of dynamic TDD with device-to-device (D2D) were analyzed based on simulation and analytical results. The authors of [33], [37], [38] assumed a small cell scenario, however, the line-of-sight (LoS)/non-line-of-sight (NLoS) pathloss model is not considered, and the performance impact of BS density needs to be discussed in greater details. In [34], the interference performance of dynamic TDD with distributed interference coordination was analyzed based on simulation and analytical results; however, the authors assumed a fully loaded SCN, and the BS idle mode operation was not considered. In [35], the performance impact of self-backhauling with dynamic TDD was analyzed based on simulation and analytical results. Moreover, in [35], the authors assumed a piecewise pathloss model to investigate the performance impact of LoS and NLoS transmission. However, the authors assumed the same pathloss component and LoS probability for all intra-link and inter-link paths, which is over-simpled and a more complicated pathloss model needs to be explored.

C. Dense SCNs with Full Duplex

In [39], the authors assumed an FD SCN scenario, and studied the feasibility of interference alignment (IA).In [30], the authors assumed a heterogeneous SCN scenario with FD, where the small BSs (SBSs) worked in FD mode and the UEs worked in HD mode. In [40], the authors considered a hybrid duplex SCN scenario, where the BSs could select FD/HD mode and the UEs worked in HD mode. In [41], the authors studied the performance of FD multiple-input multiple-output (MIMO) SCN, where the BSs worked in FD mode and the UEs worked in HD mode. Most previous works only assumed HD UE because it is difficult for UE to perform self-interference cancellation (SIC). However, recent technology has shown that the UE has potential in reducing the SI to the level of noise power [42], which makes it possible for manufacturing the FD UE. Moreover, the process of replacing

HD UE with FD UE may take a long period of time. As a result, it is anticipated that the FD UEs will coexist with the HD UEs in a FD SCN. Therefore it is interesting to investigate the performance of SCN with a hybrid of FD BSs, FD UEs and HD UEs.

TABLE II
CONTRIBUTIONS OF THE THESIS COMPARED TO EXISTING WORKS

Existing works	Contributions of the Thesis
[4]	Numerically tractable results are obtained for the UL coverage probability and the UL area spectral efficiency (ASE) performance using a piecewise path loss model, incorporating both LoS and NLoS transmissions.
[14]	The performance of synchronous dynamic TDD is quantified as SCNs evolve into dense ones.
[30]	Derive closed-form expressions for the probabilities of BS mode selection, considering a realistic SCN scenario with a hybrid of FD BSs and FD/HD UEs.

The contributions of the Thesis compared to existing works are highlighted in Table II.

III. Performance Analysis for the UL of Dense SCNs

In this Chapter, the performance analysis for the UL of dense SCNs is presented.

A. System Model

Different from the assumption that only UEs' deployment follows HPPP distribution [4], in this research, we assume that both BSs and UEs are distributed following HPPPs with densities λ $\mathrm{BSs/km^2}$ and λ^{UE} $\mathrm{UEs/km^2}$, respectively. Here, we assume that $\lambda^{\mathrm{UE}} \gg \lambda$ so that all the BSs are activated to serve at least one UE. Each UE is assumed to associate with the BS with the smallest path loss. We focus on UL and consider a randomly tagged BS, which is denoted as the typical BS located at the origin. With the assumption of $\lambda^{\mathrm{UE}} \gg \lambda$, on each time-frequency resource block, each BS has one active UE in its coverage area. The UE associated with the typical BS is denoted as the typical UE, and the other UEs using the same time-frequency resource block are denoted as the interfering UEs. The distance from the typical UE to the typical BS is denoted by R, which is a random variable whose distribution will be analyzed later. Throughout the Thesis, we use the upper case letters, e.g., R, to denote a random variable and use the lower case letters, e.g., r, to denote specific instance of the random variable.

The link from the typical UE to the typical BS has a LoS path or a NLoS path with probability $\Pr^{\mathrm{L}}(r)$ and $1-\Pr^{\mathrm{L}}(r)$, respectively, where such probability can be computed by the following piecewise function [6],

$$\Pr^{\mathrm{L}}(r) = \begin{cases} \Pr_1^{\mathrm{L}}(r), & 0 < r \leq d_1 \\ \Pr_2^{\mathrm{L}}(r), & d_1 < r < d_2 \\ \vdots & \vdots \\ \Pr_N^{\mathrm{L}}(r), & r > d_{N-1} \end{cases}. \tag{1}$$

The distance dependent path loss is expressed as $\zeta(r)$ with r being the distance, and the path loss gain is $\zeta(r)^{-1}$, where the path loss of each link is modeled as (2), which is shown on the top of next page.

$$\zeta(r)=\begin{cases}\begin{cases}A_1^{\mathrm{L}}r^{\alpha_1^{\mathrm{L}}}, & \text{LoS with probability } \Pr_1^{\mathrm{L}}(r)\\ A_1^{\mathrm{NL}}r^{\alpha_1^{\mathrm{NL}}}, & \text{NLoS with probability } \left(1-\Pr_1^{\mathrm{L}}(r)\right)\end{cases}, & 0<r\le d_1\\ \begin{cases}A_2^{\mathrm{L}}r^{\alpha_2^{\mathrm{L}}}, & \text{LoS with probability } \Pr_2^{\mathrm{L}}(r)\\ A_2^{\mathrm{NL}}r^{\alpha_2^{\mathrm{NL}}}, & \text{NLoS with probability } \left(1-\Pr_2^{\mathrm{L}}(r)\right)\end{cases}, & d_1<r<d_2\\ \vdots & & \vdots\\ \begin{cases}A_N^{\mathrm{L}}r^{\alpha_N^{\mathrm{L}}}, & \text{LoS with probability } \Pr_N^{\mathrm{L}}(r)\\ A_N^{\mathrm{NL}}r^{\alpha_N^{\mathrm{NL}}}, & \text{NLoS with probability } \left(1-\Pr_N^{\mathrm{L}}(r)\right)\end{cases}, & r>d_{N-1}\end{cases}, \tag{2}$$

In (2), for $n\in\{1,2,\cdots,N\}$, A_n^{L} is the path loss of LoS path at a reference distance of $r=1$, A_n^{NL} is the path loss of NLoS path at a reference distance of $r=1$, α_n^{L} is the path loss exponent of LoS link, and α_n^{NL} is the path loss exponent of NLoS link.

The UL transmission power of UE k located at a distance of r is denoted by P_k, and is subject to a semi-static power control (PC) mechanism, i.e., the fractional path loss compensation (FPC) scheme [8]. Based on this FPC scheme, P_k is modeled as

$$P_k=P_0\zeta(r)^{\epsilon}, \tag{3}$$

where P_0 is the baseline power on the considered RB at the UE, $\epsilon\in(0,1]$ is the FPC factor, and $\zeta(r)$ is expressed in (2).

In (3), the distance-based fractional power compensation term $\zeta(r)^{\epsilon}$ is denoted by $\beta(r)$ and written as

$$\beta(r)=\zeta(r)^{\epsilon}. \tag{4}$$

Therefore, the received signal power at the typical BS can be written as

$$\begin{aligned}P^{\mathrm{sig}}&=P_0\beta(R)\zeta(R)^{-1}g\\&=P_0\zeta(R)^{(\epsilon-1)}g,\end{aligned} \tag{5}$$

where g denotes the channel gain of the multi-path fading channel and is an i.i.d. exponential distributed random variable. Hence, g follows an exponential distribution with

unit mean.

As a result, the SINR at the typical BS of the typical UE can be expressed as

$$\text{SINR} = \frac{P^{\text{sig}}}{\sigma^2 + I_Z}, \tag{6}$$

where σ^2 is the noise power, Z is the set of interfering UEs, and I_Z is the interference given by

$$I_Z = \sum_{Z} P_0 \beta \left(R_z\right) \zeta \left(D_z\right)^{-1} g_z, \tag{7}$$

where g_z denotes the channel gain of the multi-path fading channel of interferer $z \in Z$, and is an i.i.d. exponential distributed random variable, which follows an exponential distribution with unit mean. The distance of interferer $z \in Z$ to its serving BS is denoted by R_z, and the distance of interferer $z \in Z$ to the typical BS is denoted by D_z. The details of the distribution of R_z and R are given in Subchapter III-C. Since $D_z \gg R_z$, D_z can be approximated by the distance from the serving BS of interferer z to the typical BS.

B. Analysis Based on the Proposed Path Loss Model

The UL coverage probability for the typical BS can be formulated as

$$P^{\text{cov}}\left(\lambda, T\right) = \Pr\left[\text{SINR} > T\right], \tag{8}$$

where T is the SINR threshold.

The area spectral efficiency (ASE) in $\mathrm{bps/Hz/km^2}$ for a given λ can be formulated as [6]

$$A^{\text{ASE}}\left(\lambda, T_0\right) = \lambda \int_{T_0}^{\infty} \log_2\left(1 + x\right) f_X\left(\lambda, x\right) dx, \tag{9}$$

where T_0 is the minimum working SINR for the considered SCN, and $f_X\left(\lambda, x\right)$ is the PDF of the SINR observed at the typical BS for a particular value of λ.

Based on the definition of $P^{\text{cov}}\left(\lambda, T\right)$, which is the complementary cumulative distribution function (CCDF) of SINR, $f_X\left(\lambda, x\right)$ can be computed as

$$f_X(\lambda, x) = \frac{\partial\left(1 - P^{\text{cov}}(\lambda, x)\right)}{\partial x}. \tag{10}$$

Based on the system model presented in Subchapter III-A, we can calculate $P^{\text{cov}}(\lambda, T)$ and present it in the following theorem.

Theorem 1. *$P^{cov}(\lambda, T)$ can be derived as*

$$P^{cov}(\lambda, T) = \sum_{n=1}^{N} \left(T_n^{\text{L}} + T_n^{\text{NL}}\right), \tag{11}$$

where

$$\begin{aligned} T_n^{\text{L}} &= \int_{d_{n-1}}^{d_n} \boldsymbol{Pr}\left[\frac{P_0 g\left(A^{L} r^{\alpha^{L}}\right)^{(\epsilon-1)}}{\sigma^2 + I_Z} > T \middle| \boldsymbol{LoS}\right] f_{R,n}^{L}(r) dr, \\ T_n^{\text{NL}} &= \int_{d_{n-1}}^{d_n} \boldsymbol{Pr}\left[\frac{P_0 g\left(A^{NL} r^{\alpha^{NL}}\right)^{(\epsilon-1)}}{\sigma^2 + I_Z} > T \middle| \boldsymbol{NLoS}\right] f_{R,n}^{NL}(r)\, dr, \end{aligned} \tag{12}$$

and d_0 and d_N are respectively defined as 0 and ∞.

Moreover, $f_{R,n}^{L}(r)$ and $f_{R,n}^{NL}(r)$ can be respectively derived as

$$\begin{aligned} & f_{R,n}^{L}(r) \\ &= \exp\left(-\int_0^{r_1} \left(1 - \boldsymbol{P}\text{r}_n^{\text{L}}(u)\right) 2\pi u \lambda du\right) \\ &\quad \times \exp\left(-\int_0^{r} \boldsymbol{P}\text{r}_n^{\text{L}}(u)\, 2\pi u \lambda du\right) \\ &\quad \times \boldsymbol{P}\text{r}_n^{\text{L}}(r)\, 2\pi r \lambda, \quad (d_{n-1} < r < d_n), \end{aligned} \tag{13}$$

and

$$\begin{aligned} & f_{R,n}^{NL}(r) \\ &= \exp\left(-\int_0^{r_2} \boldsymbol{P}\text{r}_n^{\text{L}}(u)\, 2\pi u \lambda du\right) \\ &\quad \times \exp\left(-\int_0^{r} \left(1 - \boldsymbol{P}\text{r}_n^{\text{L}}(u)\right) 2\pi u \lambda du\right) \\ &\quad \times \left(1 - \boldsymbol{P}\text{r}_n^{\text{L}}(r)\right) 2\pi r \lambda, \quad (d_{n-1} < r < d_n), \end{aligned} \tag{14}$$

where r_1 and r_2 are determined respectively by

$$r_1 = \left(A^L r^{\alpha^L} / A^{NL}\right)^{1/\alpha^{NL}}, \tag{15}$$

and

$$r_2 = \left(A^{NL} r^{\alpha^{NL}} / A^L\right)^{1/\alpha^L}. \tag{16}$$

Furthermore, $Pr\left[\frac{P_0 g\left(A^L r^{\alpha^L}\right)^{(\epsilon-1)}}{\sigma^2+I_Z} > T \middle| LoS\right]$ *and* $Pr\left[\frac{P_0 g\left(A^{NL} r^{\alpha^{NL}}\right)^{(\epsilon-1)}}{\sigma^2+I_Z} > T \middle| NLoS\right]$ *are respectively computed by*

$$\begin{aligned} &Pr\left[\frac{P_0 g\left(A^L r^{\alpha^L}\right)^{(\epsilon-1)}}{\sigma^2+I_Z} > T \middle| LoS\right] \\ &= \exp\left(-\frac{T\sigma^2}{P_0\left(A^L r^{\alpha^L}\right)^{(\epsilon-1)}}\right) \mathscr{L}_{I_Z}\left(\frac{T}{P_0\left(A^L r^{\alpha^L}\right)^{(\epsilon-1)}}\right), \end{aligned} \tag{17}$$

and

$$\begin{aligned} &Pr\left[\frac{P_0 g\left(A^{NL} r^{\alpha^{NL}}\right)^{(\epsilon-1)}}{\sigma^2+I_Z} > T \middle| NLoS\right] \\ &= \exp\left(-\frac{T\sigma^2}{P_0\left(A^{NL} r^{\alpha^{NL}}\right)^{(\epsilon-1)}}\right) \mathscr{L}_{I_Z}\left(\frac{T}{P_0\left(A^{NL} r^{\alpha^{NL}}\right)^{(\epsilon-1)}}\right), \end{aligned} \tag{18}$$

where $\mathscr{L}_{I_Z}(s)$ *is the Laplace transform of RV* I_Z *evaluated at* s*.*

Proof: See Appendix A. ■

As can be observed from Theorem 1, the piece-wise path loss function for LoS transmission, the piece-wise path loss function for NLoS transmission, and the piece-wise LoS probability function play active roles in determining the final result of $P^{\text{cov}}(\lambda, T)$. We will investigate their impacts on network performance in detail in the following Subchapters. Plugging $P^{\text{cov}}(\lambda, T)$ obtained from (11) into (10) , we can get the result of the ASE using (9).

C. Study of A 3GPP Special Case

As a special case for Theorem 1, we consider a path loss function adopted in the 3GPP as [8]

$$\zeta(r)=\begin{cases}A^{\mathrm{L}}r^{\alpha^{\mathrm{L}}}, & \text{LoS with probability } \mathrm{Pr}^{\mathrm{L}}(r)\\ A^{\mathrm{NL}}r^{\alpha^{\mathrm{NL}}}, & \text{NLoS with probability } \left(1-\mathrm{Pr}^{\mathrm{L}}(r)\right)\end{cases}, \tag{19}$$

together with a linear LoS probability function of $\mathrm{P}r^{L}(r)$, defined in the 3GPP as [43]

$$\mathrm{Pr}^{\mathrm{L}}(r)=\begin{cases}1-\frac{r}{d_1}, & 0<r\leq d_1\\ 0, & r>d_1\end{cases}, \tag{20}$$

where d_1 is the cut-off distance of the LoS link.

For the 3GPP special case, according to Theorem 1, $P^{\mathrm{cov}}(\lambda,\gamma)$ can then be computed by

$$P^{\mathrm{cov}}(\lambda,T)=\sum_{n=1}^{2}\left(T_n^{\mathrm{L}}+T_n^{\mathrm{NL}}\right). \tag{21}$$

In the following Subchapters, we will investigate the results of T_1^{L}, T_1^{NL}, T_2^{L}, and T_2^{NL}, respectively.

1) The Result of T_1^{L}: Regarding the result of T_1^{L}, which is the coverage probability when the typical UE is associated with the typical BS with a LoS link of distance less than d_1, we present Lemma 2 in the following.

Lemma 2. *When the typical UE is associated with a LoS BS of a distance less than d_1, the coverage probability T_1^{L} can be computed by*

$$T_1^{\mathrm{L}}=\int_0^{d_1} e^{-\frac{T\sigma^2}{P_0\left(A^{L}r^{\alpha^{L}}\right)^{(\epsilon-1)}}}\mathscr{L}_{I_Z}\left(\frac{T}{P_0\left(A^{L}r^{\alpha^{L}}\right)^{(\epsilon-1)}}\right)f_{R,1}^{L}(r)dr, \tag{22}$$

where

$$\begin{aligned}&f_{R,1}^{L}(r)\\&=\exp\left(-\pi\lambda r^2+2\pi\lambda\left(\tfrac{r^3}{3d_1}-\tfrac{r_1^3}{3d_1}\right)\right)\left(1-\tfrac{r}{d_1}\right)2\pi r\lambda,\end{aligned} \tag{23}$$

and the Laplace transform $\mathscr{L}_{I_Z}(s)$ *is expressed as*

$$\begin{aligned}
&\mathscr{L}_{I_Z}(s)\\
&=\exp\left\{-2\pi\lambda\int_r^{d_1}\left(1-\tfrac{x}{d_1}\right)\right.\\
&\quad\left.\times\int_0^{\infty}\left(\tfrac{1}{1+s^{-1}P_0^{-1}\beta(u)^{-1}\zeta(x)}f_{R_z}^{1\mathrm{L}}(u)\,du\middle|\,\textit{LoS}\right)xdx\right\}\\
&\quad\times\exp\left\{-2\pi\lambda\int_{r_1}^{d_1}\left(\tfrac{x}{d_1}\right)\right.\\
&\quad\left.\times\int_0^{\infty}\left(\tfrac{1}{1+s^{-1}P_0^{-1}\beta(u)^{-1}\zeta(x)}f_{R_z}^{1\mathrm{NL}}(u)\,du\middle|\,\textit{NLoS}\right)xdx\right\}\\
&\quad\times\exp\left\{-2\pi\lambda\int_{d_1}^{\infty}1\right.\\
&\quad\left.\times\int_0^{\infty}\left(\tfrac{1}{1+s^{-1}P_0^{-1}\beta(u)^{-1}\zeta(x)}f_{R_z}^{2\mathrm{NL}}(u)\,du\middle|\,\textit{NLoS}\right)xdx\right\}.
\end{aligned}\tag{24}$$

According to the HPPP system model, the distribution of R_z *is the same as* R*, but bounded by* x*. The PDF of* R_z *can be written as*

$$f_{R_z}(u)=\begin{cases}f_{R_z,1}^{L}(u), & \textit{LoS},\ 0<u\le x\\ f_{R_z,1}^{1NL}(u), & \textit{NLoS},\ 0<u\le x_1\\ f_{R_z,1}^{2NL}(u), & \textit{NLoS},\ y_1<u\le d_1\\ f_{R_z,2}^{NL}(u), & \textit{NLoS},\ d_1<u\le x\end{cases},\tag{25}$$

where

$$\begin{aligned}
&f_{R_z,1}^{L}(u)\\
&=\exp\left(-\pi\lambda u^2+2\pi\lambda\left(\tfrac{u^3}{3d_1}-\tfrac{u_1^3}{3d_1}\right)\right)\\
&\quad\times\left(1-\tfrac{u}{d_1}\right)2\pi u\lambda,
\end{aligned}\tag{26}$$

$$\begin{aligned}
&f_{R_z,1}^{1NL}(u)\\
&=\exp\left(-\pi\lambda u_2^2+2\pi\lambda\left(\tfrac{u_2^3}{3d_1}-\tfrac{u^3}{3d_1}\right)\right)\\
&\quad\times\left(\tfrac{u}{d_1}\right)2\pi u\lambda,
\end{aligned}\tag{27}$$

$$f_{R_z,1}^{2NL}(u)=\exp\left(2\pi\lambda\left(-\frac{d_1^2}{6}-\frac{u^3}{3d_1}\right)\right)\left(\frac{u}{d_1}\right)2\pi u\lambda,\tag{28}$$

and

$$f_{R_z,2}^{NL}(u) = \exp\left(-\pi\lambda u^2\right) 2\pi u\lambda, \tag{29}$$

where

$$u_1 = \left(A^L u^{\alpha^L}/A^{NL}\right)^{1/\alpha^{NL}}, \tag{30}$$

and

$$u_2 = \left(A^{NL} u^{\alpha^{NL}}/A^{L}\right)^{1/\alpha^{L}}, \tag{31}$$

Specifically, when the interference comes from a LoS path, $f_{R_z}^{\mathrm{1L}}(u)$ *can be derived as*

$$f_{R_z}^{\mathrm{1L}}(u) = \begin{cases} f_{R_z,1}^{L}(u), & \textit{LoS},\ 0 < u \le x \\ f_{R_z,1}^{1NL}(u), & \textit{NLoS},\ 0 < u \le x_1 \end{cases}, \tag{32}$$

where

$$x_1 = \left(A^L x^{\alpha^L}/A^{NL}\right)^{1/\alpha^{NL}}. \tag{33}$$

Conditioned on $x \le d_1$*, when the interference path is NLoS,* $f_{R_z}^{\mathrm{1NL}}(u)$ *can be derived as*

$$\begin{aligned} &f_{R_z}^{\mathrm{1NL}}(u) \\ &= \begin{cases} \begin{cases} f_{R,1}^{L}(u), & \textit{LoS}, \quad 0 < u \le x_2 \\ f_{R,1}^{1NL}(u), & \textit{NLoS}, \quad 0 < u \le x \end{cases}, & r_1 < x \le y_1 \\ \begin{cases} f_{R,1}^{L}(u), & \textit{LoS}, \quad 0 < u \le d \\ f_{R,1}^{1NL}(u), & \textit{NLoS}, \quad 0 < u \le y_1 \\ f_{R,1}^{2NL}(u), & \textit{NLoS}, \quad y_1 < u \le x \end{cases}, & y_1 < x \le d_1 \end{cases} \end{aligned} \tag{34}$$

where

$$y_1 = \left(A^L d_1^{\alpha^L} / A^{NL}\right)^{1/\alpha^{NL}}, \tag{35}$$

and

$$x_2 = \left(A^{NL} x^{\alpha^{NL}} / A^L\right)^{1/\alpha^L}. \tag{36}$$

Conditioned on $x > d_1$, when the interference path is NLoS, $f_{R_z}^{2\mathrm{NL}}(u)$ can be derived as

$$f_{R_z}^{2\mathrm{NL}}(u) = \begin{cases} f_{R_z,1}^{L}(u), & \textit{LoS},\ 0 < u \le d_1 \\ f_{R_z,1}^{1NL}(u), & \textit{NLoS},\ 0 < u \le y_1 \\ f_{R_z,}^{2NL}(u), & \textit{NLoS},\ y_1 < u \le d_1 \\ f_{R_z,2}^{NL}(u), & \textit{NLoS},\ d_1 < u \le x \end{cases}. \tag{37}$$

Proof: See Appendix B. ■

2) The Result of T_1^{NL}: Regarding the result of T_1^{NL}, which is the coverage probability when the typical UE is associated with the typical BS with a NLoS link of distance less than d_1, we propose Lemma 3 in the following.

Lemma 3. *T_1^{NL} can be derived as*

$$T_1^{NL} = \int_0^{d_1} e^{-\frac{T\sigma^2}{P_0 r^{\alpha^{NL}(\epsilon-1)}}} \mathscr{L}_{I_Z}\left(\frac{T}{P_0 r^{\alpha^{NL}(\epsilon-1)}}\right) f_{R,1}^{NL}(r)\, dr, \tag{38}$$

where

$$f_{R,1}^{NL}(r) = \begin{cases} \exp\left(-\pi\lambda r_2^2 + 2\pi\lambda\left(\frac{r_2^3}{3d_1} - \frac{r^3}{3d_1}\right)\right) \\ \times\left(\frac{r}{d_1}\right) 2\pi r\lambda, & 0 < r \le y_1 \\ \exp\left(-\frac{\pi\lambda d_1^2}{3} - \frac{2\pi\lambda r^3}{3d_1}\right) \\ \times\left(\frac{r}{d_1}\right) 2\pi r\lambda, & y_1 < r \le d_1 \end{cases}, \tag{39}$$

and the Laplace transform $\mathscr{L}_{I_Z}(s)$ *for* $0 < r \leq y_1$ *and* $y_1 < r \leq d_1$ *are respectively expressed as*

$$\begin{aligned}
&\mathscr{L}_{I_Z}(s) \\
&= \exp\left(-2\pi\lambda \int_{r_2}^{d_1} \left(1-\tfrac{x}{d_1}\right)\right. \\
&\times \int_0^{\infty} \left(\tfrac{1}{1+s^{-1}P_0^{-1}\beta(u)^{-1}\zeta(x)} f_{R_z}^{\mathrm{1L}}(u)\, du \middle| \textit{LoS} \right) xdx \Big) \\
&\times \exp\left(-2\pi\lambda \int_{r}^{d_1} \left(\tfrac{x}{d_1}\right)\right. \\
&\times \int_0^{\infty} \left(\tfrac{1}{1+s^{-1}P_0^{-1}\beta(u)^{-1}\zeta(x)} f_{R_z}^{\mathrm{1NL}}(u)\, du \middle| \textit{NLoS} \right) xdx \Big) \\
&\times \exp\left(-2\pi\lambda \int_{d_1}^{\infty} 1\right. \\
&\times \int_0^{\infty} \left(\tfrac{1}{1+s^{-1}P_0^{-1}\beta(u)^{-1}\zeta(x)} f_{R_z}^{\mathrm{2NL}}(u)\, du \middle| \textit{NLoS} \right) xdx \Big),
\end{aligned} \tag{40}$$

and

$$\begin{aligned}
&\mathscr{L}_{I_Z}(s) \\
&= \exp\left(-2\pi\lambda \int_{r}^{d_1} \tfrac{x}{d_1}\right. \\
&\times \int_0^{\infty} \left(\tfrac{1}{1+s^{-1}P_0^{-1}\beta(u)^{-1}\zeta(x)} f_{R_z}^{\mathrm{1NL}}(u)\, du \middle| \textit{NLoS} \right) xdx \Big) \\
&\times \exp\left(-2\pi\lambda \int_{d_1}^{\infty} 1\right. \\
&\times \int_0^{\infty} \left(\tfrac{1}{1+s^{-1}P_0^{-1}\beta(u)^{-1}\zeta(x)} f_{R_z}^{\mathrm{2NL}}(u)\, du \middle| \textit{NLoS} \right) xdx \Big),
\end{aligned} \tag{41}$$

where $r_2 = \left(A^L r^{\alpha^{NL}}/A^{NL}\right)^{1/\alpha^L}$.

Proof: The proof is very similar to that in Appendix B. Thus it is omitted for brevity. ■

3) The Result of T_2^L*:* The result of T_2^{L} is the coverage probability when the typical UE is associated with the typical BS with a LoS link of distance larger than d_1. From Theorem 1, T_2^{L} can be derived as

$$T_2^{\mathrm{L}} = \int_{d_1}^{\infty} \Pr\left[\frac{P_0 g \left(A^{\mathrm{L}} r^{\alpha^{\mathrm{L}}}\right)^{(\epsilon-1)}}{\sigma^2 + I_Z} > T \middle| \mathrm{LoS} \right] f_{R,2}^{\mathrm{L}}(r) dr. \tag{42}$$

According to Theorem 1 and (20), $f_{R,2}^{\mathrm{L}}(r)$ can be calculated by

$$\begin{aligned} & f_{R,2}^{\mathrm{L}}(r) \\ & = \exp\left(-\int_0^{r_1}\left(1-\mathrm{P}r^{L}(u)\right)2\pi u\lambda du\right) \\ & \quad \times \exp\left(-\int_0^{r}\mathrm{P}r^{L}(u)\,2\pi u\lambda du\right)\times 0\times 2\pi r\lambda \\ & = 0, \quad (r>d_1). \end{aligned} \tag{43}$$

Plugging (43) into (42), yields

$$T_2^{\mathrm{L}} = 0. \tag{44}$$

4) The Result of T_2^{NL}: Regarding the result of T_2^{NL}, which is the coverage probability when the typical UE is associated with the typical BS with a NLoS link of distance larger than d_1, we propose Lemma 4 in the following.

Lemma 4. *T_2^{NL} can be derived as*

$$T_2^{NL}=\int_{d_1}^{\infty} e^{-\frac{T\sigma^2}{P_0 r^{\alpha^{NL}(\epsilon-1)}}}\mathscr{L}_{I_Z}\left(\frac{T}{P_0 r^{\alpha^{NL}(\epsilon-1)}}\right) f_{R,2}^{NL}(r)\,dr, \tag{45}$$

where

$$f_{R,2}^{NL}(r) = \exp\left(-\pi\lambda r^2\right)2\pi r\lambda, \tag{46}$$

and the Laplace transform $\mathscr{L}_{I_Z}(s)$ is expressed as

$$\begin{aligned} & \mathscr{L}_{I_Z}(s) \\ & = \exp\left(-2\pi\lambda\int_r^{\infty} 1\right. \\ & \left.\times\int_0^{\infty}\left(\frac{1}{1+s^{-1}P_0^{-1}\beta(u)^{-1}\zeta(x)} f_{R_z}^{2NL}(u)\,du\middle|\, \textit{NLoS}\right)xdx\right). \end{aligned} \tag{47}$$

Proof: The proof is very similar to that in Appendix B. Thus it is omitted for brevity..

■

5) Evaluation Using the Gauss-Laguerre Quadrature: To improve the tractability of the derived results, we propose to approximate the infinite integral of outer-most integrals in (45) by the Gauss-Laguerre quadrature [44], expressed as

$$\int_0^{\infty} f(u)\, e^{-u} du \approx \sum_{i=1}^{n} \omega_i f(u_i), \tag{48}$$

where n is the degree of Laguerre polynomial, and u_i and ω_i are the *i*-th abscissas and weight of the quadrature. For practical use, n should be set to a value above 10 to ensure good numerical accuracy [44].

To utilize the Gauss-Laguerre quadrature, the outer-most integral in (45) is rewritten by using the change of variable $\tilde{r} = \pi\lambda r^2$. To evaluate (45) by means of the Gauss-Laguerre quadrature, we propose Lemma 5 in the following.

Lemma 5. *By using the Gauss-Laguerre quadrature as shown in (48), (45) can be approximated and simplified as*

$$\begin{aligned} & T_2^{NL} \\ & \approx \sum_{i=1}^{n} \omega_i \exp\left(- \frac{T\sigma^2}{P_0 \left(\sqrt{\left[u_i + \pi\lambda (d_1)^2\right] (\pi\lambda)^{-1}} \right)^{\alpha^{NL}(\epsilon-1)}} \right. \\ & \quad \left. - \pi\lambda (d_1)^2 \right) \\ & \quad \times \mathscr{L}_{I_Z} \left(\frac{T}{P_0 \sqrt{\left[u_i + \pi\lambda (d_1)^2\right] (\pi\lambda)^{-1}}^{\alpha^{NL}(\epsilon-1)}} \right). \end{aligned} \tag{49}$$

Proof: See Appendix C. ■

Thanks to Lemma 5, the 3-fold integral computation in (45) can now be simplified as a 2-fold integral computation, which improves the tractability of our results.

D. Simulation and Discussion

In this Subchapter, we present numerical and simulation results to establish the accuracy of our analysis and further study the performance of the UL of dense SCNs. We adopt the following parameters according to the 3GPP recommendations [8], [45]: d_1 = 0.3 km, α^{L} = 2.09, α^{NL} = 3.75, P_0 = -76 dBm, σ^2 = -99 dBm (with a noise figure of 5 dB at each BS). We first consider a sparse network in Subchapter III-D1, and then we analyze a dense network in the Subchapters III-D2 and III-D3.

1) Validation of the Analytical Results of $P^{\mathrm{cov}}(\lambda, T)$: For comparison, we first compute analytical results using a single-slope path loss model that does not differentiate LoS and NLoS transmissions [4]. Note that in [4], only one path loss exponent is defined and denoted by α, the value of which is $\alpha = \alpha^{\mathrm{NL}} = 3.75$. The results of $P^{\mathrm{cov}}(\lambda, T)$ in a sparse network scenario with $\lambda = 10\,\mathrm{BSs/km^2}$, $\alpha = 3.75$, and $\epsilon = 0.7$ are plotted in Fig. 1.

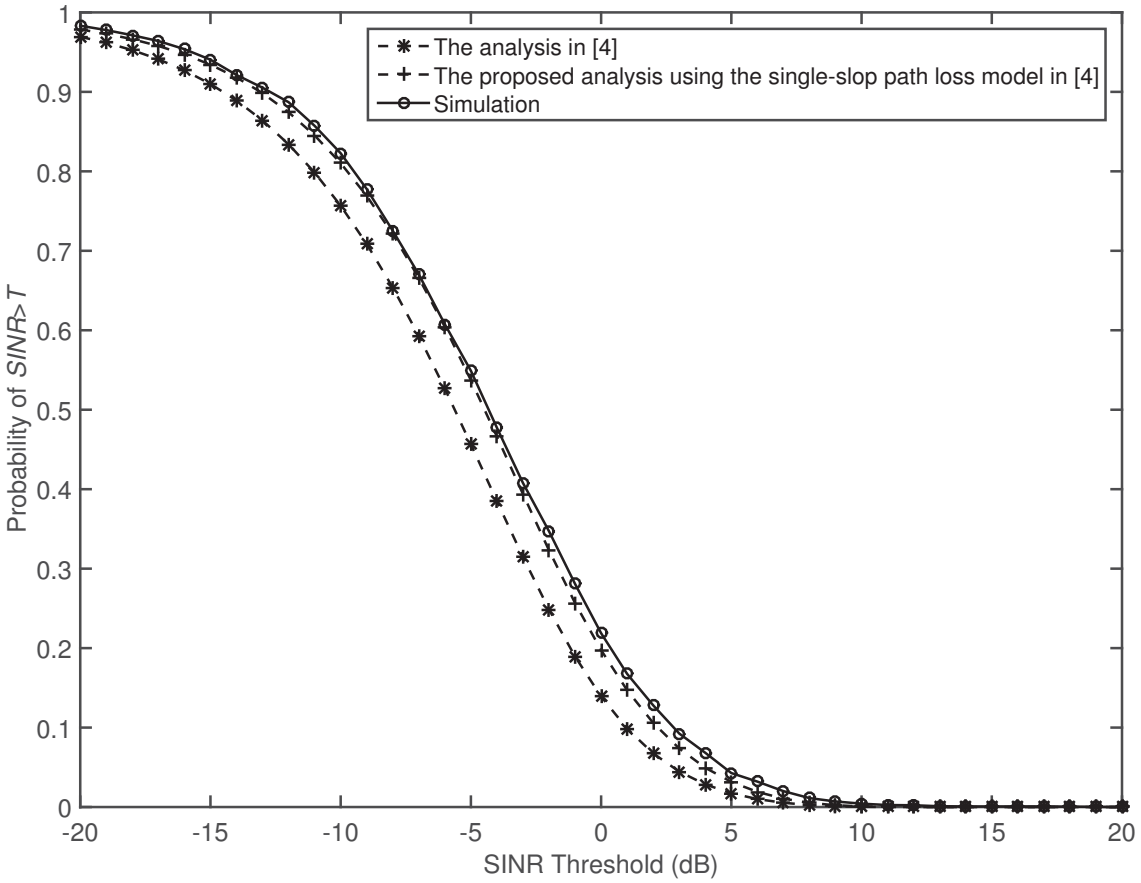

Fig. 1. The coverage probability $P^{\mathrm{cov}}(\lambda, T)$ vs. the SINR threshold in [4] with $\lambda = 10\,\mathrm{BSs/km^2}$, $\alpha = 3.75$, and $\epsilon = 0.7$.

In the case of the single-slope path loss model [4], as can be observed from Fig. 1, our analytical result is much more accurate than that in [4] because our system model assumptions are more reasonable than those in [4]: first, the distributions of BSs and UEs are modeled as two independent HPPPs, instead of the assumption that only UEs are distributed according to a HPPP [4]; second, the dependence of BS and UE positions are discussed, instead of being ignored [4].

In the case of the 3GPP path loss model [8], the results of $P^{\mathrm{cov}}(\lambda, T)$ in a sparse network

scenario with $\lambda = 10\,\mathrm{BSs/km^2}$ and in a dense network scenario with $\lambda = 10^3\,\mathrm{BSs/km^2}$ are plotted in Fig. 2. As can be observed from Fig. 2, our analytical results match the simulation results very well, and thus we will only use analytical results of $P^{\mathrm{cov}}(\lambda, T)$ in our discussion hereafter.

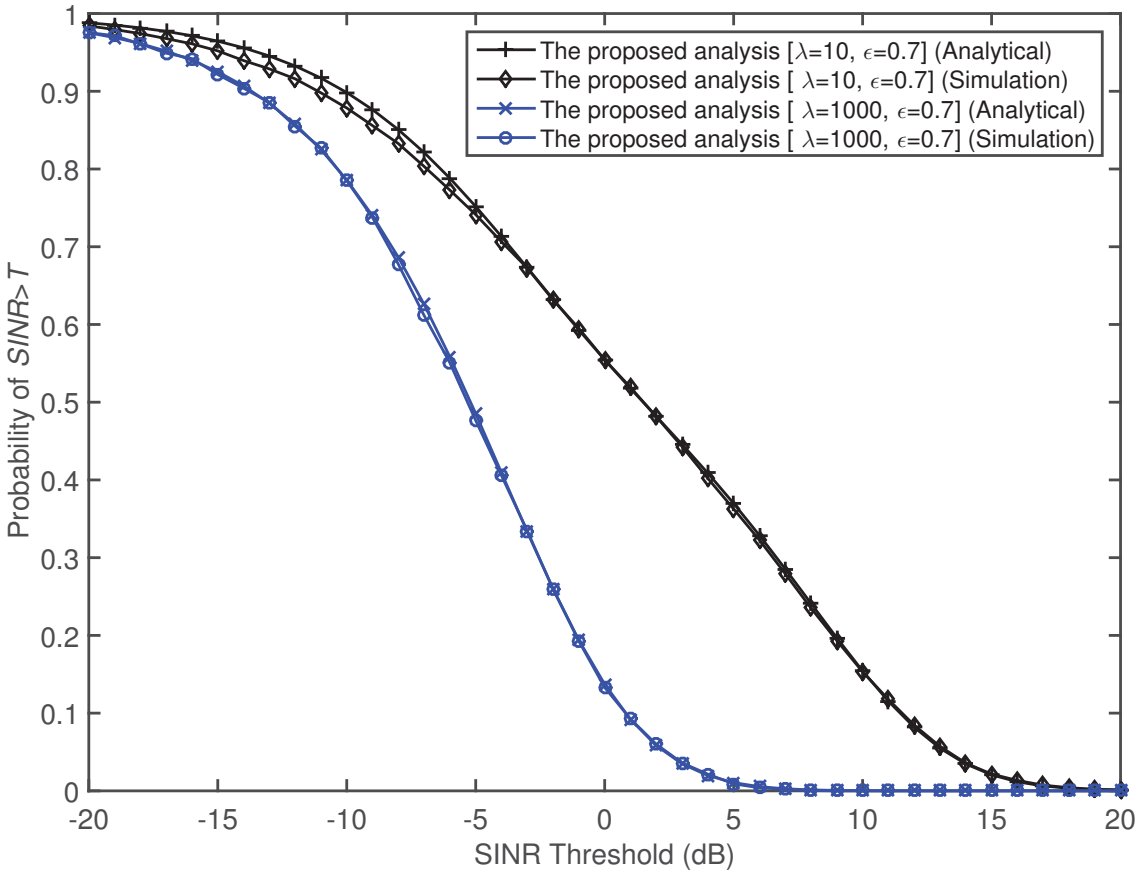

Fig. 2. The coverage probability $P^{\mathrm{cov}}(\lambda, T)$ vs. the SINR threshold with $\lambda = 10\,\mathrm{BSs/km^2}$ and $\lambda = 10^3\,\mathrm{BSs/km^2}$.

As can be seen from Fig. 2, for the case of $\lambda = 10\,\mathrm{BSs/km^2}$, when the SINR threshold is small (e.g., $T < -4$dB), the analytical result of the coverage probability is larger than the simulation result. This is because in our analysis, the approximation of replacing the location of UE by that of its serving BS, may exclude the cases of strong interfering UEs located at the proximity of the typical BS, thus underestimating the total interference, and overestimating the coverage probability. However, as the SINR threshold increases (e.g., $T > -4$dB), the impact of the overestimation of the coverage probability will decrease, and our analytical result matches the simulation result well.

Another interesting finding as can be observed from Fig. 2 is that the analytical result with a larger BS density is more accurate than that with a smaller BS density. This is because in denser networks, the distance between a UE and its serving BS is smaller, and the approximation of replacing the location of a UE by that of its serving BS has less impact on the estimation of the total interference, thus making the analytical result more accurate.

2) The Results of $P^{\text{cov}}(\lambda, T)$ vs. λ: The results of $P^{\text{cov}}(\lambda, T)$ against the BS density for $T = 0$ dB are plotted in Fig. 3. From Fig. 3, we can observe that when considering both LoS and NLoS transmissions, the coverage probability presents a significantly different behavior. When the SCN is sparse and thus noise-limited, the coverage probability given by the proposed analysis grows as λ increases, similarly as that observed in [4]. However, when the network is dense enough, the coverage probability decreases as λ increases, due to the transition of a large number of interference paths from NLoS to LoS, which is not captured in [4]. Particularly, during this region, interference increases at a faster rate than the signal due to the transition from mostly NLoS interference to LoS interference, thereby causing a drop in the SINR hence the coverage probability. In more detail, the coverage probability given by the proposed analysis peaks at a certain density λ_0. When λ increases above λ_0, interfering UEs become closer to the typical BS and their interfering signals start reaching the typical BS via strong LoS paths. When λ is further increased far above λ_0, the coverage probability decreases at a slower pace because both the signal power and the interference power are LoS dominated and increase at approximately the same rate. There are still more and more interferers whose signal reach the typical BS via LoS paths but their effect is smaller than the dominating interferers.

It should also be noted that the coverage probability with different FPC factor ϵ exhibits different trends. Specifically, when the SCN is sparse, adopting a higher ϵ (e.g., $\epsilon = 0.8$) leads to a higher coverage probability. This is because the sparse SCN is noise-limited and hence increasing the transmission power provides better coverage performance. However, when the SCN is dense, adopting a lower ϵ (e.g., $\epsilon = 0.6$) leads to higher coverage proba-

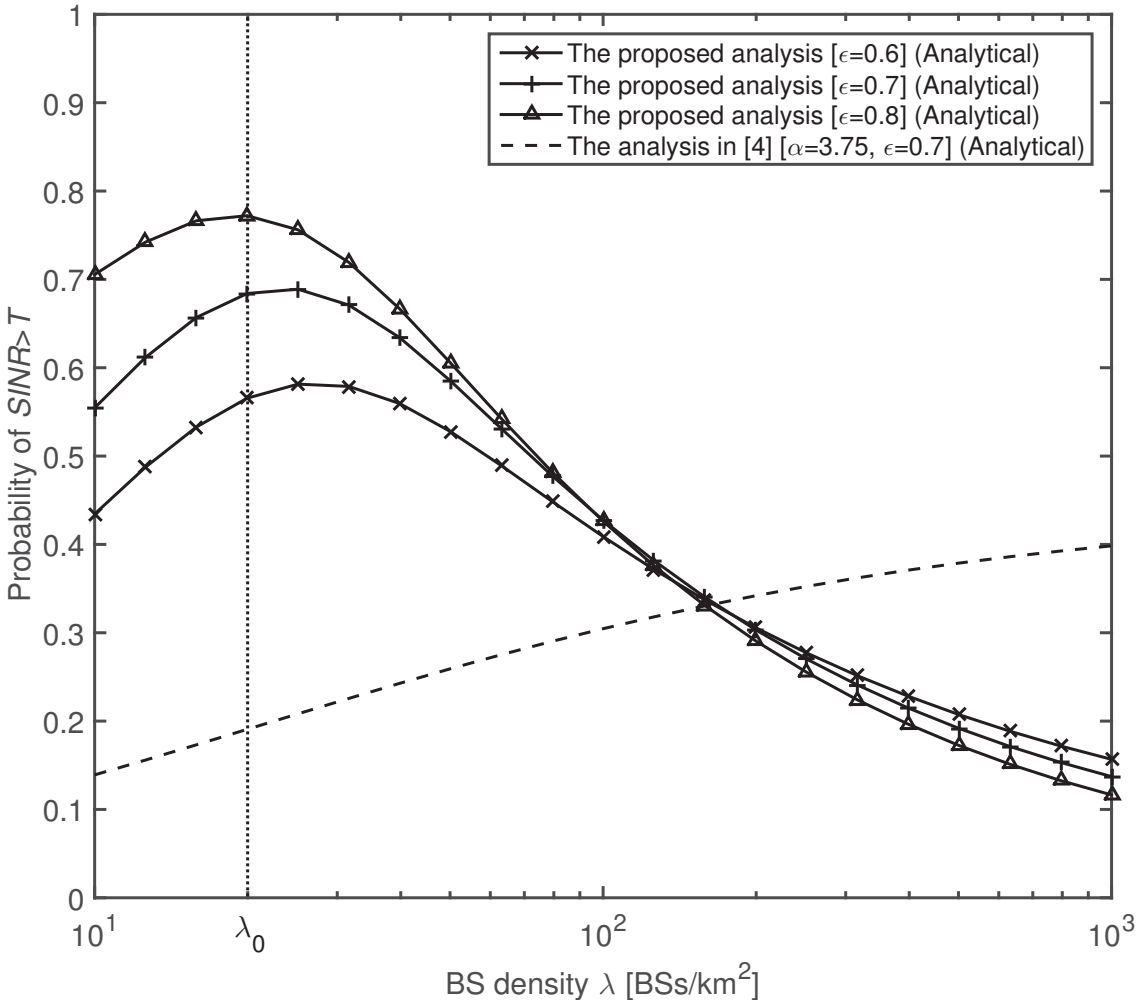

Fig. 3. The coverage probability $P^{\text{cov}}(\lambda, T)$ vs. the BS density with different ϵ and SINR threshold $T = 0$ dB.

bility. This is because the dense SCN is interference-limited, and the network experiences a surplus of strong LoS interference instead of shortage of UL transmission power, and hence decreasing the transmission power provides better coverage performance. Therefore, our results suggest that in dense SCNs, increasing the UL transmission power may degrade the coverage probability. Such observation is further investigated in terms of ASE in the following Subchapter.

3) The Results of $A^{\text{ASE}}(\lambda, T_0)$ vs. λ: In this Subchapter, we investigate the ASE with T_0 = 0 dB based on the analytical results of $P^{\text{cov}}(\lambda, T)$. The results of $A^{\text{ASE}}(\lambda, T_0)$ obtained by comparing the proposed analysis with the analysis from [4] are plotted in Fig. 4.

As can be seen from Fig. 4, the analysis from [4] indicates that when the SCN is dense

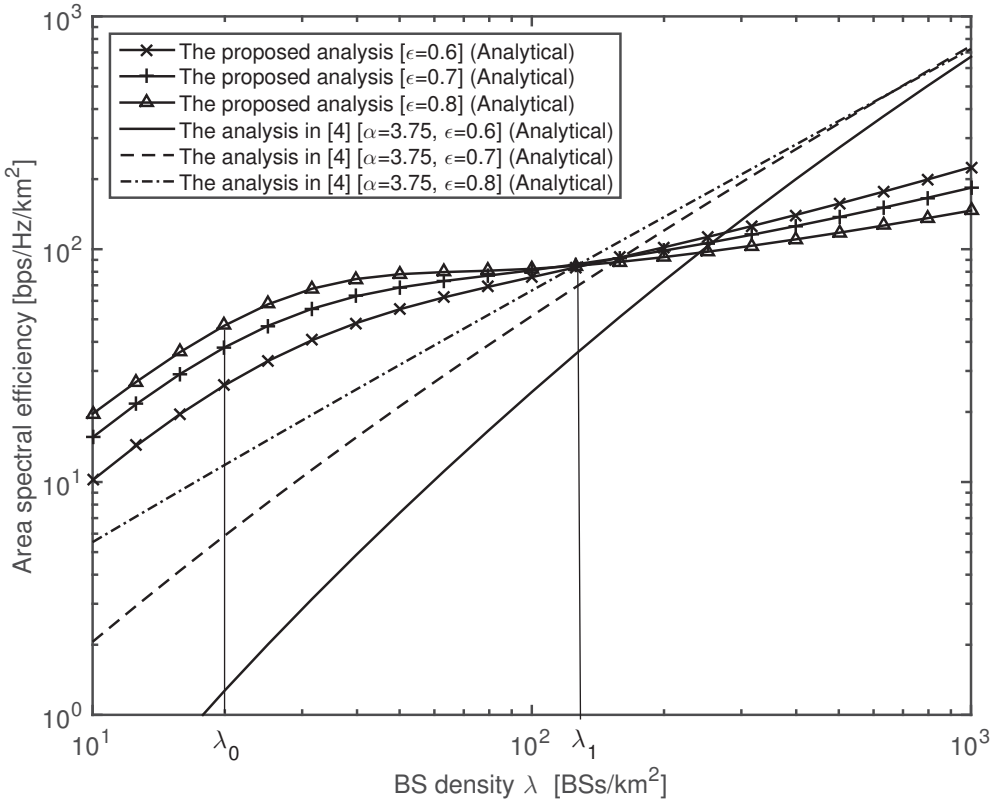

Fig. 4. Area spectral efficiency $A^{\mathrm{ASE}}(\lambda, T_0)$ vs. the BS density with different ϵ and SINR threshold $T_0 = 0$ dB. λ_0 and λ_1 correspond to the BS density when the ASE given by the proposed analysis starts to suffer from a slow growth and when it starts to pick up the growth, respectively.

enough, the ASE increases linearly with λ. In contrast, our proposed analysis reveals a more complicated ASE trend. Specifically, when the SCN is relatively sparse, i.e., $10^0 \sim 10^1$ BSs/km^2, the ASE quickly increases with λ since the network is generally noise-limited, and thus having UEs closer to their serving BSs improves performance. When the SCN is extremely dense, i.e., around 10^3 BSs/km^2, the ASE increases linearly with λ because both the signal power and the interference power are LoS dominated. As for the practical range of λ for the existing and the future cellular networks, i.e., $10^1 \sim 10^3$ BSs/km^2 [1], the ASE trend is interesting. First, when $\lambda \in [\lambda_0, \lambda_1]$, where λ_0 is around 20 and λ_1 ($\lambda_1 > \lambda_0$) is around 125 in Fig. 4, the ASE exhibits a slow-down in the rate of growth due to the fast decrease of coverage probability shown in Fig. 3. Thereafter, when $\lambda \geq \lambda_1$, the ASE exhibits an acceleration in the growth rate due to the slow-down in the decrease of coverage

probability also shown in Fig. 3. Our finding, the ASE may exhibits a slow-down in the rate of growth as the BS density increases, is similar to our results reported for the DL of SCNs [6], which indicates the significant impact of the path loss model incorporating both NLoS and LoS transmissions. Such impact makes a difference for dense SCNs in terms of the ASE both quantitatively and qualitatively, comparing to that with a simplistic path loss model that does not differentiate LoS and NLoS transmissions.

Our proposed analysis also shows another important finding. A smaller UL power compensation factor ϵ (e.g., $\epsilon = 0.6$) can greatly boost the ASE performance in 5G dense SCNs [1], i.e., $10^2 \sim 10^3$ BSs/km^2, while a larger ϵ (e.g., $\epsilon = 0.8$) is more suitable for sparse SCNs, i.e., $10^1 \sim 10^2$ BSs/km^2. This contradicts the results in [4] where a larger UL power compensation factor was predicted to always result in a better ASE in the practical range of BS density, i.e., $10^1 \sim 10^3$ BSs/km^2, as shown in Fig. 4. Therefore, our theoretical analysis indicates that the performance impact of LoS and NLoS transmissions on UL SCNs with UL power compensation is also significant both quantitatively and qualitatively, compared with the previous work in [4] that does not differentiate LoS and NLoS transmissions. Interestingly, our new finding implies that its is possible to save UE battery and meanwhile achieve a high ASE in the UL of 5G dense SCNs, if ϵ is optimized. The intuition is that in dense SCNs, the network experiences a surplus of strong LoS interference instead of shortage of UL transmission power, and thus reducing the transmission powers of a large number of interferers turns out to be a good strategy that enhances the ASE. Note that our conclusion is made from the investigated set of parameters, and it is of significant interest to further study the generality of this conclusion in other network models and with other parameter sets.

4) Discussion on Various Values of α^{L}: In this Subchapter, we change the value of α^{L} from 2.09 to 1.09 and 3.09, respectively, to investigate the performance impact of α^{L}. In Fig. 5, the analytical results of $P^{\mathrm{cov}}(\lambda, 0)$ with T_0 = 0 dB and with various α^{L} and various ϵ are compared.

As can be seen from Fig. 5, the smaller the α^{L}, the larger the difference between the

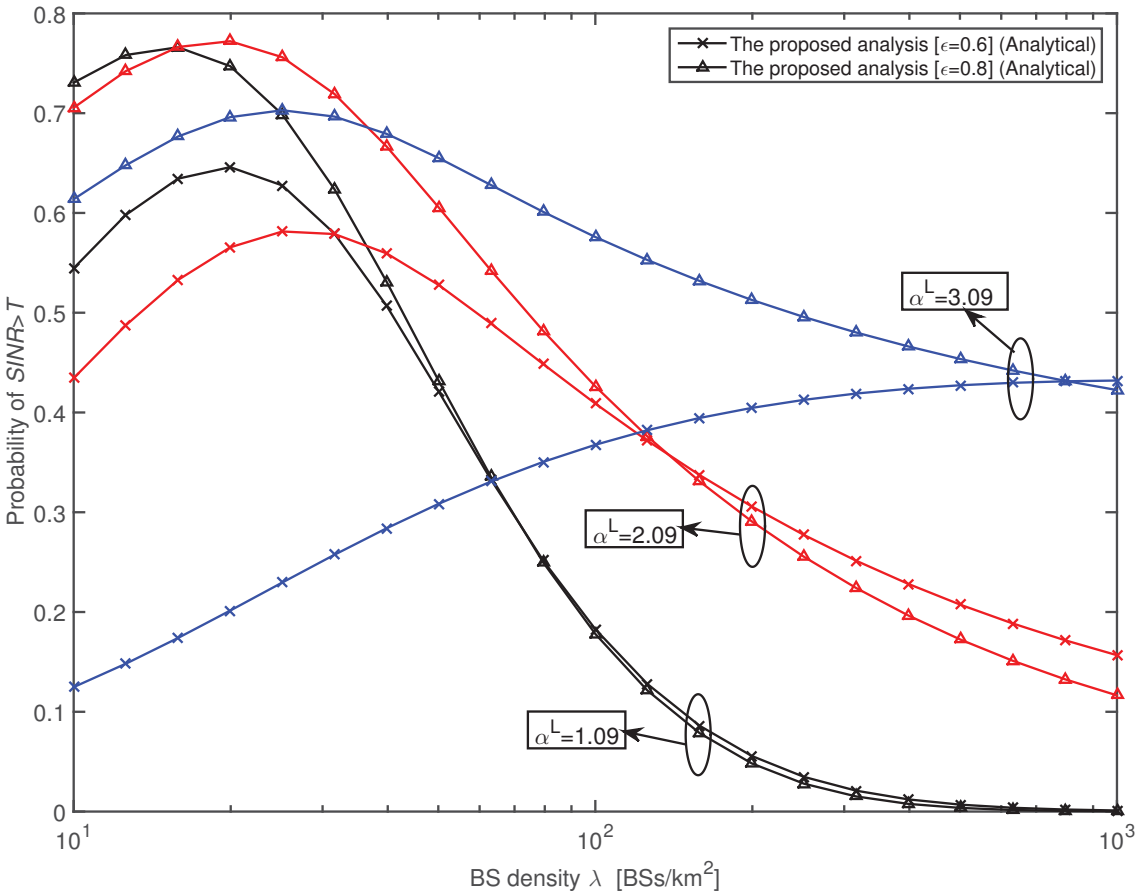

Fig. 5. The coverage probability $P^{\text{cov}}(\lambda, T)$ vs. the BS density with different ϵ and α^{L}. SINR threshold $T = 0$ dB.

NLoS path loss exponent α^{NL} and α^{L}. As a result, performance impact of the transition of interference from the NLoS transmission to the LoS transmission becomes more drastic as λ increases. In other words, the slow growth of the $P^{\text{cov}}(\lambda, 0)$ is more obvious to observe. For example, when α^{L} takes a near-field path loss exponent such as 1.09, the decrease of the $P^{\text{cov}}(\lambda, 0)$ at $\lambda \in [\lambda_0, \lambda_1]$ BSs/km^2 is substantial and it hardly recovers after λ_1.

As has been discussed in the Subchapter III-D2, when the SCN is sparse, adopting a higher ϵ leads to a higher coverage probability. However, as λ increases, adopting a lower ϵ leads to a higher coverage probability. The BS density around which the coverage probability with smaller ϵ surpasses that with larger ϵ is defined as the transition point of ϵ. As can be seen from Fig. 5, the transition point of various ϵ increases as α^{L} increases. It indicates that in dense SCNs with smaller α^{L}, the coverage probability using a smaller ϵ can soon outperform that using a larger ϵ as the SCN becomes denser.

5) Investigation of a Different Path Loss Model: In this Subchapter, we investigate the UL ASE performance assuming a more complicated path loss model, in which the LoS probability is defined as follows [8]

$$\Pr^{\mathrm{L}}(r) = \begin{cases} 1 - 5\exp\left(-\frac{R_1}{r}\right), & 0 < r \leq d_1 \\ 5\exp\left(-\frac{r}{R_2}\right), & r > d_1 \end{cases}, \tag{50}$$

where $R_1 = 0.156$ km, $R_2 = 0.03$ km, and $d_1 = \frac{R_1}{\ln 10}$. The simulation results of the area spectral efficiency $A^{\mathrm{ASE}}(\lambda, T_0)$ vs. the BS density is shown in Fig. 6.

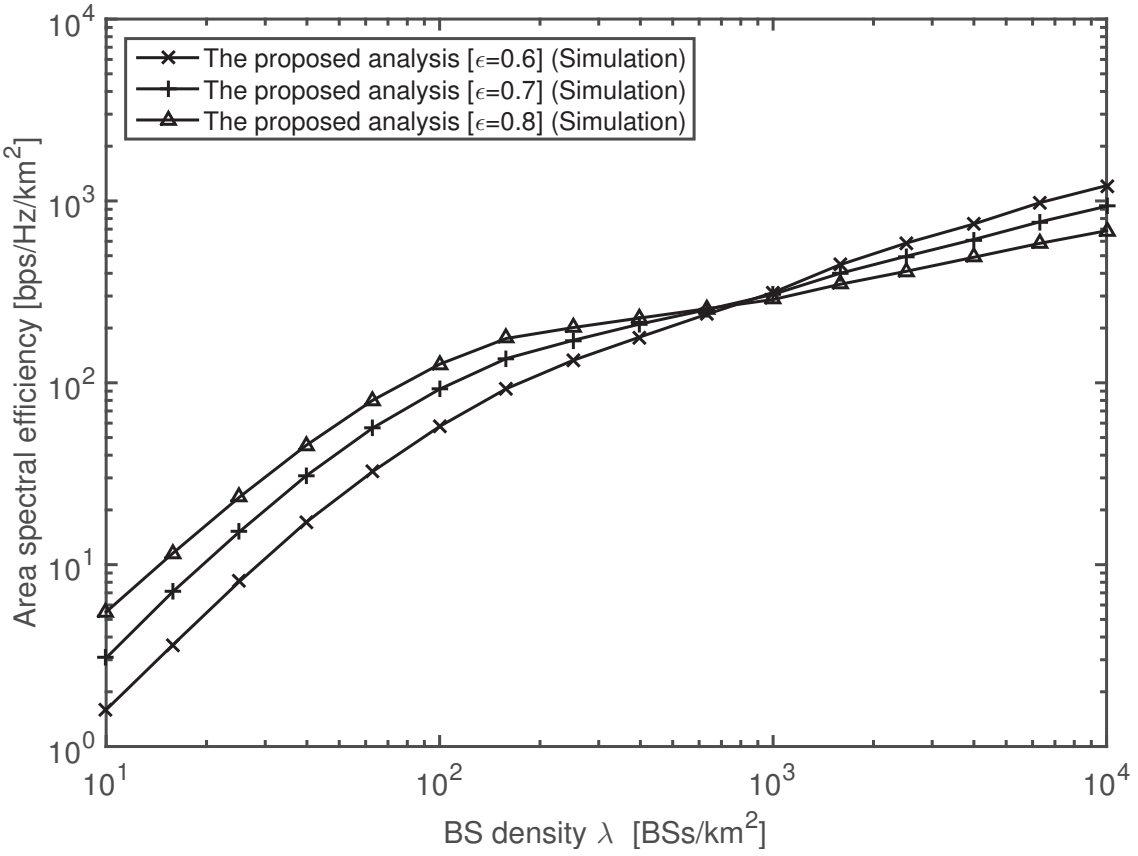

Fig. 6. Area spectral efficiency $A^{\mathrm{ASE}}(\lambda, T_0)$ vs. the BS density with the exponential LoS probability model, different ϵ and SINR threshold $T_0 = 0$ dB.

As can be seen from Fig. 6, the area spectral efficiency with the exponential LoS probability model exhibits a slow-down in the rate of growth in certain BS density regions, which qualitatively confirms our observations in Subchapter III-D3 with the linear LoS probability model. Specifically, in Fig. 6, the numerical result for λ_0 is around 10^2 BSs/km^2.

Furthermore, the area spectral efficiency with the exponential LoS probability model exhibits a similar trend as discussed in Subchapter III-D3 with the linear LoS probability model, i.e., using a smaller UL power compensation factor ϵ can outperform that using a larger ϵ as the SCN becomes denser.

6) Investigation of the Performance Impact of Ricean Fading: In this Subchapter, we investigate the UL ASE performance assuming a linear path loss model including the Ricean fading. Here we adopt a practical model of Ricean fading [21] with K factor $K = 15$ dB. The simulation results of the area spectral efficiency $A^{\mathrm{ASE}}(\lambda, T_0)$ vs. the BS density is shown in Fig. 7.

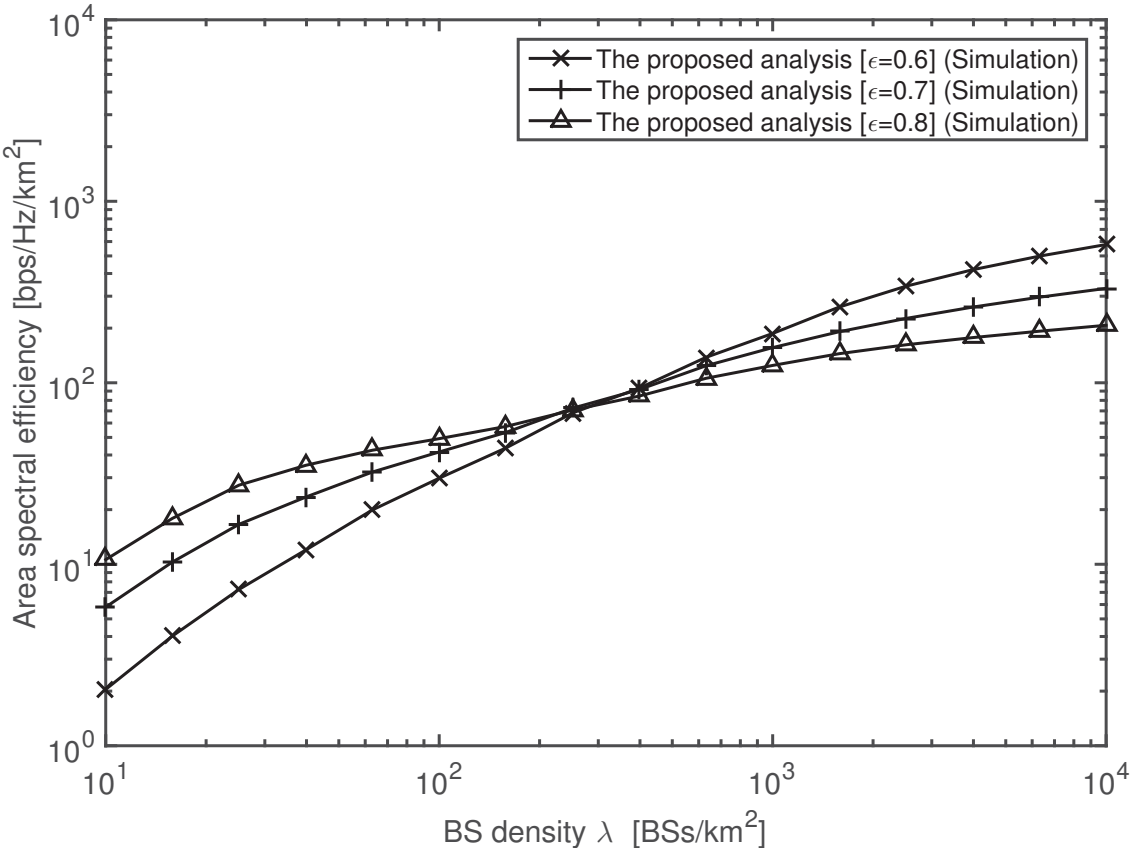

Fig. 7. Area spectral efficiency $A^{\mathrm{ASE}}(\lambda, T_0)$ vs. the BS density with the linear LoS probability model, different ϵ and SINR threshold $T_0 = 0$ dB, including the Ricean fading.

As can be seen from Fig. 7, the area spectral efficiency with the linear LoS probability model and the Ricean fading exhibits a slow-down in the rate of growth as the BS density increases, which qualitatively confirms our observations in Subchapter III-D3 for the linear

LoS probability model and the Rayleigh fading. Furthermore, the area spectral efficiency with the Ricean fading exhibits a similar trend as discussed in Subchapter III-D3 with the Rayleigh fading, i.e., using a smaller UL power compensation factor ϵ can outperform that using a larger ϵ as the SCN becomes denser. Since the simulation results of Ricean fading and Rayleigh fading are not qualitatively different, we suggest to use a simplified model with the Rayleigh fading in theoretical analysis.

E. Conclusion

In this Chapter, we have investigated the impact of a piecewise linear path loss model incorporating both LoS and NLoS transmissions in the performance of the UL of dense SCNs. Analytical results were obtained for the coverage probability and the ASE performance. The results show that LoS and NLoS transmissions have a significant impact in the ASE of the UL of dense SCNs, both quantitatively and qualitatively, compared with previous works that does not differentiate LoS and NLoS transmissions. Specifically, we found that

- The ASE may suffer from a slow growth as the UE density increases in the UL of dense SCNs.
- The ASE with a smaller UL power compensation factor considerably outperforms that with a larger UL power compensation factor in dense SCNs. The reverse is true for sparse SCNs.

As our future work, we will consider other factors of realistic networks in the theoretical analysis for SCNs, such as the introduction of Ricean fading or Nakagami fading, because the multi-path fading model is also affected by the LoS and NLoS transmissions.

IV. Performance Analysis of Dense SCNs with Dynamic TDD

In this Chapter, the performance analysis of dense SCNs with dynamic TDD is presented.

A. System Model

1) General Network Scenario: We consider a cellular network with BSs deployed on a plane according to a homogeneous Poisson point process (HPPP) Φ with a density of λ BSs/km^2. Active UEs are distributed as a HPPP Φ_{UE} with density λ_{UE}. Here, we only consider active UEs in the network because non-active UEs do not trigger data transmissions. In practice, a BS will mute its transmission, if there is no UE connected to it, which reduces inter-cell interference and energy consumption [46]. Note that such BS idle mode operation is not trivial, which even changes the capacity scaling law [46]. Since UEs are randomly and uniformly distributed in the network, we assume that the active BSs also follow an HPPP distribution $\tilde{\Phi}$, the density of which is denoted by $\tilde{\lambda}$ BSs/km^2. Note that $0 \leq \tilde{\lambda} \leq \lambda$, and a larger λ_{UE} leads to a larger $\tilde{\lambda}$. From [47], [48], $\tilde{\lambda}$ is given by

$$\tilde{\lambda} = \lambda \left[1 - \frac{1}{\left(1 + \frac{\lambda_{\mathrm{UE}}}{q\lambda}\right)^q} \right], \tag{51}$$

where q takes an empirical value around 3.5~4 [47], [48].

For each active UE, the probabilities of it requesting DL and UL data are respectively denoted by p^{D} and p^{U}, with $p^{\mathrm{D}} + p^{\mathrm{U}} = 1$. Besides, we assume that each request is large enough to be transmitted for at least one TDD frame, which consists of T subframes. In the sequel, *the DL or UL subframe number per frame* will be shortened as *the DL or UL subframe number*, because subframes are meant within one frame.

We focus on the UL of a randomly picked BS from Φ, named the typical BS, and the DL of a randomly picked UE from the UEs served by the typical BS, defined as the typical UE. We assume that at any subframe in any small cell, there is exactly one active transmission, either on the DL with probability p^{D}, or on the UL with probability p^{U} . Then the set of transmitting BSs at the subframe of interest is described by a PPP Φ^{D} with

density $\lambda^{\mathrm{D}} = \tilde{\lambda} p^{\mathrm{D}}$, and the set of transmitting UEs at the subframe of interest is described by a PPP Φ^{U} with density $\lambda^{\mathrm{U}} = \tilde{\lambda} p^{\mathrm{U}}$. The system model is shown in Fig. 8.

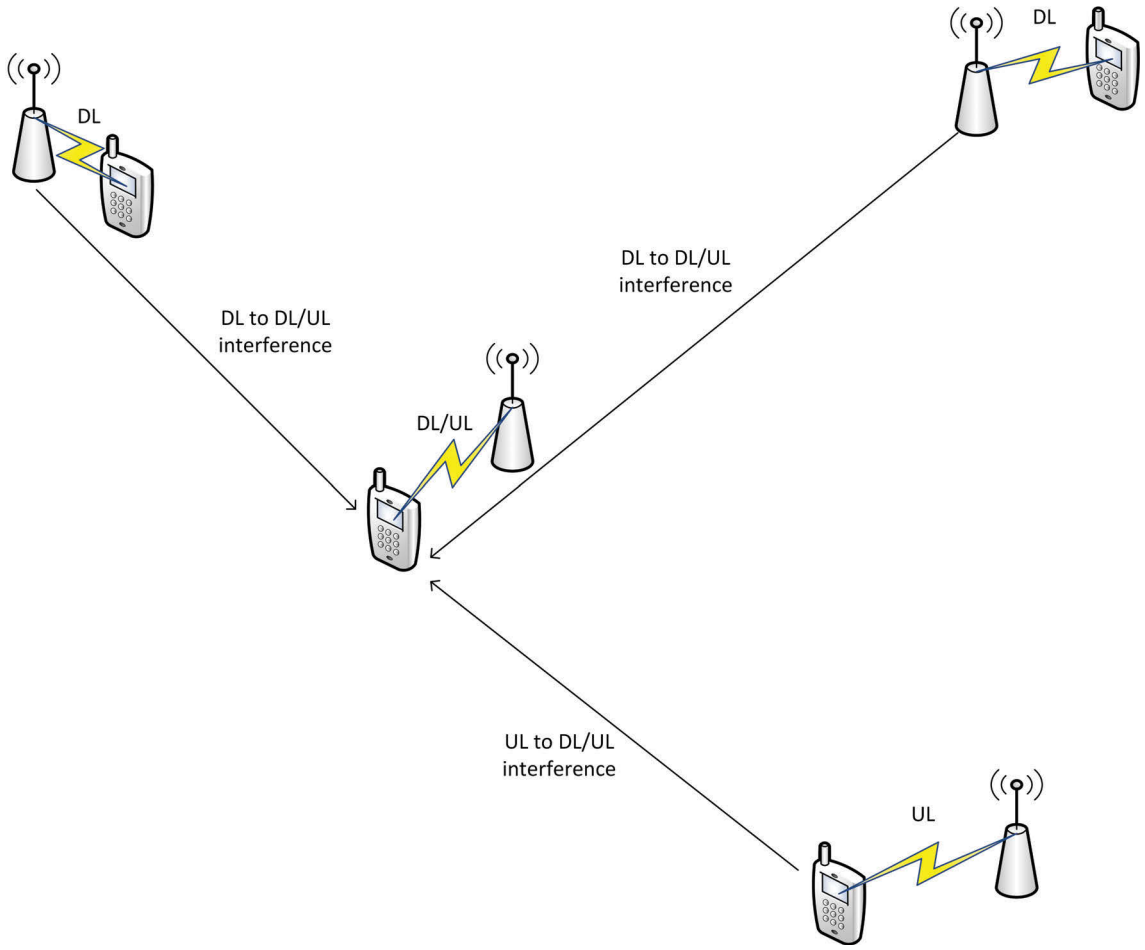

Fig. 8. Dynamic TDD scenarios.

Following [6], we adopt a general and practical path loss model, in which the path loss $\zeta(r)$ associated with distance r is segmented into N pieces written as

$$\zeta^{Dir}(r) = \begin{cases} \zeta_1^{Dir}(r), & \text{when } 0 \le r \le d_1 \\ \zeta_2^{Dir}(r), & \text{when } d_1 < r \le d_2 \\ \vdots & \vdots \\ \zeta_N^{Dir}(r), & \text{when } r > d_{N-1} \end{cases}, \tag{52}$$

where the string variable Dir denotes the path loss direction and takes the value of 'B2U',

'B2B' and 'U2U' for the BS-to-UE path loss, the BS-to-BS path loss and the UE-to-UE path loss, respectively. Besides, each piece $\zeta_n^{Dir}(r), n \in \{1, 2, \ldots, N\}$, is modeled as

$$\zeta_n^{Dir}(r) = \begin{cases} \zeta_n^{Dir,\mathrm{L}}(r) = \frac{A_n^{Dir,\mathrm{L}}}{r^{\alpha_n^{Dir,\mathrm{L}}}}, & \text{LoS: } \mathrm{Pr}_n^{Dir,\mathrm{L}}(r) \\ \zeta_n^{Dir,\mathrm{NL}}(r) = \frac{A_n^{Dir,\mathrm{NL}}}{r^{\alpha_n^{Dir,\mathrm{NL}}}}, & \text{NLoS: } 1 - \mathrm{Pr}_n^{Dir,\mathrm{L}}(r) \end{cases}, \tag{53}$$

where $\zeta_n^{Dir,\mathrm{L}}(r)$ and $\zeta_n^{Dir,\mathrm{NL}}(r)$ are the n-th piece path loss functions for the LoS transmission and the NLoS transmission, respectively, $A_n^{Dir,\mathrm{L}}$ and $A_n^{Dir,\mathrm{NL}}$ are the path losses at a reference distance $r = 1$ for the LoS and the NLoS cases, respectively, and $\alpha_n^{Dir,\mathrm{L}}$ and $\alpha_n^{Dir,\mathrm{NL}}$ are the path loss exponents for the LoS and the NLoS cases, respectively. In practice, $A_n^{Dir,\mathrm{L}}$, $A_n^{Dir,\mathrm{NL}}$, $\alpha_n^{Dir,\mathrm{L}}$ and $\alpha_n^{Dir,\mathrm{NL}}$ are constants obtainable from field tests [8].

Moreover, $\mathrm{Pr}_n^{Dir,\mathrm{L}}(r)$ is the n-th piece LoS probability function for the event that there is a LoS path between a transmitter and a receiver separated by a distance r.

In this research, we assume a practical user association strategy (UAS), in which each UE is connected to the BS with the strongest received signal strength (i.e., with the largest $\zeta(r)$) [6]. Moreover, we assume that each BS/UE is equipped with an isotropic antenna, and that the multi-path fading between a transmitter and a receiver is modeled as independent and identically distributed (i.i.d.) Rayleigh fading [6]. Note we have found in previous work that a general multi-path fading model based on Rician fading has a minor impact on the performance of SCNs, i.e., change the results quantitatively but not qualitatively, and thus its incorporation into theoretical analyses is less urgent [49].

2) Synchronous Networks: Regarding TDD frames, we focus on the analysis of the synchronous networks. Fig. 9 shows an example of such TDD configuration structure in LTE with $T = 10$ [8]. In Fig. 9, TDD frames of different cells are aligned in the time domain. One TDD frame is composed of $T = 10$ subframes, and the time length of each subframe is 1 millisecond [8]. As an example, we assume that BS 1 and BS 2 use the TDD configurations with 6 and 8 DL subframes, respectively. Note that the current LTE behaviour in dynamic TDD is first DL and then UL. For this synchronous network with TDD frame alignment, we have the following two remarks.

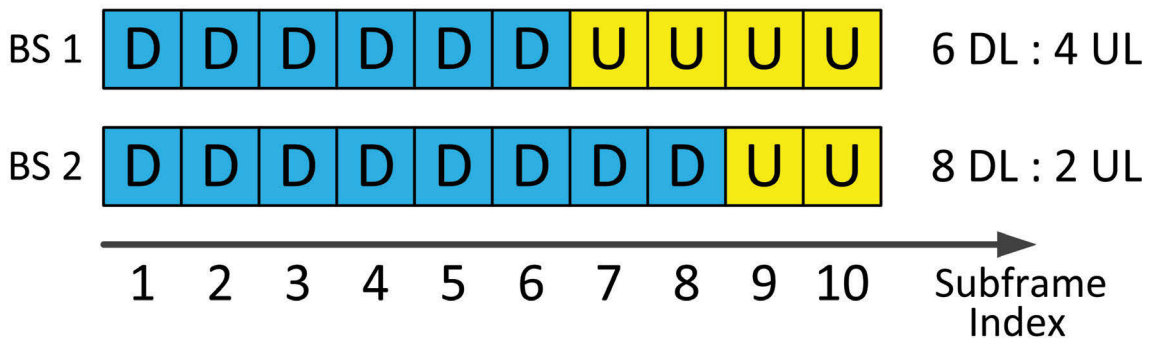

Fig. 9. An example of the LTE TDD configurations. ('D' and 'U' denote a DL subframe and an UL one, respectively.)

Remark 1: The first few subframes are more likely to carry DL transmissions than the last few ones. The opposite conclusion applies for the UL. This leads to a subframe dependent MAC layer performance of dynamic TDD.

Remark 2: The subframes in the middle of the frame are more likely to be subject to inter-cell inter-link interference than those at the beginning and at the end. This implies a subframe dependent PHY layer performance of dynamic TDD.

In this research, we explore these two Remarks, and study the system performance of synchronous dynamic TDD, with the consideration of the DL-before-UL TDD configuration structure adopted in LTE (see Fig. 9).

3) Performance Metrics:

a) MAC-layer Performance Metrics: For the l-th subframe ($l \in \{1, 2, \ldots, T\}$), we define the subframe dependent DL TRU and UL TRU as the probability of the BS transmitting DL signals and that of UEs transmitting UL signals, respectively, which are denoted by q_l^{D} and q_l^{U}. In other words, q_l^{D} and q_l^{U} characterize how much time resource is *actually* used for DL and UL, respectively. Note that we may or may not have $q_l^{\mathrm{D}} + q_l^{\mathrm{U}} = 1$, depending on whether we have a dynamic enough TDD and the traffic conditions.

Moreover, we define the average DL TRU κ^{D} and the average UL TRU κ^{U} as the mean value of q_l^{D} and q_l^{U} across all of the T subframes:

$$\begin{cases} \kappa^{\mathrm{D}} = \frac{1}{T} \sum_{l=1}^{T} q_l^{\mathrm{D}} \\ \kappa^{\mathrm{U}} = \frac{1}{T} \sum_{l=1}^{T} q_l^{\mathrm{U}} \end{cases}. \tag{54}$$

Finally, we define the average total TRU κ as the sum of κ^{D} and κ^{U}, which is written as

$$\kappa = \kappa^{\mathrm{D}} + \kappa^{\mathrm{U}}. \tag{55}$$

In the following Subchapters, we will investigate the performance of q_l^{Link}, κ^{Link} and κ considering Remark 1, where the string variable $Link$ denotes the link direction and takes the value of 'D' and 'U' for the DL and the UL, respectively.

b) PHY-layer Performance Metrics: Based on the system model presented in Subchapter IV-A1, we can define the coverage probability that the typical UE's DL/UL SINR is above a designated threshold γ as

$$p^{\mathrm{cov},Link}(\lambda,\gamma) = \Pr\left[\mathrm{SINR}^{Link} > \gamma\right]. \tag{56}$$

Moreover, the DL/UL SINR is calculated by

$$\mathrm{SINR}^{Link} = \frac{P^{Link}\zeta_{b_o}^{\mathrm{B2U}}(r)\,h}{I_{\mathrm{agg}}^{Link,\mathrm{D}} + I_{\mathrm{agg}}^{Link,\mathrm{U}} + P_{\mathrm{N}}^{Link}}, \tag{57}$$

where P^{Link} is the transmission power, r is the distance from the typical UE to the typical BS denoted by b_o, h is the Rayleigh channel gain modeled as an exponentially distributed random variable (RV) with a mean of one as mentioned above, P_{N}^{Link} is the additive white Gaussian noise (AWGN) power, and $I_{\mathrm{agg}}^{Link,\mathrm{D}}$ ($I_{\mathrm{agg}}^{Link,\mathrm{U}}$) is the DL (UL) cumulative interference, respectively. It is important to note that:

- For the DL, P^{Link} takes the value of the BS power, i.e., P^{D}, which is usually a cell-specific constant to maintain a stable DL coverage [8]. Besides, P_{N}^{Link} should be the AWGN at the UE side, i.e., $P_{\mathrm{N}}^{\mathrm{D}}$.
- For the UL, P^{Link} takes the value of the UE power, i.e., P^{U}, which is assumed as a constant in this research [8]. Besides, P_{N}^{Link} should be the AWGN at the BS side, i.e., $P_{\mathrm{N}}^{\mathrm{U}}$.
- Due to the existence of inter-cell inter-link interference, $I_{\mathrm{agg}}^{\mathrm{D}}$ and $I_{\mathrm{agg}}^{\mathrm{U}}$ are probabilistic interference emitted from interfering BSs and interfering UEs, respectively.

For clarity, the notation of variables is summarized in Table III.

TABLE III
NOTATION OF VARIABLES FOR DYNAMIC TDD

Notation	Items
q_l^{D}, q_l^{U}	Subframe dependent DL TRU and UL TRU
κ, κ^{D}, κ^{U}	Average total TRU, DL TRU and UL TRU
P^{D}, P^{U}	DL and UL transmission power
$I_{\mathrm{agg}}^{Link,\mathrm{D}}$, $I_{\mathrm{agg}}^{Link,\mathrm{U}}$	DL and UL cumulative interference
$P_{\mathrm{N}}^{\mathrm{D}}$, $P_{\mathrm{N}}^{\mathrm{U}}$.	DL and UL AWGN power

c) Combined Performance Metrics: According to [6], the SINR-dependent DL/UL area spectral efficiency (ASE) in bps/Hz/km^2 can be defined by

$$ASE^{Link}(\lambda,\gamma_0)=\kappa^{Link}\lambda\int_{\gamma_0}^{+\infty}\log_2(1+\gamma)\,f_{\Gamma}^{Link}(\lambda,\gamma)\,d\gamma, \tag{58}$$

where κ^{Link} is the DL/UL time resource utilization characterizing how much time resource is actually used for the DL/UL, γ_0 is the minimum working SINR for the considered SCN, and $f_{\Gamma}^{Link}(\lambda,\gamma)$ is the probability density function (PDF) of SINR^{Link} at a particular BS density λ.

Based on the definition of $p^{\mathrm{cov},Link}(\lambda,\gamma)$ in (56), which is the complementary cumulative distribution function (CCDF) of the DL/UL SINR, $f_{\Gamma}^{Link}(\lambda,\gamma)$ can be computed by

$$f_{\Gamma}^{Link}(\lambda,\gamma)=\frac{\partial\left(1-p^{\mathrm{cov},Link}(\lambda,\gamma)\right)}{\partial\gamma}. \tag{59}$$

B. Main Results of the MAC Layer Analysis

The main goal of this Subchapter is to derive theoretical results on the DL/UL TRU defined in Subchapter IV-A3. Note that computing q_l^{D} and q_l^{U} is a non-trivial task for synchronous dynamic TDD, because it involves the following distributions:

- the distribution of the UE number in an active BS, which will be shown to follow a truncated Negative Binomial distribution in Subchapter IV-B1;
- the distribution of the DL/UL data request numbers in an active BS, which will be shown to follow a Binomial distribution in Subchapter IV-B2;

- the dynamic TDD subframe splitting strategy and the corresponding distribution of the DL/UL subframe number, which will be shown to follow an aggregated Binomial distribution in Subchapter IV-B3; and finally
- the prior information about the TDD frame structure, such as the DL-before-UL structure adopted in LTE [8] (see Fig. 9), which will lead to subframe dependent results of q_l^{D} and q_l^{U} to be presented in Subchapter IV-B4.

1) The Distribution of the UE Number in an active BS: A Truncated Negative Binomial Distribution: According to [47], the per-BS coverage area size X can be characterized by a Gamma distribution [47], [50], [51], and the probability density function (PDF) of X can be expressed as

$$f_X(x) = (q\lambda)^q \, x^{q-1} \frac{\exp(-q\lambda x)}{\Gamma(q)}, \tag{60}$$

where $\Gamma(\cdot)$ is the Gamma function [52]. Note that the Gamma approximation was shown to be very accurate in [47], assuming a nearest-distance UAS, where an empirical value of 3.5 was suggested for q. In this work, a more realistic received signal strength based UAS is adopted, and thus the corresponding result in [47] cannot be directly applied. Instead, we need to derive a new approximation for the adopted UAS considering probabilistic LoS and NLoS transmissions. Intuitively speaking, from a typical UE's point of view, the equivalent BS density of the considered UAS based on probabilistic LoS and NLoS transmissions should be larger than that of the nearest-distance UAS based on single-slope path loss transmissions. In other words, the existence of LoS BSs provides more candidate BSs for a typical UE to connect with, and thus the equivalent BS density increases for each UE. We have proved that based on the considered path loss model and the adopted UAS, the per-BS coverage area size can be approximated tightly with the gamma approximation in (60) [46]. Moreover, the value of q in (60) is obtained according to the derived lower bound and the upper bound presented in Theorems 3 and 4 of [46], respectively.

Then, the UE number per BS can be denoted by a random variable (RV) K, and the

probability mass function (PMF) of K can be derived as

$$\begin{aligned} f_K(k) &= \Pr[K=k] \\ &\overset{(a)}{=} \int_0^{+\infty} \frac{(\rho x)^k}{k!} \exp(-\rho x) f_X(x) dx \\ &\overset{(b)}{=} \frac{\Gamma(k+q)}{\Gamma(k+1)\Gamma(q)} \left(\frac{\rho}{\rho+q\lambda}\right)^k \left(\frac{q\lambda}{\rho+q\lambda}\right)^q, \end{aligned} \tag{61}$$

where (a) is due to the HPPP distribution of UEs and (b) is obtained from (60). It can be seem from (61) that K follows a Negative Binomial distribution [52], i.e., $K \sim$ NB $\left(q, \frac{\rho}{\rho+q\lambda}\right)$.

As discussed in Subchapter IV-A1, we assume that a BS with $K = 0$ is not active, which will be ignored in our analysis due to its muted transmission. Hence, we focus on the active BSs and further study *the distribution of the UE number per active BS*, which is denoted by a positive RV $\tilde{K}$. Considering (61) and the fact that the only difference between K and $\tilde{K}$ lies in $\tilde{K} \neq 0$, we can conclude that $\tilde{K}$ follows a truncated Negative Binomial distribution, i.e., $\tilde{K} \sim$ truncNB $\left(q, \frac{\rho}{\rho+q\lambda}\right)$. More specifically, the PMF of $\tilde{K}$ is denoted by $f_{\tilde{K}}\left(\tilde{k}\right), \tilde{k} \in \{1, 2, \ldots, +\infty\}$, and it is given by

$$f_{\tilde{K}}\left(\tilde{k}\right) = \Pr\left[\tilde{K} = \tilde{k}\right] = \frac{f_K\left(\tilde{k}\right)}{1 - f_K(0)}, \tag{62}$$

where the denominator $(1 - f_K(0))$ represents the probability of a BS being active, i.e., $\tilde{\lambda}/\lambda$.

2) The Distribution of the DL/UL Data Request Number in an Active BS: A Binomial Distribution: After obtaining $f_{\tilde{K}}\left(\tilde{k}\right)$, we need to further study the distribution of the DL/UL data request number in an active BS, so that a tailored TDD configuration can be determined in a dynamic TDD network.

For clarity, the DL and UL data request numbers in an active BS are denoted by RVs M^{D} and M^{U}, respectively. Since we assume that each UE generates one request of either

DL data or UL data (see Subchapter IV-A1), it is easy to show that

$$M^{\mathrm{D}} + M^{\mathrm{U}} = \tilde{K}. \tag{63}$$

As discussed in Subchapter IV-A1, for each UE in an active BS, the probability of it requesting DL data and UL data is p^{D} and p^{U}, respectively. Hence, for a given UE number $\tilde{k}$, M^{D} and M^{U} follow Binomial distributions [52], i.e., $M^{\mathrm{D}} \sim \mathrm{Bi}\left(\tilde{k}, p^{\mathrm{D}}\right)$ and $M^{\mathrm{U}} \sim \mathrm{Bi}\left(\tilde{k}, p^{\mathrm{U}}\right)$. More specifically, the PMFs of M^{D} and M^{U} can be respectively written as

$$f_{M^{\mathrm{D}}}\left(m^{\mathrm{D}}\right) = \begin{pmatrix} \tilde{k} \\ m^{\mathrm{D}} \end{pmatrix} \left(p^{\mathrm{D}}\right)^{m^{\mathrm{D}}} \left(1-p^{\mathrm{D}}\right)^{\tilde{k}-m^{\mathrm{D}}}, \tag{64}$$

and

$$f_{M^{\mathrm{U}}}\left(m^{\mathrm{U}}\right) = \begin{pmatrix} \tilde{k} \\ m^{\mathrm{U}} \end{pmatrix} \left(p^{\mathrm{U}}\right)^{m^{\mathrm{U}}} \left(1-p^{\mathrm{U}}\right)^{\tilde{k}-m^{\mathrm{U}}}. \tag{65}$$

3) The Distribution of the DL/UL Subframe Number with Dynamic TDD: An Aggregated Binomial Distribution: After knowing the distribution of the DL data request number M^{D} in an active BS, we are now ready to consider dynamic TDD, and derive the distribution of the DL subframe number in an active BS. For a given UE number $\tilde{k}$, the DL subframe number in an active BS is denoted by N^{D}. Here, we adopt a dynamic TDD algorithm to choose the DL subframe number, which matches the DL subframe ratio with the DL data request ratio [53]. In more detail, for certain values of m^{D} and $\tilde{k}$, the DL subframe number $n\left(m^{\mathrm{D}}, \tilde{k}\right)$ is determined by

$$n\left(m^{\mathrm{D}}, \tilde{k}\right) = \mathrm{round}\left(\frac{m^{\mathrm{D}}}{\tilde{k}} T\right), \tag{66}$$

where $\mathrm{round}\,(x)$ is an operator that rounds a real value x to its nearest integer. In (66), $\frac{m^{\mathrm{D}}}{\tilde{k}}$ can be deemed as the DL data request ratio, because *(i)* m^{D} denotes the DL data request number with its distribution characterized in (64); and *(ii)* $\tilde{k}$ represents the UE number, and thus the total number of the DL and UL data requests. As a result, $\frac{m^{\mathrm{D}}}{\tilde{k}} T$ yields the desirable

DL subframe number that matches the DL subframe ratio with the DL data request ratio. Due to the integer nature of the DL subframe number, we use the round operator to generate a valid DL subframe number that is nearest to $\frac{m^{\mathrm{D}}}{\tilde{k}}T$ in (66).

Based on (66), the PMF of N^{D} is denoted by $f_{N^{\mathrm{D}}}\left(n^{\mathrm{D}}\right), n^{\mathrm{D}} \in \{0, 1, \ldots, T\}$, and it can be derived as

$$\begin{aligned} f_{N^{\mathrm{D}}}\left(n^{\mathrm{D}}\right) &= \Pr\left[N^{\mathrm{D}} = n^{\mathrm{D}}\right] \\ &\overset{(a)}{=} \sum_{m^{\mathrm{D}}=0}^{\tilde{k}} I\left\{\text{round}\left(\frac{m^{\mathrm{D}}}{\tilde{k}}T\right) = n^{\mathrm{D}}\right\} f_{M^{\mathrm{D}}}\left(m^{\mathrm{D}}\right), \end{aligned} \tag{67}$$

where (66) is plugged into (a), and $I\{X\}$ is an indicator function that outputs one when X is true and zero otherwise. Besides, $f_{M^{\mathrm{D}}}\left(m^{\mathrm{D}}\right)$ is computed by (64). Due to the existence of the indicator function in (67), $f_{N^{\mathrm{D}}}\left(n^{\mathrm{D}}\right)$ can be viewed as an aggregated PMF of Binomial PMFs, since N^{D} is computed from M^{D} according to a many-to-one mapping in (66).

Because the total subframe number in a frame is T, and each subframe should be either a DL one or an UL one, it is apparent that $N^{\mathrm{D}} + N^{\mathrm{U}} = T$, and thus we have

$$f_{N^{\mathrm{U}}}\left(n^{\mathrm{U}}\right) = f_{N^{\mathrm{D}}}\left(T - n^{\mathrm{U}}\right). \tag{68}$$

4) The Subframe Dependent DL/UL TRU: In this Subchapter, we present our main results on the subframe dependent DL/UL TRUs q_l^{D} and q_l^{U} for dynamic TDD in Theorem 6.

Theorem 6. *For dynamic TDD, q_l^{D} and q_l^{U} are given by*

$$\begin{cases} q_l^{\mathrm{D}} = \sum_{\tilde{k}=1}^{+\infty}\left(1 - \sum_{i=0}^{l-1} f_{N^{\mathrm{D}}}(i)\right) f_{\tilde{K}}\left(\tilde{k}\right) \\ q_l^{\mathrm{U}} = \sum_{\tilde{k}=1}^{+\infty}\sum_{i=0}^{l-1} f_{N^{\mathrm{D}}}(i)\, f_{\tilde{K}}\left(\tilde{k}\right) \end{cases}, \tag{69}$$

where $f_{N^{\mathrm{D}}}(i)$ and $f_{\tilde{K}}\left(\tilde{k}\right)$ are given by (67) and (62), respectively.

Proof: See Appendix D. ■

5) The Probabilities of Inter-Cell Inter-Link Interference: With the knowledge on the probability of each subframe being a DL one or an UL one, we can conduct an interesting study on the probabilities of inter-cell inter-link interference for dynamic TDD in the

synchronous case. For clarify, such probabilities are formally defined as follows:

- The probability of the DL-to-UL interference is denoted by $\Pr^{\mathrm{D2U}}$ and defined as $\Pr\left[Z = \text{'D'} \middle| S = \text{'U'}\right]$, where Z and S denote the link directions for the interference and the signal, respectively. Note that the probability of the UL-to-UL interference is denoted by $\Pr^{\mathrm{U2U}}$ and defined as $\Pr\left[Z = \text{'U'} \middle| S = \text{'U'}\right]$. From the definition of $\Pr^{\mathrm{D2U}}$ and $\Pr^{\mathrm{U2U}}$, we have $\Pr^{\mathrm{D2U}} + \Pr^{\mathrm{U2U}} = 1$.
- Similarly, the probability of the UL-to-DL interference is defined by

$$\Pr^{\mathrm{U2D}} \triangleq \Pr\left[Z = \text{'U'} \middle| S = \text{'D'}\right].$$

  Besides, the probability of the DL-to-DL interference is defined by

$$\Pr^{\mathrm{D2D}} \triangleq \Pr\left[Z = \text{'D'} \middle| S = \text{'D'}\right],$$

  with $\Pr^{\mathrm{U2D}} + \Pr^{\mathrm{D2D}} = 1$.

Our main results on $\Pr^{\mathrm{D2U}}$ and $\Pr^{\mathrm{U2D}}$ are summarized in Theorem 7.

Theorem 7. *$\Pr^{\mathrm{D2U}}$ and $\Pr^{\mathrm{U2D}}$ can be derived in closed-form expressions as*

$$\begin{cases} \Pr^{\mathrm{D2U}} = \frac{\sum_{l=1}^{T} q_l^{\mathrm{D}} q_l^{\mathrm{U}}}{\sum_{j=1}^{T} q_j^{\mathrm{U}}} \\ \Pr^{\mathrm{U2D}} = \frac{\sum_{l=1}^{T} q_l^{\mathrm{U}} q_l^{\mathrm{D}}}{\sum_{j=1}^{T} q_j^{\mathrm{D}}} \end{cases}, \tag{70}$$

where q_l^{D} and q_l^{U} are obtained from (69).

Proof: See Appendix E. ■

As discussed at the beginning of Subchapter IV-B, for static TDD, we have $\Pr^{\mathrm{D2U}} = \Pr^{\mathrm{U2D}} = 0$ since all the TDD subframes are of the same sequence and well-aligned. For dynamic TDD in the *asynchronous* case, we have $\Pr^{\mathrm{D2U}} = p^{\mathrm{D}}$ and $\Pr^{\mathrm{U2D}} = p^{\mathrm{U}}$ [32], due to the random collision of the dynamic TDD subframes. On the other hand, as shown in Theorem 7, $\Pr^{\mathrm{D2U}}$ and $\Pr^{\mathrm{U2D}}$ for dynamic TDD in the *synchronous* case are much more complex, which are expected to have a major impact on the evaluation of $I_{\mathrm{agg}}^{\mathrm{D}}$ and $I_{\mathrm{agg}}^{\mathrm{U}}$ in (57).

6) The Average DL/UL/Total TRU: From Theorem 6, and Equations (54) and (55), we can obtain the results on the average DL/UL/total TRU for dynamic TDD, which are summarized in Lemma 8.

Lemma 8. *For dynamic TDD,* $\left\{\kappa^{\mathrm{D}}, \kappa^{\mathrm{U}}, \kappa\right\}$ *is given by*

$$\begin{cases} \kappa^{\mathrm{D}} = \frac{1}{T}\sum_{l=1}^{T}\sum_{\tilde{k}=1}^{+\infty}\left(1-\sum_{i=0}^{l-1} f_{N^{\mathrm{D}}}\left(i\right)\right) f_{\tilde{K}}\left(\tilde{k}\right) \\ \kappa^{\mathrm{U}} = \frac{1}{T}\sum_{l=1}^{T}\sum_{\tilde{k}=1}^{+\infty}\sum_{i=0}^{l-1} f_{N^{\mathrm{D}}}\left(i\right) f_{\tilde{K}}\left(\tilde{k}\right) \\ \kappa = 1 \end{cases}, \tag{71}$$

where $f_{N^{\mathrm{D}}}(i)$ *and* $f_{\tilde{K}}\left(\tilde{k}\right)$ *are given by (67) and (62), respectively.*

Proof: The proof is straightforward by plugging (69) into (54) and (55). ■

Lemma 8 not only quantifies the average MAC layer performance of dynamic TDD, but also shows from a theoretical viewpoint that dynamic TDD can always achieve a full resource utilization, thanks to the smart adaption of DL/UL subframes to DL/UL data requests.

Next, we present our main results on κ^{D}, κ^{U} and κ for static TDD in Theorem 9.

Theorem 9. *For static TDD,* $\left\{\kappa^{\mathrm{D}}, \kappa^{\mathrm{U}}, \kappa\right\}$ *can be derived as*

$$\begin{cases} \kappa^{\mathrm{D}} = \left(1-\sum_{\tilde{k}=1}^{+\infty}\left(1-p^{\mathrm{D}}\right)^{\tilde{k}} f_{\tilde{K}}\left(\tilde{k}\right)\right)\frac{N_0^{\mathrm{D}}}{T} \\ \kappa^{\mathrm{U}} = \left(1-\sum_{\tilde{k}=1}^{+\infty}\left(1-p^{\mathrm{U}}\right)^{\tilde{k}} f_{\tilde{K}}\left(\tilde{k}\right)\right)\frac{N_0^{\mathrm{U}}}{T} \\ \kappa = \frac{1}{T}\sum_{\tilde{k}=1}^{+\infty}\left[\left(1-\left(p^{\mathrm{U}}\right)^{\tilde{k}}\right)N_0^{\mathrm{D}} + \left(1-\left(p^{\mathrm{D}}\right)^{\tilde{k}}\right)N_0^{\mathrm{U}}\right] f_{\tilde{K}}\left(\tilde{k}\right) \end{cases}, \tag{72}$$

where $f_{\tilde{K}}\left(\tilde{k}\right)$ *is obtained from (62), and* N_0^{D} *and* N_0^{U} *are the designated subframe numbers for the DL and the UL in static TDD, respectively, which satisfy* $N_0^{\mathrm{D}} + N_0^{\mathrm{U}} = T$.

Proof: See Appendix F. ■

From Lemma 8 and Theorem 9, we can further quantify the additional total TRU achieved

by dynamic TDD as

$$\kappa^{\mathrm{ADD}} = \frac{1}{T}\sum_{\tilde{k}=1}^{+\infty}\left[\left(p^{\mathrm{U}}\right)^{\tilde{k}} N_0^{\mathrm{D}} + \left(p^{\mathrm{D}}\right)^{\tilde{k}} N_0^{\mathrm{U}}\right] f_{\tilde{K}}\left(\tilde{k}\right), \tag{73}$$

where κ^{ADD} measures the difference of κ in (71) and that in (72).

In addition, we present the performance limit of κ^{ADD} in Lemma 10.

Lemma 10. *When $\lambda \to +\infty$, the limit of κ^{ADD} is given by*

$$\lim_{\lambda\to+\infty} \kappa^{\mathrm{ADD}} = \frac{p^{\mathrm{D}} N_0^{\mathrm{U}}}{T} + \frac{p^{\mathrm{U}} N_0^{\mathrm{D}}}{T}. \tag{74}$$

Proof: From (62), we have $\lim_{\lambda\to+\infty} \Pr\left[\tilde{K}=1\right] = 1$. Hence, using Lemma 8, we can draw the following conclusion for dynamic TDD:

$$\begin{cases} \lim_{\lambda\to+\infty} \kappa^{\mathrm{D}} = 1 - f_{N^{\mathrm{D}}}(0) = 1 - p^{\mathrm{U}} = p^{\mathrm{D}} \\ \lim_{\lambda\to+\infty} \kappa^{\mathrm{U}} = 1 - f_{N^{\mathrm{U}}}(0) = 1 - p^{\mathrm{D}} = p^{\mathrm{U}} \end{cases}. \tag{75}$$

Based on $\lim_{\lambda\to+\infty} \Pr\left[\tilde{K}=1\right] = 1$ and Theorem 9, we can obtain the following conclusion for static TDD:

$$\begin{cases} \lim_{\lambda\to+\infty} \kappa^{\mathrm{D}} = \left(1-\left(1-p^{\mathrm{D}}\right)\right)\frac{N_0^{\mathrm{D}}}{T} = \frac{p^{\mathrm{D}} N_0^{\mathrm{D}}}{T} \\ \lim_{\lambda\to+\infty} \kappa^{\mathrm{U}} = \left(1-\left(1-p^{\mathrm{U}}\right)\right)\frac{N_0^{\mathrm{U}}}{T} = \frac{p^{\mathrm{U}} N_0^{\mathrm{U}}}{T} \end{cases}. \tag{76}$$

Our proof is completed by comparing (75) with (76). ■

Note that in (74) of Lemma 10, the first and the second terms are contributed from the DL and the UL, respectively.

C. Main Results of the PHY Layer Analysis

The main goal of this Subchapter is to derive theoretical results on the DL/UL coverage probability defined in Subchapter IV-A3. Note that computing $p^{\mathrm{cov,D}}(\lambda,\gamma)$ and $p^{\mathrm{cov,U}}(\lambda,\gamma)$ is a non-trivial task for dynamic TDD, because it involves the following characteristics:

- Two new kinds of inter-cell inter-link interference, i.e., the DL-to-UL and UL-to-DL interference, are introduced in the analysis of the coverage probability. For accurate

performance analysis, the dependent relationship between interfering BS and typical BS, as well as that between interfering UE and typical UE, should be considered carefully. The details will be shown in Subchapter IV-C1.

- The UL performance is the bottleneck of dynamic TDD and we need to manage the detrimental DL-to-UL interference. The UL coverage probability with full IC will be derived in Subchapter IV-C2. Note that having results cancelling a subset of interferers would be ideal, and other interference mitigation methods exist, e.g., clustering, UL power boosting, etc., which are left as possible future work.
- The theoretical analysis of the coverage probability will be applied to a 3GPP special case, and the results will be shown in Subchapter IV-C3.

1) Coverage Probability without Interference Cancellation: Based on the system model presented in Subchapter IV-A, we can calculate coverage probability $p^{\mathrm{cov},Link}(\lambda,\gamma)$ and present it in the following theorem.

Theorem 11. *$p^{\mathrm{cov},Link}(\lambda,\gamma)$ can be derived as*

$$p^{\mathrm{cov},Link}(\lambda,\gamma)=\sum_{n=1}^{N}\left(T_n^{\mathrm{L},Link}+T_n^{\mathrm{NL},Link}\right), \tag{77}$$

where

$$\begin{aligned} T_n^{\mathrm{L},Link}&=\textstyle\int_{d_{n-1}}^{d_n} \boldsymbol{Pr}\left[\mathrm{SINR}^{Link}>\gamma\middle|\, r,\mathrm{LoS}\right] f_{R,n}^{\mathrm{L}}(r)dr,\\ T_n^{\mathrm{NL},Link}&=\textstyle\int_{d_{n-1}}^{d_n} \boldsymbol{Pr}\left[\mathrm{SINR}^{Link}>\gamma\middle|\, r,\mathrm{NLoS}\right] f_{R,n}^{\mathrm{NL}}(r)\,dr, \end{aligned} \tag{78}$$

and d_0 and d_N are respectively defined as 0 and ∞.

Furthermore, $\Pr\left[\mathrm{SINR}^{Link}>\gamma\middle|\, \boldsymbol{LoS}\right]$ *and* $\Pr\left[\mathrm{SINR}^{Link}>\gamma\middle|\, \boldsymbol{NLoS}\right]$ *are respectively computed by*

$$\begin{aligned} &\Pr\left[\mathrm{SINR}^{Link}>\gamma\middle|\,\mathrm{LoS}\right]\\ &\overset{(a)}{=}\exp\left(-\tfrac{\gamma P_{\mathrm{N}}^{Link}}{P^{Link}\zeta_{b_o}^{\mathrm{B2U}}}\right)\mathscr{L}_{I_{\mathrm{agg}}^{Link,\mathrm{D}}}\left(\tfrac{\gamma}{P^{Link}\zeta_{b_o}^{\mathrm{B2U,L}}}\right)\\ &\times\mathscr{L}_{I_{\mathrm{agg}}^{Link,\mathrm{U}}}\left(\tfrac{\gamma}{P^{Link}\zeta_{b_o}^{\mathrm{B2U,L}}}\right), \end{aligned} \tag{79}$$

and

$$\begin{aligned}&\Pr\left[\mathrm{SINR}^{Link}>\gamma\middle|\,\mathrm{NLoS}\right]\\&=\exp\left(-\tfrac{\gamma P_{\mathrm{N}}^{Link}}{P^{Link}\zeta_{b_o}^{\mathrm{B2U}}}\right)\mathscr{L}_{I_{\mathrm{agg}}^{Link,\mathrm{D}}}\left(\tfrac{\gamma}{P^{Link}\zeta_{b_o}^{\mathrm{B2U,NL}}}\right)\\&\times\mathscr{L}_{I_{\mathrm{agg}}^{Link,\mathrm{U}}}\left(\tfrac{\gamma}{P^{Link}\zeta_{b_o}^{\mathrm{B2U,NL}}}\right),\end{aligned}\tag{80}$$

where (a) *is due to the independence of RV* $I_{\mathrm{agg}}^{Link,\mathrm{D}}$ *and* $I_{\mathrm{agg}}^{Link,\mathrm{U}}$*, moreover,* $\mathscr{L}_{I_{\mathrm{agg}}^{Link,\mathrm{U}}}(s)$ *and* $\mathscr{L}_{I_{\mathrm{agg}}^{Link,\mathrm{U}}}(s)$ *are the Laplace transform of RV* $I_{\mathrm{agg}}^{Link,\mathrm{D}}$ *and* $I_{\mathrm{agg}}^{Link,\mathrm{U}}$ *evaluated at* s *respectively.*

Proof: See Appendix G. ■

Note that the DL-to-DL interference and the UL-to-UL interference of dense cellular networks have been studied in our previous papers [6], [54]. Different from [6]and [54], in this research, we focus on the downlink and uplink performance analysis of dense small cell networks with dynamic TDD. Moreover, the novelties of the PHY layer analysis lie in the analysis of the inter-cell inter-link interference, i.e., the DL-to-UL interference $I_{\mathrm{agg}}^{\mathrm{U,D}}$ and the UL-to-DL interference $I_{\mathrm{agg}}^{\mathrm{D,U}}$. The Laplace transforms of the inter-cell inter-link interference, i.e., $\mathscr{L}_{I_{\mathrm{agg}}^{\mathrm{U,D}}}(s)$ and $\mathscr{L}_{I_{\mathrm{agg}}^{\mathrm{D,U}}}(s)$, can be characterized by the following two Lemmas.

Lemma 12. *The Laplace transform* $\mathscr{L}_{I_{\mathrm{agg}}^{\mathrm{U,D}}}(s)$ *of the DL-to-UL interference* $I_{\mathrm{agg}}^{\mathrm{U,D}}$*, i.e., the aggregate interference from DL transmitting BS to the UL typical BS, evaluated at* s *can be computed as*

$$\mathscr{L}_{I_{\mathrm{agg}}^{\mathrm{U,D}}}(s)=\exp\left(-2\pi p^{\mathrm{D}}\tilde{\lambda}\int_r^{\infty}\left[\tfrac{1}{1+(sP^{\mathrm{D}}\zeta^{D2U})^{-1}}\right]xdx\right).\tag{81}$$

Proof: By assuming the distance between BSs (x) are larger than the distance from the typical UE to the typical BS (r), (81) is proved. ■

Lemma 13. *The Laplace transform* $\mathscr{L}_{I_{\mathrm{agg}}^{\mathrm{D,U}}}(s)$ *of the UL-to-DL interference* $I_{\mathrm{agg}}^{\mathrm{D,U}}$*, i.e., the aggregate interference from UL transmitting UE to the DL typical UE, evaluated at* s *can be computed as*

$$\mathscr{L}_{I_{\mathrm{agg}}^{\mathrm{D,U}}}(s)=\exp\left(-2\pi p^{\mathrm{U}}\tilde{\lambda}\int_r^{\infty}\left[\tfrac{1}{1+(sP^{\mathrm{U}}\zeta^{U2U})^{-1}}\right]xdx\right).\tag{82}$$

Proof: By assuming the locations of UEs are replaced by their serving BSs, and the

distance between BSs (x) are larger than the distance from the typical UE to the typical BS (r), (82) is proved. ■

Note that the UL performance of dynamic TDD is important because the UL SINR is vulnerable to the DL-to-UL interference [53]. If the DL-to-UL interference is not properly treated, the UL coverage probability of dynamic TDD will suffer from a performance loss compared with static TDD. Therefore we propose a simple full interference cancellation (IC) scheme for the UL of dynamic TDD, which will be addressed in the following Subchapter.

2) Coverage Probability with Interference Cancellation: In this Subchapter, we consider a simple full interference cancellation (IC) scheme to demonstrate the gain with interference mitigation. We assume that for the UL of dynamic TDD, all the DL transmitters with instantaneous interference power above δ can be cancelled at the typical BS.

Lemma 14. *The Laplace transform with IC $\mathscr{L}_{I_{\mathrm{agg}}^{\mathrm{D,U}}}(s)$ of $I_{\mathrm{agg}}^{\mathrm{D,U}}$ evaluated at s can be computed as*

$$\begin{aligned}
&\mathscr{L}_{I_{\mathrm{agg}}^{\mathrm{D,U}}}(s)\\
&=\exp\left(-2\pi p^{\mathrm{D}}\lambda\int_0^{d_1}\left(1-\mathbb{E}\left[\mathit{1}\left(h<\tfrac{\delta}{P^{\mathrm{B}}\zeta^{B2B,L}}\right)\right.\right.\right.\\
&\left.\left.\left.\times\exp\left(-sP^{\mathrm{B}}\zeta^{B2B,L}h\right)\right]\right)\left(1-\tfrac{x}{d_1}\right)xdx\right)\\
&\times\exp\left(-2\pi p^{\mathrm{D}}\lambda\int_0^{d_1}\left(1-\mathbb{E}\left[\mathit{1}\left(h<\tfrac{\delta}{P^{\mathrm{B}}\zeta^{B2B,NL}}\right)\right.\right.\right.\\
&\left.\left.\left.\times\exp\left(-sP^{\mathrm{B}}\zeta^{B2B,NL}h\right)\right]\right)\left(\tfrac{x}{d_1}\right)xdx\right)\\
&\times\exp\left(-2\pi p^{\mathrm{D}}\lambda\int_{d_1}^{\infty}\left(1-\mathbb{E}\left[\mathit{1}\left(h<\tfrac{\delta}{P^{\mathrm{B}}\zeta^{B2B,NL}}\right)\right.\right.\right.\\
&\left.\left.\left.\times\exp\left(-sP^{\mathrm{B}}\zeta^{B2B,NL}h\right)\right]\right)xdx\right),
\end{aligned}\tag{83}$$

where the expectation over h can be derived as

$$\begin{aligned}
&\mathbb{E}\left[\mathit{1}\left(h<\tfrac{\delta}{P^{\mathrm{B}}\zeta^{B2B}}\right)\exp\left(-sP^{\mathrm{B}}\zeta^{B2B}h\right)\right]\\
&=\int_0^{\frac{\delta}{P^{\mathrm{B}}\zeta^{B2B}}}\exp\left(-sP^{\mathrm{B}}\zeta^{B2B}h\right)\exp\left(-h\right)dh\\
&=-\tfrac{1}{sP^{\mathrm{B}}\zeta^{B2B}+1}\left(\exp\left(-\tfrac{\delta\left(sP^{\mathrm{B}}\zeta^{B2B}+1\right)}{P^{\mathrm{B}}\zeta^{B2B}}\right)-1\right).
\end{aligned}\tag{84}$$

Proof: By assuming the fading h of interference is smaller than $\frac{\delta}{P^{\mathrm{B}}\zeta^{\mathrm{B2B}}}$, Lemma 14 is proved. ■

3) Study of A 3GPP Special Case: As a special case for Theorem 11, we consider a path loss function adopted in the 3GPP as [8]

$$\zeta\left(r\right)=\begin{cases}A^{\mathrm{L}}r^{\alpha^{\mathrm{L}}}, & \text{LoS with probability } \mathrm{Pr}^{\mathrm{L}}\left(r\right)\\ A^{\mathrm{NL}}r^{\alpha^{\mathrm{NL}}}, & \text{NLoS with probability } \left(1-\mathrm{Pr}^{\mathrm{L}}\left(r\right)\right)\end{cases}, \tag{85}$$

together with a linear LoS probability function of $\mathrm{P}r^{L}\left(r\right)$, defined in the 3GPP as [8]

$$\mathrm{Pr}^{\mathrm{B2U,L}}\left(r\right)=\mathrm{Pr}^{\mathrm{B2B,L}}\left(r\right)=\begin{cases}1-\frac{r}{d_1}, & 0<r\leq d_1\\ 0, & r>d_1\end{cases}, \tag{86}$$

where d_1 is the cut-off distance of the LoS link.

In addition, a simple LoS probability function for $\mathrm{Pr}^{\mathrm{U2U,L}}\left(r\right)$ is given by [8]

$$\mathrm{Pr}^{\mathrm{U2U,L}}\left(r\right)=\begin{cases}1, & 0<r\leq 50\,\mathrm{m}\\ 0, & r>50\,\mathrm{m}\end{cases}. \tag{87}$$

For the 3GPP special case, according to Theorem 11, $p^{\mathrm{cov},Link}\left(\lambda,\gamma\right)$ can then be computed by

$$p^{\mathrm{cov},Link}\left(\lambda,\gamma\right)=\sum_{n=1}^{2}\left(T_n^{\mathrm{L},Link}+T_n^{\mathrm{NL},Link}\right). \tag{88}$$

The details of the DL/UL results of $T_1^{\mathrm{L},Link}$, $T_1^{\mathrm{NL},Link}$, $T_2^{\mathrm{L},Link}$, and $T_2^{\mathrm{NL},Link}$ are investigated in Appendix H and Appendix I respectively.

D. Simulation Results

In this Subchapter, we present numerical results to validate the accuracy of our analysis. In our simulation, we adopt the following parameters recommended by the 3GPP [8]. In (53), $N=2$ and for $n\in\{1,2\}$, $A_n^{\mathrm{B2U,L}}=10^{-10.38}$, $A_n^{\mathrm{B2U,NL}}=10^{-14.54}$, $A_n^{\mathrm{B2B,L}}=10^{-9.84}$, $A_n^{\mathrm{B2B,NL}}=10^{-16.94}$, $A_n^{\mathrm{U2U,L}}=10^{-9.85}$, $A_n^{\mathrm{U2U,NL}}=10^{-17.58}$, $\alpha_n^{\mathrm{B2U,L}}=2.09$, $\alpha_n^{\mathrm{B2U,NL}}=3.75$, $\alpha_n^{\mathrm{B2B,L}}=2$, $\alpha_n^{\mathrm{B2B,NL}}=4$, $\alpha_n^{\mathrm{U2U,L}}=2$, $\alpha_n^{\mathrm{U2U,NL}}=4$.

Besides, according to [8], the power values are set to: $P_{\mathrm{N}}^{\mathrm{D}}=-95$ dBm, $P_{\mathrm{N}}^{\mathrm{U}}=-91$ dBm, $P^{\mathrm{D}}=24$ dBm, and $P^{\mathrm{U}}=23\,\mathrm{dBm}$ [8]. In addition, the UE density is set to $\rho=$

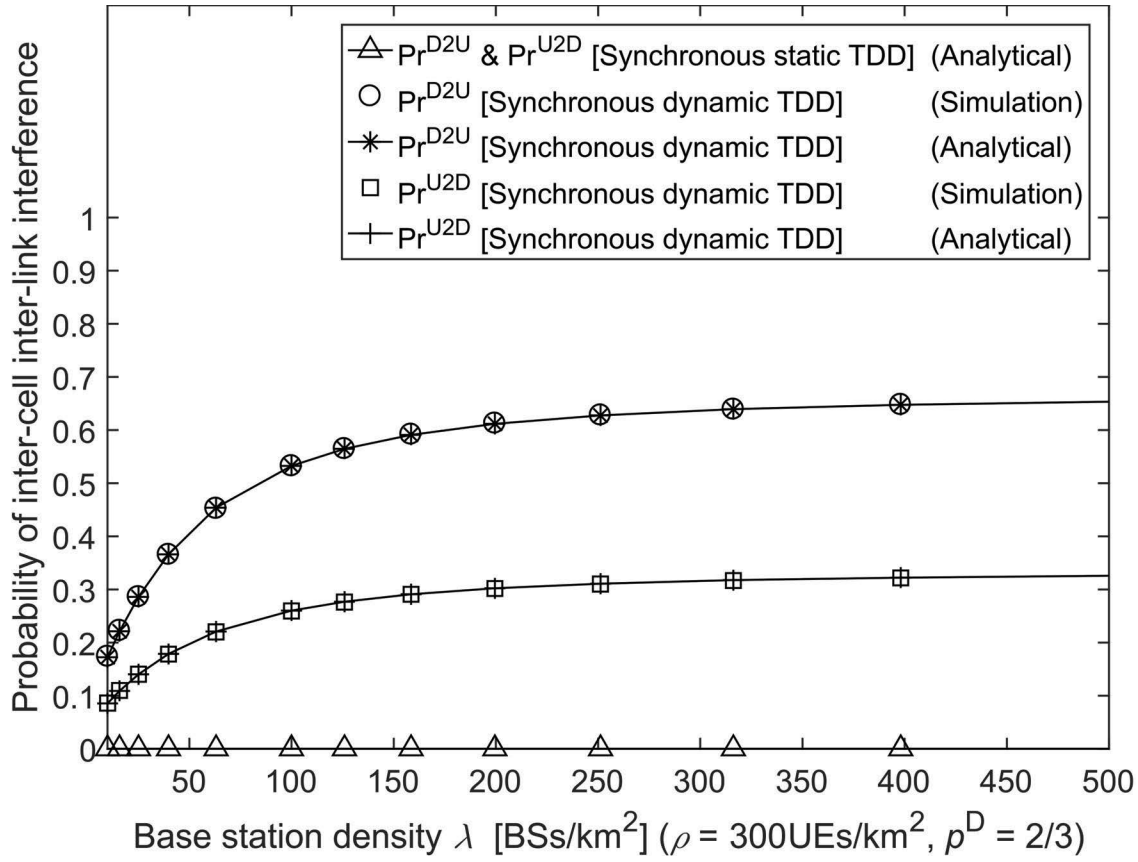

Fig. 10. The probability of inter-cell inter-link interference.

$300\,\text{UEs/km}^2$, which leads to $q = 4.05$ in (60) [46]. Finally, we assume that $\gamma = 1$, $p^{\mathrm{D}} = \frac{2}{3}$ and $T = 10$. Thus, for static TDD, we have $N_0^{\mathrm{D}} = 7$ and $N_0^{\mathrm{U}} = 3$ in (72), which achieves the best match with p^{D} and p^{U}, according to (66).

1) Validation of the Results on the Probabilities of Inter-Cell Inter-Link Interference: The analytical and simulation results of $\mathrm{Pr}^{\mathrm{D2U}}$ and $\mathrm{Pr}^{\mathrm{U2D}}$ are plotted in Fig. 10. From this figure, we can draw the following observations:

- The analytical and simulation results match well, which validates the accuracy of our analysis.
- For static TDD, $\mathrm{Pr}^{\mathrm{D2U}}$ and $\mathrm{Pr}^{\mathrm{U2D}}$ are zeros.
- For dynamic TDD in the synchronous case, as the BS density λ increases, $\mathrm{Pr}^{\mathrm{D2U}}$ and $\mathrm{Pr}^{\mathrm{U2D}}$ gradually grow and converge to the results of dynamic TDD in the asynchronous case. This is because:
  - when λ increases, the UE number in each active BS decreases; and

– hence, when λ is high enough to reach the limit of one UE per active BS, all the subframes will be used as either DL ones or UL ones, the probability of which solely depends on p^{D} or p^{U}.

2) Validation of the Results on the Time Resource Utilization: The analytical and simulation results of κ^{D} and κ^{U} are plotted in Fig. 11. From this figure, we can see that:

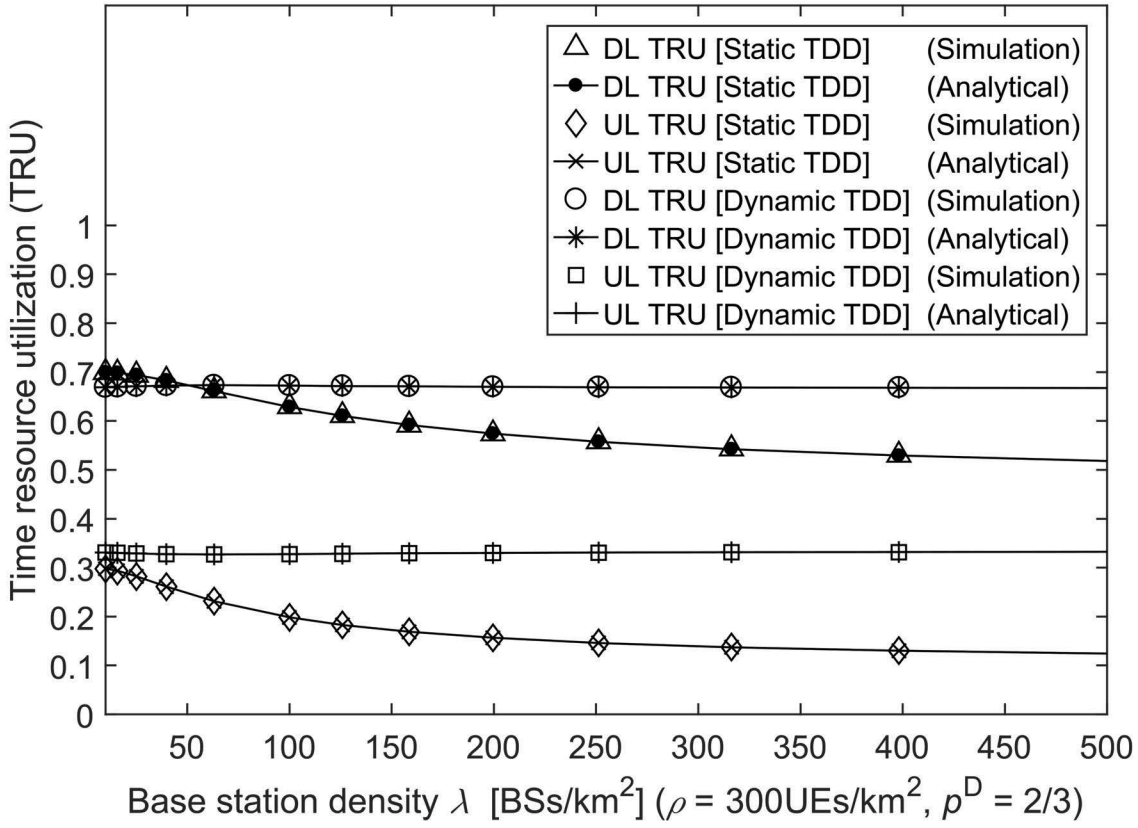

Fig. 11. The average DL/UL TRU κ^{D} and κ^{U}.

- For static TDD, κ^{D} starts from 0.7 and decreases as λ increases. This is because $N_0^{\mathrm{D}} = 7$ and $T = 10$, and thus static TDD maintains $N_0^{\mathrm{U}} = 3$ UL subframes even if there is no UL data request in a BS, leading to a large time resource waste. Moreover, the sum of κ^{D} and κ^{U} is much less than one when λ is large, e.g., $\lambda = 500\,\mathrm{BSs/km}^2$, showing the inefficiency of static TDD in dense SCNs.
- For dynamic TDD, κ^{D} converges to $p^{\mathrm{D}} = \frac{2}{3}$ as λ increases. This is because when λ is high enough to reach the limit of one UE per active BS, all the subframes will be used as DL ones with a probability of p^{D}. Moreover, the sum of κ^{D} and κ^{U} always

equals to one, thanks to the dynamic adaption of DL/UL subframes to DL/UL data requests.

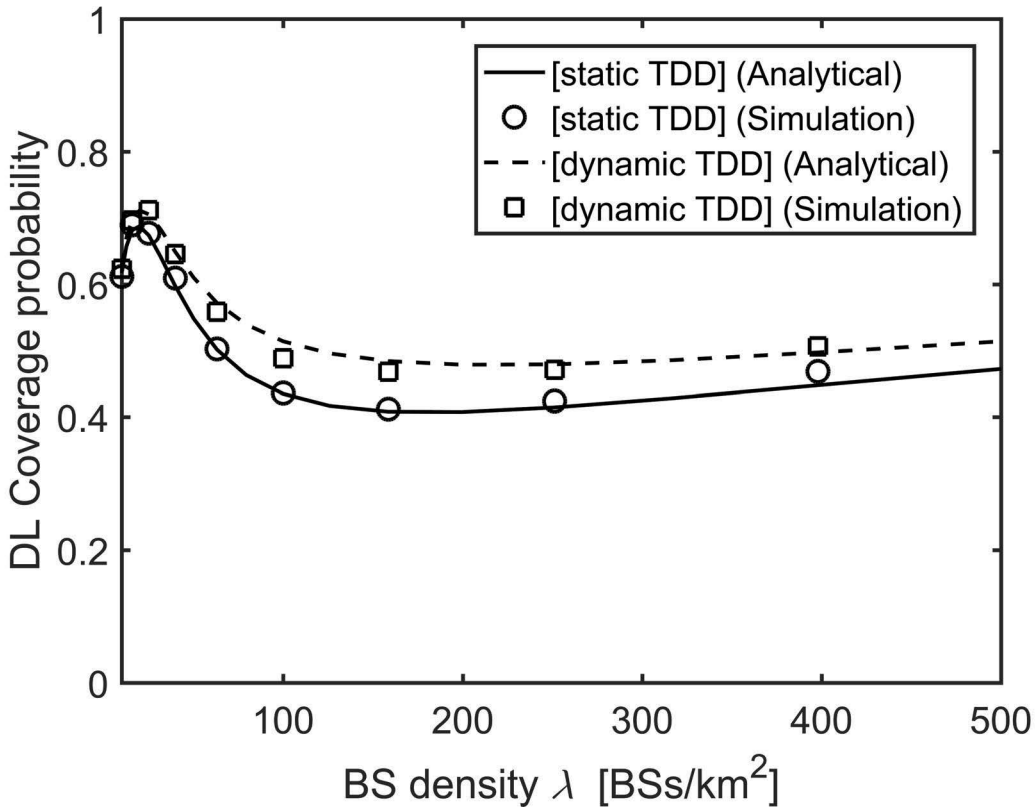

Fig. 12. The DL coverage probability $p^{\mathrm{cov,D}}(\lambda,\gamma)$ vs. the BS density λ with SINR threshold $\gamma = 0\,\mathrm{dB}$.

3) Validation of the Analytical Results of $p^{\mathrm{cov},Link}(\lambda,\gamma)$: In the case of the linear 3GPP path loss model as proposed in Subchapter IV-C3, the results of $p^{\mathrm{cov,D}}(\lambda,\gamma)$ and $p^{\mathrm{cov,U}}(\lambda,\gamma)$ against the BS density for $\gamma = 0$ dB are plotted in Fig. 12 and Fig. 13 respectively. Note that our analytical results on $\mathrm{Pr}^{\mathrm{D2U}}$ and $\mathrm{Pr}^{\mathrm{U2D}}$ are used for the simulation of $I^{\mathrm{D}}_{\mathrm{agg}}$ and $I^{\mathrm{U}}_{\mathrm{agg}}$ in (57). As can be observed from Fig. 12 and Fig. 13, our analytical results with the assumptions in Lemma 12 and Lemma 13 match the simulation results well, and thus we will only use analytical results of $p^{\mathrm{cov},Link}(\lambda,\gamma)$ in our discussion hereafter.

From Fig. 12, we can observe that:

- For static TDD, when considering both LoS and NLoS transmissions, the DL coverage probability shows a complicated performance trend. The details are described as

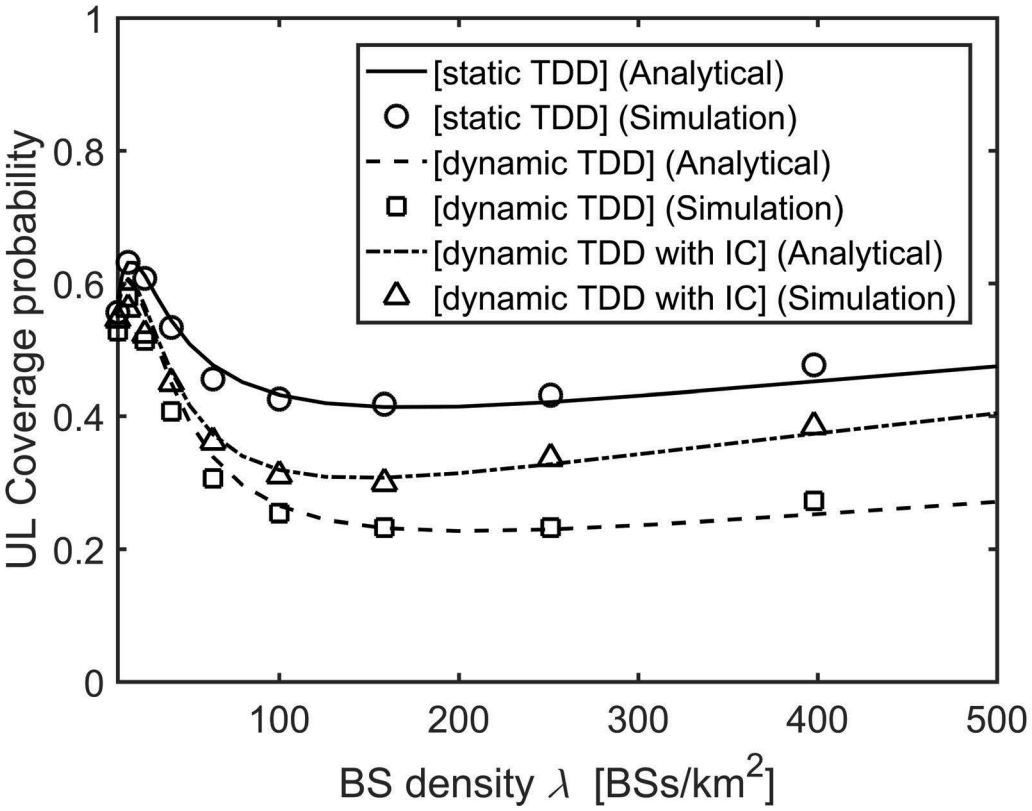

Fig. 13. The UL coverage probability $p^{\mathrm{cov,U}}(\lambda,\gamma)$ vs. the BS density λ with SINR threshold $\gamma = 0\,\mathrm{dB}$.

follows:

- When the SCN is sparse and thus noise-limited, the DL coverage probability of static TDD given by the proposed analysis grows as λ increases.
- However, when the network is dense enough, the DL coverage probability decreases as λ increases, due to the transition of a large number of interference paths from NLoS to LoS. Particularly, during this region, interference increases at a faster rate than the signal due to the transition from mostly NLoS interference to LoS interference, thereby causing a drop in the SINR hence the coverage probability.
- In more detail, the coverage probability given by the proposed analysis peaks at a certain density λ_0. When λ is further increased far above λ_0, the coverage probability decreases at a slower pace because both the signal power and the

interference power are LoS dominated and increase at approximately the same rate. There are still more and more interferers whose signal reach the typical BS via LoS paths but their effect is smaller than the dominating interferers.

  - At last, the coverage probability picks up the increasing speed because the number of interferers is limited by the UE density ρ.

- For dynamic TDD, the DL coverage probability presents a similar behavior compared to the static TDD. Note that the DL coverage probability of dynamic TDD performs better than the static TDD, due to part of the strong DL interference becomes weak UL interference in the scenario of DL of dynamic TDD.

From Fig. 13, we can observe that:

- On one hand, when considering both LoS and NLoS transmissions, the UL coverage probability of dynamic TDD presents a similar behavior compared to the static TDD, due to the similar reason as the DL.
- On the other hand, the UL coverage probability of dynamic TDD performs worse than the static TDD, due to part of the weak UL interference becomes strong DL interference in the scenario of UL of dynamic TDD. Therefore it is necessary to apply the interference cancellation (IC) scheme to the UL of dynamic TDD. With the IC proposed in subsec IV-C2, the UL coverage probability of dynamic TDD is enhanced, although still poorer than the static TDD.

However, from Fig. 13, we should not conclude that for the UL dynamic TDD exhibits no significant performance gain compared with static TDD due to the detrimental DL-to-UL interference. Instead, we need to investigate the ASE performance, which includes the time resource utilization and is shown in the following Subchapter.

4) The ASE Performance: From Fig. 14, we can conclude that:

- For static TDD, the DL ASE also shows a complicated performance trend. The details are described as follows:
  - When the SCN is sparse and thus noise-limited, the DL ASE of static TDD given by the proposed analysis grows as λ increases.

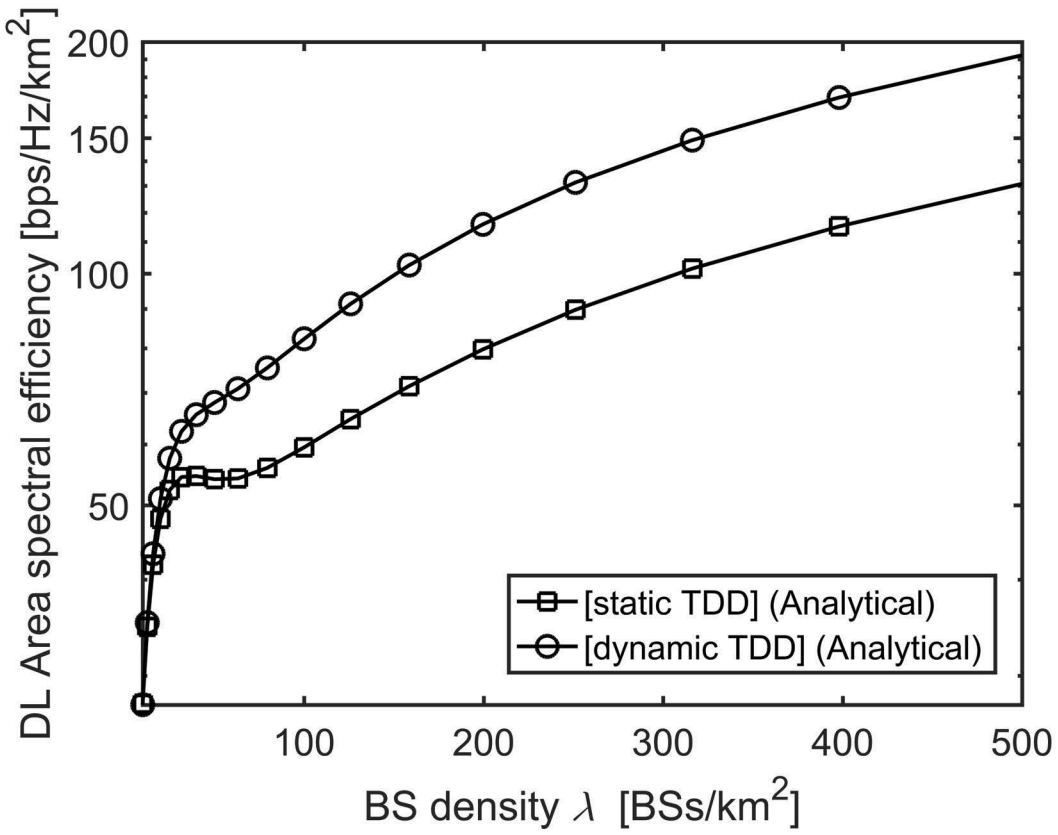

Fig. 14. DL area spectral efficiency $ASE^{\mathrm{D}}(\lambda, \gamma_0)$ vs. the BS density λ with SINR threshold $\gamma_0 = 0$ dB.

  - However, when the network is dense enough, the DL ASE decreases as λ increases, due to the decrease of coverage probability and TRU.
  - When λ is further increased, the DL ASE picks up the increasing speed, because the increasing effect of active BS density and coverage probability is stronger than the decreasing effect of TRU.

- For dynamic TDD, the details of the behavior of the DL ASE are described as follows:
  - When the SCN is sparse and thus noise-limited, the DL ASE grows as λ increases. When the network is dense enough, the DL ASE increases at a slower rate as λ increases, due to the decrease of coverage probability. Note that the effect of the decrease of coverage probability is weaker than the increase of active BS density, as a result, the DL ASE of dynamic TDD keeps increasing and doesn't present decrease. When λ is further increased, the DL ASE slightly picks up the

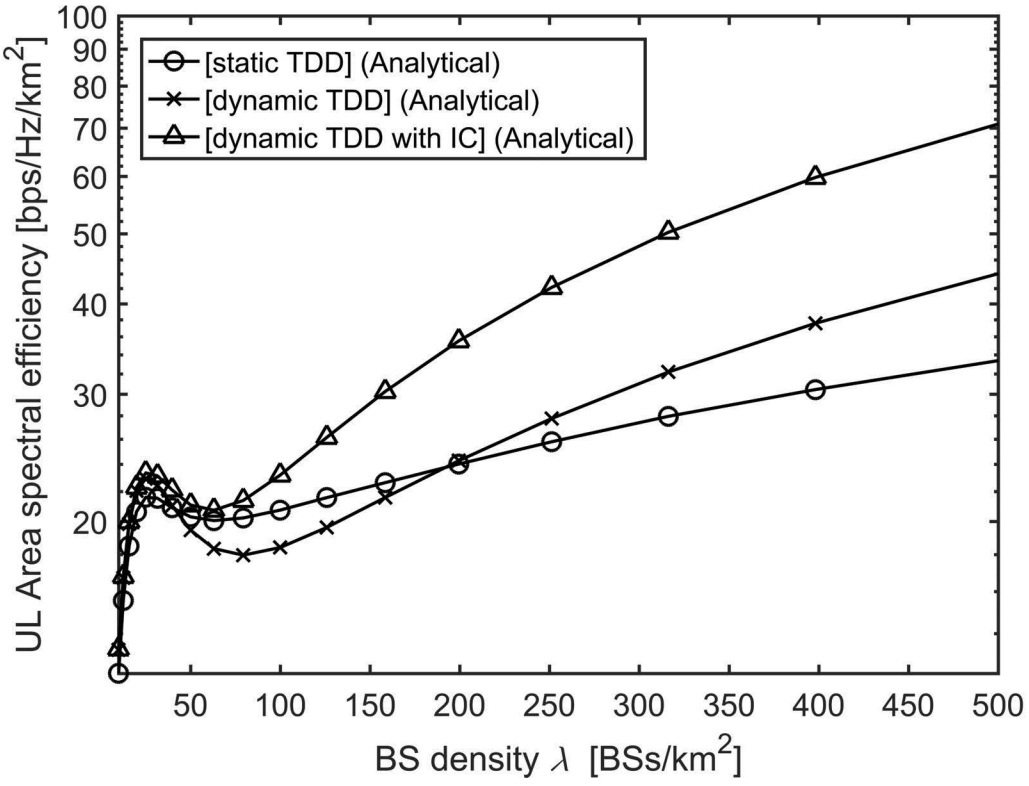

Fig. 15. UL area spectral efficiency $ASE^{\mathrm{U}}(\lambda, \gamma_0)$ vs. the BS density λ with SINR threshold $\gamma_0 = 0$ dB.

increasing speed and increases almost linearly as λ increases.

– The DL ASE exhibits performance gain compared with static TDD due to the beneficial UL-to-DL interference and the TRU gain, especially for 5G dense SCNs [1], i.e., $\lambda > 100\,\mathrm{BSs/km}^2$.

From Fig. 15, we can conclude that:

- The UL ASE of dynamic TDD presents a similar behavior compared to static TDD, due to the similar reason as the DL.
- The UL performance is important because the UL SINR is vulnerable to the DL-to-UL interference [53]. If the DL-to-UL interference is not properly treated, the UL ASE of dynamic TDD will suffer from a performance loss compared with static TDD, for the BS density range of $30 < \lambda < 200\,\mathrm{BSs/km}^2$.
- To mitigate such interference, we investigate the effectiveness of the full interference cancellation (IC), which removes all DL-to-UL interfering signals based on instan-

taneous DL-to-UL interference power. As discussed in Subchapter IV-C2, the IC threshold is set as $\delta = -50$ dBm. Note that the results of full IC, i.e., cancelling a subset of interferers, would be ideal. The analysis of other interference mitigation methods, e.g., clustering, UL power boosting, etc., is left as possible future work.

- Dynamic TDD with IC can achieve larger ASE in the UL compared with static TDD, mainly due to the dynamic adaption of DL/UL subframes to DL/UL data requests. The performance gain of dynamic TDD with IC in the UL is larger as the BS density λ increases. When $\lambda = 500\,\text{BSs/km}^2$, the UL ASE of static TDD and that of dynamic TDD with full IC are around $30\,\text{bps/Hz/km}^2$ and $70\,\text{bps/Hz/km}^2$, respectively.

E. Conclusion

In this Chapter, we have investigated the impact of synchronous dynamic TDD in the performance of the DL/UL of dense SCNs. Analytical results are obtained for the DL/UL TRU, coverage probability and ASE. Specifically, we find that

- The DL/UL TRU varies across TDD subframes, and that of dynamic TDD can achieve an increasingly higher average total TRU than static TDD with the network densification of up to $75.4\,\%$.
- With the beneficial UL-to-DL interference and MAC layer gain, dynamic TDD can achieve an increasingly higher average DL ASE than static TDD with the network densification of up to $50\,\%$.
- With the MAC layer gain and proper IC, dynamic TDD can achieve an increasingly higher average UL ASE than static TDD with the network densification of up to $100\,\%$.

As our future work, we will consider other factors of realistic networks in the theoretical analysis for SCNs, such as the introduction of Rician fading or Nakagami fading, because the multi-path fading model is also affected by the LoS and NLoS transmissions.

V. Performance Analysis of Dense SCNs with Full Duplex

In this Chapter, the performance analysis of dense SCNs with full duplex is presented.

A. System Model

1) Network Scenario: In this Subchapter, we present the network scenario considered in the Thesis. Note that in this research we only focus on the MAC layer performance analysis, and the considered network scenario is used to derive the distribution of the UE number in an active BS, which will be shown in Subchapter V-B1. The PHY layer performance analysis will be left as our future work.

We consider a cellular network with BSs deployed on a plane according to a homogeneous Poisson point process (HPPP) Φ with a density of λ BSs/km^2. Active UEs are also Poisson distributed in the considered network with a density of ρ UEs/km^2. Here, we only consider active UEs in the network because non-active UEs do not trigger data transmission, and thus they are ignored in our analysis.

In practice, a BS will mute its transmission if there is no UE connected to it, which reduces inter-cell interference and energy consumption [46]. Note that such BS idle mode operation is not trivial, which even changes the capacity scaling law [55]. Since UEs are randomly and uniformly distributed in the network, we assume that the active BSs also follow an HPPP distribution $\tilde{\Phi}$ [47], the density of which is denoted by $\tilde{\lambda}$ BSs/km^2. Note that $0 \leq \tilde{\lambda} \leq \lambda$, and a larger ρ leads to a larger $\tilde{\lambda}$. From [47], [48], $\tilde{\lambda}$ is given by $\tilde{\lambda} = \lambda \left[1 - \frac{1}{\left(1+\frac{\rho}{q\lambda}\right)^q}\right]$, where q takes an empirical value around 3.5~4 [47], [48].

2) BS Mode Selection: In this Subchapter, we introduce the scheme of BS mode selection with FD. We consider a realistic SCN scenario with a hybrid of FD BSs and FD/HD UEs, where all the SBSs are capable of FD communications, and the UEs are composed of a coexistence of both FD UEs and HD UEs. The active UEs may request FD, HD-DL or HD-UL type of data, and the serving BSs select mode according to the real-time DL/UL traffic. For the considered network with a hybrid of FD BSs and FD/HD UEs, we have the following three remarks.

Remark 1: For an active FD UE (FU), it may not always request FD data. When a FD UE requests DL or UL data, it can be deemed as a HD UE.

Remark 2: For an active HD UE (HU), it can also request FD data, where it demands both DL and UL data simultaneously. Since the HD UE is not capable of FD communications, it may be scheduled with another FD-HU, DL or UL data for FD communications. If there is only one active UE in the cell, and the active UE is a HD UE requesting FD data, the HU is assumed to have priority of DL communications.

Remark 3: For an active BS, it can work in FD mode only if there exists at least one FD UE requesting FD data, or there exists at least one DL-UL data pair. The DL-UL data pair is formed by one DL data request and one UL data request, or by one FD data request from a HD UE and one DL/UL data request. Otherwise the active BS will work in HD mode.

We define the four BS working modes as follows.

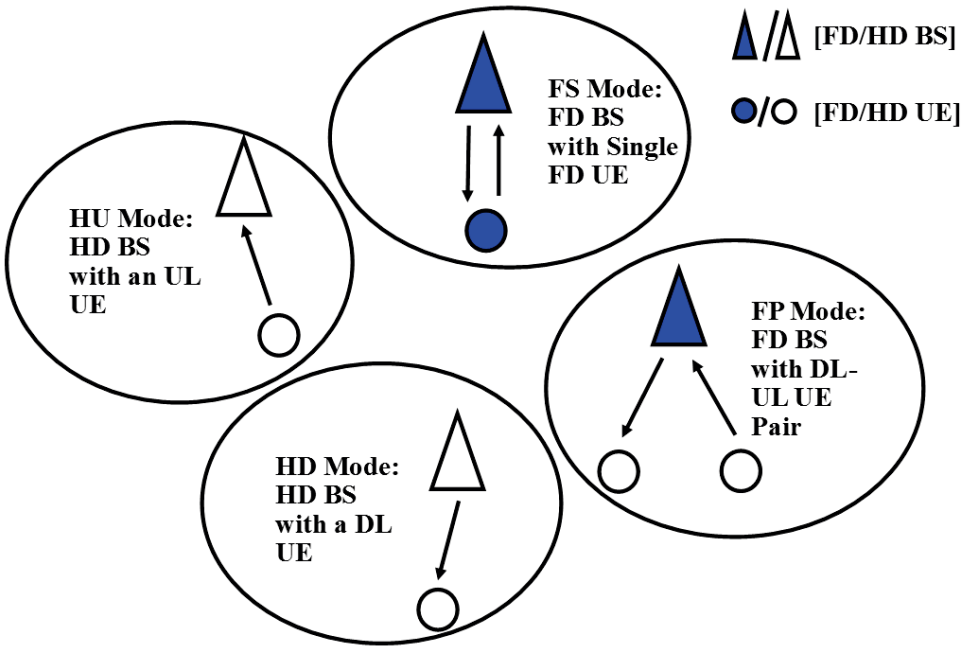

Fig. 16. A sketch of the four BS working modes.

1) FD BS with Single FD UE (FS): For an active BS, it will work in FS mode if there exists at least one FD UE requesting FD data. Note that we assume the FU requesting FD data has priority over the DL-UL data pair.
2) FD BS with DL-UL UE Pair (FP): For an active BS, it will work in FP mode if there exists at least one DL-UL data pair, and there is no FU requesting FD data.
3) HD BS with a DL UE (HD): For an active BS, it will work in HD mode if there only exists DL data; or there is only one active UE in the cell, and the active UE is a HD UE requesting FD data, as stated in **Remark 2**.
4) HD BS with an UL UE (HU): For an active BS, it will work in HU mode if there only exists UL data.

A sketch of the four BS working modes is shown in Fig. 16. Note that in this research we focus on the MAC layer performance analysis. Therefore the modelling and analysis of the PHY layer interference will be left as our future work.

3) Performance Metrics: The propotions of FD UE and HD UE are denoted as p^{FU} and p^{HU} respectively, where $p^{\mathrm{FU}} + p^{\mathrm{HU}} = 1$. For each active FD UE, the probabilities of requesting FD data, DL data and UL data are respectively denoted by p^{FF}, p^{DF} and p^{UF}, where $p^{\mathrm{FF}} + p^{\mathrm{DF}} + p^{\mathrm{UF}} = 1$. For each active HD UE, the probabilities of requesting DL data and UL data are respectively denoted by p^{FH}, p^{DH} and p^{UH}, where $p^{\mathrm{FH}} + p^{\mathrm{DH}} + p^{\mathrm{UH}} = 1$.

We denote the working mode of an active BS by a string variable Q, where Q takes the value of 'FS', 'FP', 'HD' and 'HU'. For clarity, 'FS', 'FP', 'HD' and 'HU' denote the FD mode with single UE, FD mode with a UE pair, HD DL mode and HD UL mode respectively. The probability of an active BS selecting the mode of Q are denoted by q^Q. In the following Subchapters, we will investigate the performance of q^Q. The notation of variables is summarized in Table IV.

B. Main Results of MAC Layer Analysis

1) The Distribution of the UE Number in an Active BS: Considering both active BSs and inactive BSs, the coverage area size X can be characterized by a Gamma distribution [47].

TABLE IV
NOTATION OF VARIABLES FOR FD

Notation	Items
p^{FU}, p^{HU}	FD UE and HD UE ratios
p^{FF}, p^{DF}, p^{UF}	FD data, HD-DL data and HD-UL data request probabilities of FD UE
p^{FH}, p^{DH}, p^{UH}	FD data, HD-DL data and HD-UL data request probabilities of HD UE
q^{FS}	The probability of an active BS selecting the FD mode with single UE
q^{FP}	The probability of an active BS selecting the FD mode with a UE pair
q^{HD}	The probability of an active BS selecting the HD DL mode
q^{HU}	The probability of an active BS selecting the HD UL mode

Thus, the PDF of X can be expressed by

$$f_X(x) = (q\lambda)^q \, x^{q-1} \frac{\exp(-q\lambda x)}{\Gamma(q)}, \tag{89}$$

where q is a distribution parameter and $\Gamma(\cdot)$ is the Gamma function [52].

Then, we denote the UE number per BS by a random variable (RV) K, and the probability mass function (PMF) of K can be derived as

$$\begin{aligned} f_K(k) &= \Pr[K = k] \\ &\overset{(a)}{=} \int_0^{+\infty} \frac{(\rho x)^k}{k!} \exp(-\rho x) f_X(x) dx \\ &\overset{(b)}{=} \frac{\Gamma(k+q)}{\Gamma(k+1)\Gamma(q)} \left(\frac{\rho}{\rho + q\lambda}\right)^k \left(\frac{q\lambda}{\rho + q\lambda}\right)^q, \end{aligned} \tag{90}$$

where (a) is due to the HPPP distribution of UEs and (b) is obtained from (89). It can be seen from (90) that K follows a Negative Binomial distribution [52], i.e., $K \sim \mathrm{NB}\left(q, \frac{\rho}{\rho+q\lambda}\right)$.

As discussed in Subchapter V-A1, we assume that a BS with $K = 0$ is not active, which will be ignored in our analysis due to its muted transmission. Hence, we focus on the active BSs and further study the distribution of the UE number in an active BS. For clarity, the UE number in an active BS is denoted by a positive RV $\tilde{K}$. Considering (90) and the

fact that the only difference between K and $\tilde{K}$ lies in $\tilde{K} \neq 0$, we can conclude that $\tilde{K}$ should follow a truncated Negative Binomial distribution, i.e., $\tilde{K} \sim \text{truncNB}\left(q, \frac{\rho}{\rho+q\lambda}\right)$. More specifically, the PMF of $\tilde{K}$ is denoted by $f_{\tilde{K}}\left(\tilde{k}\right), \tilde{k} \in \{1, 2, \ldots, +\infty\}$, and it is given by

$$f_{\tilde{K}}\left(\tilde{k}\right) = \Pr\left[\tilde{K} = \tilde{k}\right] = \frac{f_K\left(\tilde{k}\right)}{1 - f_K\left(0\right)}, \tag{91}$$

where the denominator $(1 - f_K(0))$ represents the probability of a BS being active. Note that based on the definition of $\tilde{\lambda}$ in Subchapter V-A1, we have $(1 - f_K(0)) = \frac{\tilde{\lambda}}{\lambda}$.

2) The Distribution of the Data Request Number in an Active BS: A Multinomial Distribution: After obtaining $f_{\tilde{K}}\left(\tilde{k}\right)$, we need to further study the distribution of the data request number in an active BS, so that the working mode of the BS can be determined in a FD network.

For clarity, the FD-FU, FD-HU, HD-DL and HD-UL data request numbers in an active BS are denoted by RVs M^{FFU}, M^{FHU}, M^{D} and M^{U}, respectively. Since we assume that each UE generates one request of FD data, DL data or UL data, it is easy to show that

$$M^{\mathrm{FF}} + M^{\mathrm{FH}} + M^{\mathrm{D}} + M^{\mathrm{U}} = \tilde{K}. \tag{92}$$

For each FD/HD UE in an active BS, the probability of it requesting FD data, DL data and UL data is p^{FF}/p^{FH}, p^{DF}/p^{DH} and p^{UF}/p^{UH}, respectively. Therefore, for a given p^{FU}, for each UE in an active BS, the probability of it requesting FD-FU data, FD-HU data, DL data and UL data is p^{FFU}, p^{FHU}, p^{D} and p^{U}, respectively, where $p^{\mathrm{FFU}} = p^{\mathrm{FU}}p^{\mathrm{FF}}$, $p^{\mathrm{FHU}} = p^{\mathrm{HU}}p^{\mathrm{FH}}$, $p^{\mathrm{D}} = p^{\mathrm{FU}}p^{\mathrm{DF}} + p^{\mathrm{HU}}p^{\mathrm{DH}}$ and $p^{\mathrm{U}} = p^{\mathrm{FU}}p^{\mathrm{UF}} + p^{\mathrm{HU}}p^{\mathrm{UH}}$. Hence, for a given UE number $\tilde{k}$, M^{FFU}, M^{FHU}, M^{D} and M^{U} follow multinomial distributions, i.e., $M^{\mathrm{FFU}}, M^{\mathrm{FHU}}, M^{\mathrm{D}}, M^{\mathrm{U}} \sim \mathrm{M}\left(\tilde{k}, p^{\mathrm{FFU}}, p^{\mathrm{FHU}}, p^{\mathrm{D}}, p^{\mathrm{U}}\right)$. More specifically, the PMF of M^{FFU}, M^{FHU}, M^{D} and M^{U} can be written as

$$\begin{aligned} &f_{M^{\mathrm{FFU}},M^{\mathrm{FHU}},M^{\mathrm{D}},M^{\mathrm{U}}}\left(m^{\mathrm{FFU}}, m^{\mathrm{FHU}}, m^{\mathrm{D}}, m^{\mathrm{U}}\right) \\ &= \tfrac{\tilde{k}!}{m^{\mathrm{FFU}}!m^{\mathrm{FHU}}!m^{\mathrm{D}}!m^{\mathrm{U}}!} \\ &\times \left(p^{\mathrm{FFU}}\right)^{m^{\mathrm{FFU}}} \left(p^{\mathrm{FHU}}\right)^{m^{\mathrm{FHU}}} \left(p^{\mathrm{D}}\right)^{m^{\mathrm{D}}} \left(p^{\mathrm{U}}\right)^{m^{\mathrm{U}}}. \end{aligned} \tag{93}$$

3) The Distribution of the Mode Selection in an Active BS: After obtaining the PMF of the DL/UL data request number in an active BS, we can further derive the distribution of the mode selection in an active BS, i.e., q^Q. In this Subchapter, we present our main results on q^Q in Theorem 15 - 18.

Theorem 15. *The probability of an active BS selecting the FS mode is given by*

$$q^{\mathrm{FS}} = \sum_{\tilde{k}=1}^{+\infty} \left(1 - \left(1 - p^{\mathrm{FFU}}\right)^{\tilde{k}}\right) f_{\tilde{K}}\left(\tilde{k}\right), \tag{94}$$

where $f_{\tilde{K}}\left(\tilde{k}\right)$ *is given by (91).*

Proof: Conditioned on $\tilde{K} = \tilde{k}$, $q_{\tilde{k}}^{\mathrm{FS}} = 1 - f_{M^{\mathrm{FFU}},M^{\mathrm{FHU}},M^{\mathrm{D}},M^{\mathrm{U}}}\left(0, m^{\mathrm{FHU}}, m^{\mathrm{D}}, m^{\mathrm{U}}\right) = 1 - \left(1 - p^{\mathrm{FFU}}\right)^{\tilde{k}}$. The unconditional probability is $q^{\mathrm{FS}} = \sum_{\tilde{k}=1}^{+\infty} q_{\tilde{k}}^{\mathrm{FS}} f_{\tilde{K}}\left(\tilde{k}\right)$. ■

Theorem 16. *The probability of an active BS selecting the FP mode is given by*

$$q^{\mathrm{FP}} = \begin{cases} 0 & \tilde{k} = 1 \\ \sum_{\tilde{k}=2}^{+\infty} \left(\left(1 - p^{\mathrm{FFU}}\right)^{\tilde{k}} - \left(p^{\mathrm{D}}\right)^{\tilde{k}} - \left(p^{\mathrm{U}}\right)^{\tilde{k}}\right) f_{\tilde{K}}\left(\tilde{k}\right) & \tilde{k} > 1 \end{cases}, \tag{95}$$

where $f_{\tilde{K}}\left(\tilde{k}\right)$ *is given by (91).*

Proof: Conditioned on $\tilde{K} = \tilde{k}$, for $\tilde{k} = 1$, $q^{\mathrm{FP}} = 0$ because there is only one active UE in the cell and it is impossible for the active BS to find a UE pair for FD communications. For $\tilde{k} > 1$, the probability of the active BS selecting FD mode is given by

$$\begin{aligned} & q_{\tilde{k}}^{\mathrm{FS}} + q_{\tilde{k}}^{\mathrm{FP}} \\ & = 1 - f_{M^{\mathrm{FFU}},M^{\mathrm{FHU}},M^{\mathrm{D}},M^{\mathrm{U}}}\left(m^{\mathrm{FFU}}, m^{\mathrm{FHU}}, \tilde{k}, m^{\mathrm{U}}\right) \\ & - f_{M^{\mathrm{FFU}},M^{\mathrm{FHU}},M^{\mathrm{D}},M^{\mathrm{U}}}\left(m^{\mathrm{FFU}}, m^{\mathrm{FHU}}, m^{\mathrm{D}}, \tilde{k}\right) \\ & = 1 - \left(p^{\mathrm{D}}\right)^{\tilde{k}} - \left(p^{\mathrm{U}}\right)^{\tilde{k}}. \end{aligned} \tag{96}$$

The unconditional probability is

$$\begin{aligned} & q^{\mathrm{FS}}+q^{\mathrm{FP}} \\ & =\sum_{\tilde{k}=2}^{+\infty}\left(q_{\tilde{k}}^{\mathrm{FS}}+q_{\tilde{k}}^{\mathrm{FP}}\right) f_{\tilde{K}}\left(\tilde{k}\right) \\ & =\sum_{\tilde{k}=2}^{+\infty}\left(1-\left(p^{\mathrm{D}}\right)^{\tilde{k}}-\left(p^{\mathrm{U}}\right)^{\tilde{k}}\right) f_{\tilde{K}}\left(\tilde{k}\right). \end{aligned} \tag{97}$$

Plugging q^{FS} given by (94) into (97) we can derive (95). ■

Theorem 17. *The probability of an active BS selecting the HD mode is given by*

$$q^{\mathrm{HD}}=\begin{cases} p^{\mathrm{FHU}}+p^{\mathrm{D}} & \tilde{k}=1 \\ \sum_{\tilde{k}=2}^{+\infty}\left(\left(p^{\mathrm{D}}\right)^{\tilde{k}}\right) f_{\tilde{K}}\left(\tilde{k}\right) & \tilde{k}>1 \end{cases}, \tag{98}$$

where $f_{\tilde{K}}\left(\tilde{k}\right)$ *is given by (91).*

Proof: Considering the definition of HD mode in Subchapter V-A2, the proof is straightforward. ■

Theorem 18. *The probability of an active BS selecting the HU mode is given by*

$$q^{\mathrm{HU}}=\sum_{\tilde{k}=1}^{+\infty}\left(\left(p^{\mathrm{U}}\right)^{\tilde{k}}\right) f_{\tilde{K}}\left(\tilde{k}\right), \tag{99}$$

where $f_{\tilde{K}}\left(\tilde{k}\right)$ *is given by (91).*

Proof: Considering the definition of HU mode in Subchapter V-A2, the proof is straightforward. ■

C. Simulation and Discussion

In this Subchapter, we present numerical results to validate the accuracy of our analysis and investigate the performance impact of different parameters.

1) Validation of the Results on the MAC Layer Analysis: In Fig. 17, we plot the analytical and simulation results of the full duplex BS ratio, i.e., the sum of q^{FS} and q^{FP}. The UE density is set to $\rho=300\,\mathrm{UEs/km}^2$, which leads to $q=4.05$ in (89) [46]. In addition, we assume that $p^{\mathrm{FF}}=p^{\mathrm{FH}}=\frac{1}{4}$, $p^{\mathrm{DF}}=p^{\mathrm{DH}}=\frac{1}{2}$, and $p^{\mathrm{UF}}=p^{\mathrm{UH}}=\frac{1}{4}$. Note that our analytical

results in this research can work with any value of the MAC layer parameters. From this

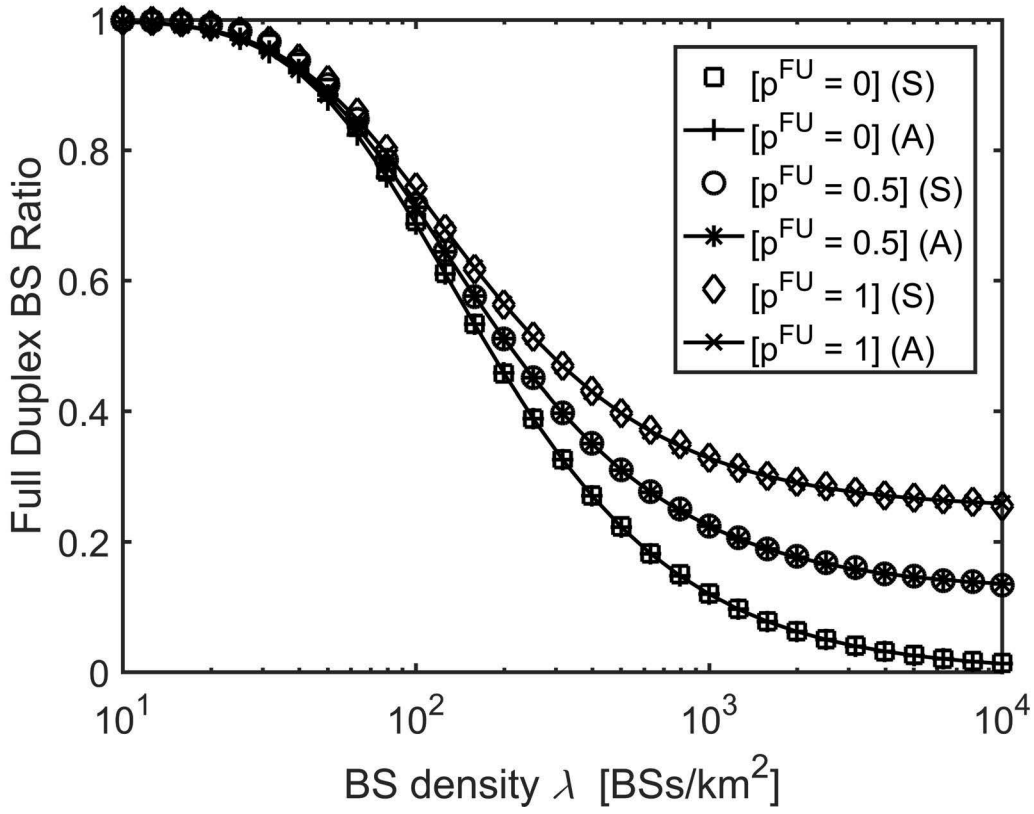

Fig. 17. The full duplex BS ratio.

figure, we can see that:

- The analytical results of the full duplex BS ratio match well with the simulation results.
- The FD BS ratio increases with the increase of the FD UE ratio.
- The FD BS ratio decreases with the increase of the BS density. This is because higher BS density leads to lower UE number per active BS, thus the probability of FD traffic existing decreases.

Since our analytical results match the simulation results well, we will only use analytical results of the FD BS ratio in our discussion hereafter.

2) Discussion of the Performance Impact of FD UE Ratio p^{FU}: In Fig. 18, we plot the results of the FD BS ratio against the FD UE Ratio p^{FU}. The BS density is set to $\lambda = 300\,\mathrm{BSs/km^2}$ and the UE density is set to $\rho = 300\,\mathrm{UEs/km^2}$. In addition, we assume that $p^{\mathrm{FF}} = p^{\mathrm{FH}} = \frac{1}{4}$, $p^{\mathrm{DF}} = p^{\mathrm{DH}} = \frac{1}{2}$, and $p^{\mathrm{UF}} = p^{\mathrm{UH}} = \frac{1}{4}$. As can be observed from

Fig. 18, the FD BS ratio increases linearly with the increase of p^{FU}, and thus we may expect a linear gain in the MAC layer performance with the increase of FD UE ratio.

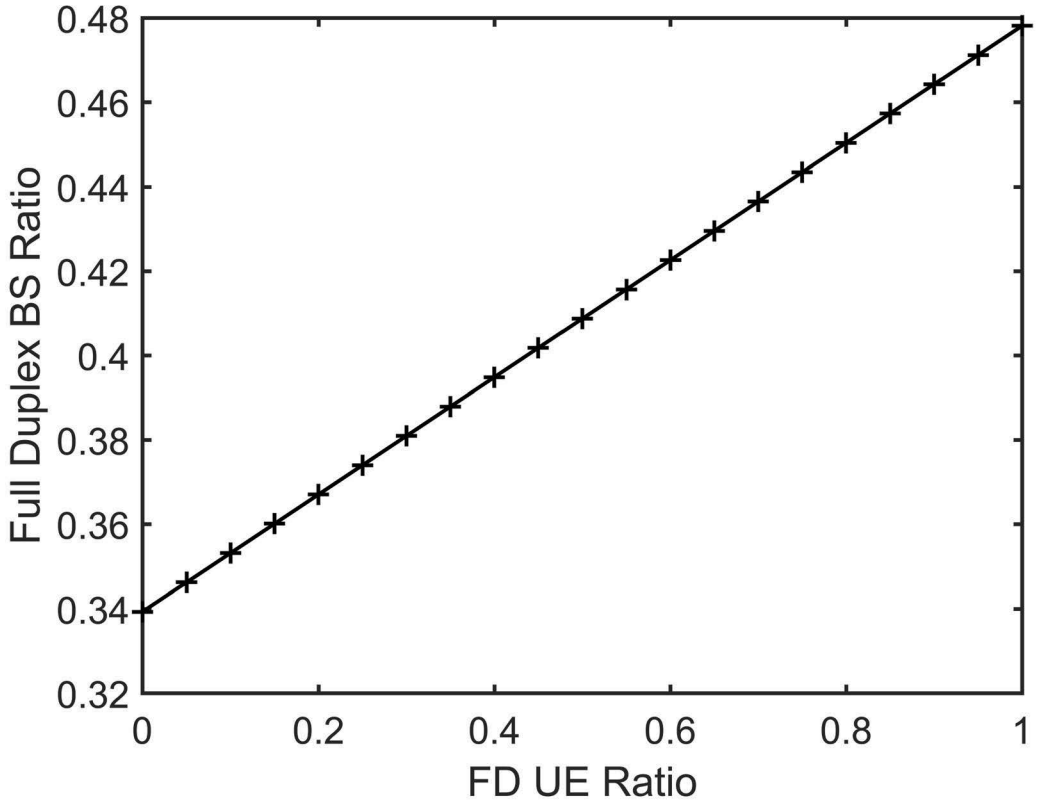

Fig. 18. The full duplex BS ratio vs. the FD UE ratio p^{FU}.

3) Discussion of the Performance Impact of FD Data Request Probability: In Fig. 19, we plot the results of the FD BS ratio against the FD data request probability. The BS density is set to $\lambda = 300\,\mathrm{BSs/km}^2$ and the UE density is set to $\rho = 300\,\mathrm{UEs/km}^2$.We assume that for FD UE and HD UE, the FD data request probability is the same, i.e., $p^{\mathrm{FF}} = p^{\mathrm{FH}}$. In addition, we assume that for each active UE, the HD-DL data request probability is twice of the HD-UL data request probability, i.e., $p^{\mathrm{DF}}/p^{\mathrm{UF}} = 2/1$ and $p^{\mathrm{DH}}/p^{\mathrm{UH}} = 2/1$. From Fig. 19, we can see that:

- The FD BS ratio increases with the increase of FD data request probability.
- The increasing speed of the FD BS ratio gradually slows down with the increase of FD data request probability. Moreover, the increasing speed of the FD BS ratio

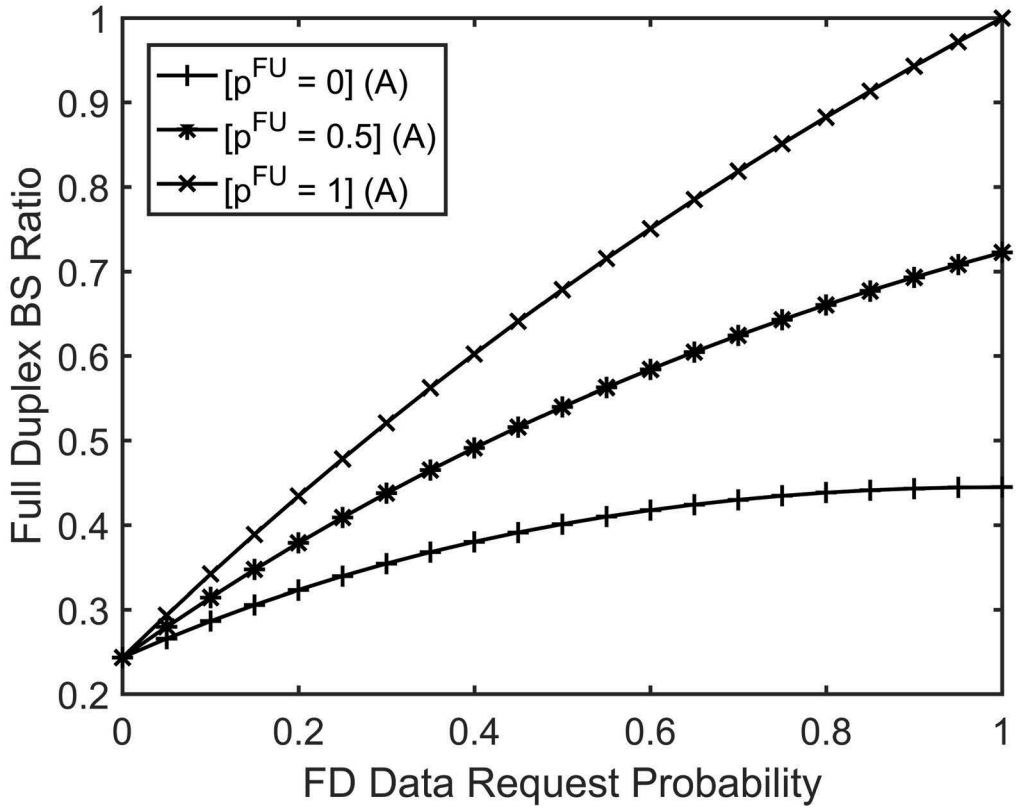

Fig. 19. The full duplex BS ratio vs. the FD data request probability.

with a larger FD UE Ratio p^{FU} lessens slower with the increase of FD data request probability, thanks to the contribution of FS mode with FD UE.

4) Discussion of the Performance Impact of UE Density ρ: In Fig. 20, we plot the results of the FD BS ratio against the UE density ρ. The BS density is set to $\lambda = 300\,\mathrm{BSs/km}^2$, besides, we assume that $p^{\mathrm{FF}} = p^{\mathrm{FH}} = \frac{1}{4}$, $p^{\mathrm{DF}} = p^{\mathrm{DH}} = \frac{1}{2}$, and $p^{\mathrm{UF}} = p^{\mathrm{UH}} = \frac{1}{4}$. From Fig. 20, we can see that:

- For different FD UE ratio p^{FU}, the FD BS ratio first increases gradually with the increase of UE density ρ, then picks up the increasing speed, and finally converges to 1 when ρ becomes large enough.
- For different FD UE ratio p^{FU}, the gap of the FD BS ratio decreases with the increase of UE density ρ.

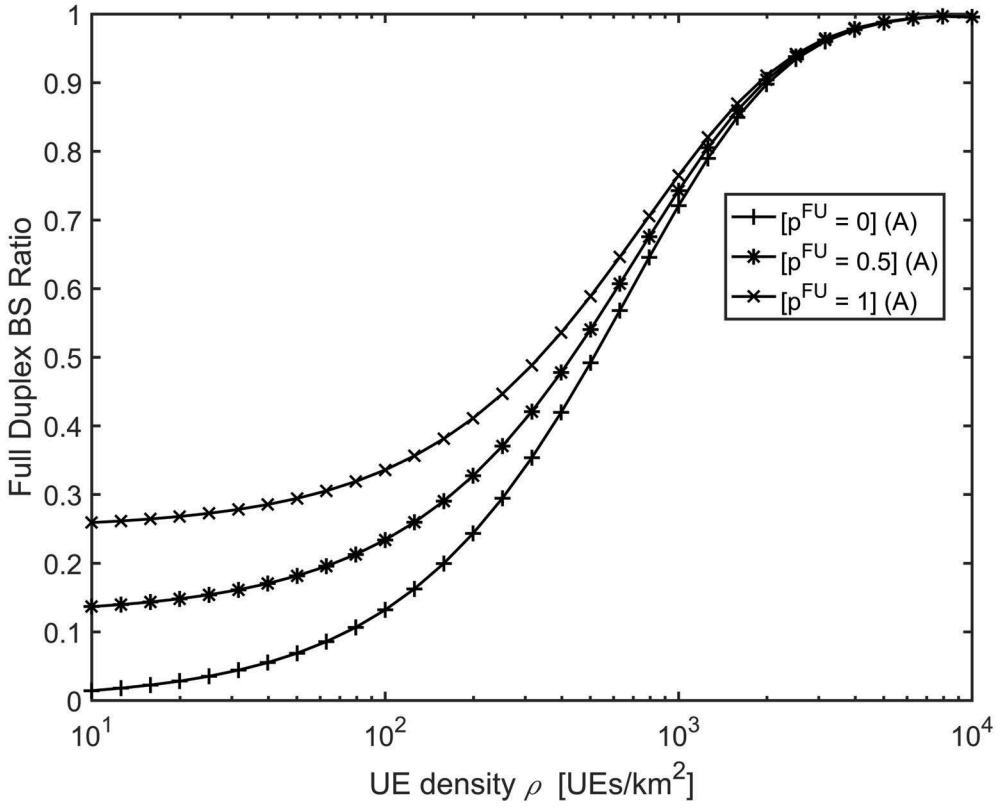

Fig. 20. The full duplex BS ratio vs. the UE density ρ.

D. Conclusion

For the first time, we analytically study the MAC layer performance of FD in a realistic SCN scenario, where BSs can select FD/HD mode according to the real-time DL/UL traffic. The analytical results are shown to match the simulation results well. As our future work, we will combine our results on the MAC layer BS mode selection with the PHY layer SINR results to derive the total area spectral efficiency for FD.

VI. Conclusion

In this Thesis, I have investigated the performance of the dense SCNs. I firstly analysed the coverage probability and the ASE for the UL of dense SCNs considering a practical path loss model incorporating both LoS and NLoS transmissions. Secondly, I studied the performance of the dense SCNs with synchronous dynamic TDD, which has been widely adopted in the existing 4G systems. I analysed the coverage probability and the ASE in the DL and UL of dense SCNs considering the synchronous dynamic TDD transmissions. I thirdly considered the FD communications in a practical SCN scenario, where BSs can select FD or HD mode according to the real-time DL/UL traffic. The analytical results in this Thesis shed new light on the performance of future 5th-generation (5G) dense SCNs.

As my future work, I will investigate the application of the proposed probabilistic interference model in a real-time scenario. Moreover, I will consider other factors of realistic networks in the theoretical analysis for SCNs, such as the unlicensed and asynchronous SCNs.

APPENDIX A: PROOF OF THEOREM 1

Given the piecewise path loss model presented in Subchapter III-A, $P^{\text{cov}}(\lambda, T)$ can be derived as

$$\begin{aligned}
&P^{\text{cov}}(\lambda, T) \\
&= \int_0^{\infty} \Pr\left[\text{SINR} > T \middle| r\right] f_R(r)\, dr \\
&= \int_0^{\infty} \Pr\left[\frac{P_0 g \zeta(r)^{(\epsilon-1)}}{\sigma^2 + I_Z} > T\right] f_R(r)\, dr \\
&= \int_0^{d_1} \Pr\left[\frac{P_0 g \left(A^{\text{L}} r^{\alpha^{\text{L}}}\right)^{(\epsilon-1)}}{\sigma^2 + I_Z} > T \middle| \text{LoS}\right] f_{R,1}^{\text{L}}(r) dr \\
&+ \int_0^{d_1} \Pr\left[\frac{P_0 g \left(A^{\text{NL}} r^{\alpha^{\text{NL}}}\right)^{(\epsilon-1)}}{\sigma^2 + I_Z} > T \middle| \text{NLoS}\right] f_{R,1}^{\text{NL}}(r)\, dr \\
&+ \dots \\
&+ \int_{d_{N-1}}^{\infty} \Pr\left[\frac{P_0 g \left(A^{\text{L}} r^{\alpha^{\text{L}}}\right)^{(\epsilon-1)}}{\sigma^2 + I_Z} > T \middle| \text{LoS}\right] f_{R,N}^{\text{L}}(r) dr \\
&+ \int_{d_{N-1}}^{\infty} \Pr\left[\frac{P_0 g \left(A^{\text{NL}} r^{\alpha^{\text{NL}}}\right)^{(\epsilon-1)}}{\sigma^2 + I_Z} > T \middle| \text{NLoS}\right] f_{R,N}^{\text{NL}}(r)\, dr \\
&\triangleq \sum_{n=1}^{N} \left(T_n^{\text{L}} + T_n^{\text{NL}}\right).
\end{aligned} \tag{100}$$

In the following, we show how to compute $f_{R,n}^{\text{L}}(r)$ and $f_{R,n}^{\text{NL}}(r)$.

To compute $f_{R,n}^{\text{L}}(r)$, we define two events as follows

Event B^{L}: The nearest BS with a LoS path to the UE is located at distance X^{L}. The CCDF of X^{L} is written as $\bar{F}_X^{\text{L}}(x) = \exp\left(-\int_0^x \Pr^{\text{L}}(u)\, 2\pi u \lambda du\right)$ [6]. Taking the derivative of $\left(1 - \bar{F}_X^{\text{L}}(x)\right)$ with regard to x, we can get the PDF of X^{L} as

$$f_X^{\text{L}}(x) = \exp\left(-\int_0^x \Pr^{\text{L}}(u)\, 2\pi u \lambda du\right) \Pr^{\text{L}}(x)\, 2\pi x \lambda. \tag{101}$$

Event C^{NL} conditioned on the value of X^{L}: Given that $X^{\text{L}} = x$, the nearest BS with a NLoS path to the UE is located farther than distance x_1, where $A^{\text{L}} x^{\alpha^{\text{L}}} = A^{\text{NL}} x_1^{\alpha^{\text{NL}}}$, and $x_1 = \left(A^{\text{L}} x^{\alpha^{\text{L}}} / A^{\text{NL}}\right)^{1/\alpha^{\text{NL}}}$. The conditional probability of C^{NL} on condition of $X^{\text{L}} = x$ can be computed by

$$\begin{aligned}
&\Pr\left[C^{\text{NL}} \middle| X^{\text{L}} = x\right] \\
&= \exp\left(-\int_0^{x_1} \left(1 - \Pr^{\text{L}}(u)\right) 2\pi u \lambda du\right).
\end{aligned} \tag{102}$$

Then, we consider the event that the UE is associated with a BS with a LoS path and such BS is located at distance R_n^{L}. $f_{R,n}^{\mathrm{L}}(r)$ can be derived as

$$\begin{aligned}
&f_{R,n}^{\mathrm{L}}(r) \\
&= f_X^{\mathrm{L}}(r) \Pr\left[C^{\mathrm{NL}} \middle| X^{\mathrm{L}} = r\right] \\
&= \exp\left(-\int_0^r \Pr^{\mathrm{L}}(u)\, 2\pi u\lambda du\right) \Pr^{\mathrm{L}}(r)\, 2\pi r\lambda \\
&\times \exp\left(-\int_0^{r_1} \left(1 - \Pr^{\mathrm{L}}(u)\right)\right. \\
&\left.\times 2\pi u\lambda du\right), \quad (d_{n-1} < r < d_n).
\end{aligned} \tag{103}$$

Having obtained $f_{R,n}^{\mathrm{L}}(r)$, we move on to evaluate $\Pr\left[\frac{P_0 g\left(A^{\mathrm{L}} r^{\alpha^{\mathrm{L}}}\right)^{(\epsilon-1)}}{\sigma^2 + I_Z} > T \middle| \mathrm{LoS}\right]$ in (17) as

$$\begin{aligned}
&\Pr\left[\frac{P_0 g\left(A^{\mathrm{L}} r^{\alpha^{\mathrm{L}}}\right)^{(\epsilon-1)}}{\sigma^2 + I_Z} > T \middle| \mathrm{LoS}\right] \\
&= \Pr\left[g > \frac{T\left(\sigma^2 + I_Z\right)}{P_0\left(A^{\mathrm{L}} r^{\alpha^{\mathrm{L}}}\right)^{(\epsilon-1)}} \middle| \mathrm{LoS}\right] \\
&= \mathbb{E}_{I_Z}\left\{\exp\left(-\frac{T\left(\sigma^2 + I_Z\right)}{P_0\left(A^{\mathrm{L}} r^{\alpha^{\mathrm{L}}}\right)^{(\epsilon-1)}}\right)\right\} \\
&= \exp\left(-\frac{T\sigma^2}{P_0\left(A^{\mathrm{L}} r^{\alpha^{\mathrm{L}}}\right)^{(\epsilon-1)}}\right) \\
&\quad \times \mathbb{E}_{I_Z}\left\{\exp\left(-\frac{TI_Z}{P_0\left(A^{\mathrm{L}} r^{\alpha^{\mathrm{L}}}\right)^{(\epsilon-1)}}\right)\right\} \\
&= \exp\left(-\frac{T\sigma^2}{P_0\left(A^{\mathrm{L}} r^{\alpha^{\mathrm{L}}}\right)^{(\epsilon-1)}}\right) \mathscr{L}_{I_Z}\left(\frac{T}{P_0\left(A^{\mathrm{L}} r^{\alpha^{\mathrm{L}}}\right)^{(\epsilon-1)}}\right),
\end{aligned} \tag{104}$$

where $\mathscr{L}_{I_Z}(s)$ is the Laplace transform of RV I_Z evaluated at s.

To compute $f_{R,n}^{\mathrm{NL}}(r)$, we define two events as follows

Event B^{NL}: The nearest BS with a NLoS path to the UE is located at distance X^{NL}. The CCDF of X^{NL} is written as $\bar{F}_X^{\mathrm{NL}}(x) = \exp\left(-\int_0^x \left(1 - \Pr^{\mathrm{L}}(u)\right) 2\pi u\lambda du\right)$. Taking the derivative of $\left(1 - \bar{F}_X^{\mathrm{L}}(x)\right)$ with regard to x, we can get the PDF of X^{NL} as

$$\begin{aligned}
&f_X^{\mathrm{NL}}(x) \\
&= \exp\left(-\int_0^x \left(1 - \Pr^{\mathrm{L}}(u)\right) 2\pi u\lambda du\right) \\
&\quad \times \left(1 - \Pr^{\mathrm{L}}(x)\right) 2\pi x\lambda.
\end{aligned} \tag{105}$$

Event C^{L} conditioned on the value of X^{NL}: Given that $X^{\mathrm{NL}}=x$, the nearest BS with a LoS path to the UE is located farther than distance x_2, where $A^{\mathrm{L}}x_2^{\alpha^{\mathrm{L}}}=A^{\mathrm{NL}}x^{\alpha^{\mathrm{NL}}}$, and $x_2=\left(A^{\mathrm{NL}}x^{\alpha^{\mathrm{NL}}}/A^{\mathrm{L}}\right)^{1/\alpha^{\mathrm{L}}}$. The conditional probability of C^{L} on condition of $X^{\mathrm{NL}}=x$ can be computed by

$$\begin{aligned}&\Pr\left[C^{\mathrm{L}}\middle|\, X^{\mathrm{NL}}=x\right]\\&=\begin{cases}\exp\left(-\int_0^{x_2}\left(\Pr^{\mathrm{L}}(u)\right)2\pi u\lambda du\right), & 0<x\le y_1\\ \exp\left(-\int_0^{d_1}\left(\Pr^{\mathrm{L}}(u)\right)2\pi u\lambda du\right), & x>y_1\end{cases}.\end{aligned}\tag{106}$$

Then, we consider the event that the UE is associated with a BS with a NLoS path and such BS is located at distance R_n^{NL}. $f_{R,n}^{\mathrm{NL}}(r)$ can be derived as

$$\begin{aligned}&f_{R,n}^{\mathrm{NL}}(r)\\&=f_X^{\mathrm{NL}}(r)\Pr\left[C^{\mathrm{L}}\middle|\, X^{\mathrm{NL}}=r\right]\\&=\exp\left(-\int_0^{r}\left(1-\Pr^{\mathrm{L}}(u)\right)2\pi u\lambda du\right)\left(1-\Pr^{\mathrm{L}}(r)\right)2\pi r\lambda\\&\times\exp\left(-\int_0^{r_2}\left(\Pr^{\mathrm{L}}(u)\right)2\pi u\lambda du\right),\quad (d_{n-1}<r<d_n).\end{aligned}\tag{107}$$

Similar to (104), $\Pr\left[\frac{P_0 g\left(A^{\mathrm{NL}}r^{\alpha^{\mathrm{NL}}}\right)^{(\epsilon-1)}}{\sigma^2+I_Z}>T\middle|\,\mathrm{NLoS}\right]$ can be computed by

$$\begin{aligned}&\Pr\left[\frac{P_0 g\left(A^{\mathrm{NL}}r^{\alpha^{\mathrm{NL}}}\right)^{(\epsilon-1)}}{\sigma^2+I_Z}>T\middle|\,\mathrm{NLoS}\right]\\&=\mathbb{E}_{I_Z}\left\{\exp\left(-\frac{T\left(\sigma^2+I_Z\right)}{P_0\left(A^{\mathrm{NL}}r^{\alpha^{\mathrm{NL}}}\right)^{(\epsilon-1)}}\right)\right\}\\&=\exp\left(-\frac{T\sigma^2}{P_0\left(A^{\mathrm{NL}}r^{\alpha^{\mathrm{NL}}}\right)^{(\epsilon-1)}}\right)\mathscr{L}_{I_Z}\left(\frac{T}{P_0\left(A^{\mathrm{NL}}r^{\alpha^{\mathrm{NL}}}\right)^{(\epsilon-1)}}\right).\end{aligned}\tag{108}$$

Our proof is completed by applying the definition of T_n^{L} and T_n^{NL} in (11).

APPENDIX B: PROOF OF LEMMA 2

Based on (21), T_1^{L} can be obtained as

$$
\begin{aligned}
&T_1^{\mathrm{L}} \\
&= \int_0^{d_1} \Pr\left[\frac{P_0 g\left(A^{\mathrm{L}} r^{\alpha^{\mathrm{L}}}\right)^{(\epsilon-1)}}{\sigma^2+I_Z} > T \middle| \mathrm{LoS}\right] f_{R,1}^{\mathrm{L}}(r) dr \\
&= \int_0^{d_1} \exp\left(-\frac{T\sigma^2}{P_0\left(A^{L} r^{\alpha^{\mathrm{L}}}\right)^{(\epsilon-1)}}\right) \\
&\quad \times \mathscr{L}_{I_Z}\left(\frac{T}{P_0\left(A^{L} r^{\alpha^{\mathrm{L}}}\right)^{(\epsilon-1)}}\right) f_{R,1}^{\mathrm{L}}(r)\, dr.
\end{aligned} \tag{109}
$$

The Laplace transform $\mathscr{L}_{I_Z}(s)$ is expressed as

$$
\begin{aligned}
&\mathscr{L}_{I_Z}(s) \\
&= \mathbb{E}_{I_Z}\left[\exp\left(-sI_Z\right)\right] \\
&= \mathbb{E}_{r_z,d_z,g_z}\left[\exp\left(-s\sum_Z P_0 \beta(r_z)\,\zeta(d_z)^{-1} g_z\right)\right] \\
&= \mathbb{E}_{r_z,d_z}\left[\prod_Z \mathbb{E}_{g_z}\left(\exp\left(-sP_0\beta(r_z)\,\zeta(d_z)^{-1} g_z\right)\right)\right] \\
&= \mathbb{E}_{r_z,d_z}\left[\prod_Z \frac{1}{1+sP_0\beta(r_z)\zeta(d_z)^{-1}}\right] \\
&= \exp\left(-2\pi\lambda \int_r^{\infty}\left(1 - \mathbb{E}_{r_z}\left[\frac{1}{1+sP_0\beta(r_z)\zeta(x)^{-1}}\right]\right) x dx\right) \\
&= \exp\left(-2\pi\lambda \int_r^{\infty} \mathbb{E}_{r_z}\left[\frac{1}{1+s^{-1}P_0^{-1}\beta(r_z)^{-1}\zeta(x)}\right] x dx\right) \\
&= \exp\left(-2\pi\lambda \int_r^{d_1}\left(1 - \frac{x}{d_1}\right)\right. \\
&\left.\times \mathbb{E}_{r_z}\left[\frac{1}{1+s^{-1}P_0^{-1}\beta(r_z)^{-1}\zeta(x)} \middle| \mathrm{LoS}\right] x dx\right) \\
&\times \exp\left(-2\pi\lambda \int_{r_1}^{d_1}\left(\frac{x}{d_1}\right)\right. \\
&\left.\times \mathbb{E}_{r_z}\left[\frac{1}{1+s^{-1}P_0^{-1}\beta(r_z)^{-1}\zeta(x)} \middle| \mathrm{NLoS}\right] x dx\right) \\
&\times \exp\left(-2\pi\lambda \int_{d_1}^{\infty} 1\right. \\
&\left.\times \mathbb{E}_{r_z}\left[\frac{1}{1+s^{-1}P_0^{-1}\beta(r_z)^{-1}\zeta(x)} \middle| \mathrm{NLoS}\right] x dx\right),
\end{aligned} \tag{110}
$$

where the expectation function averaged over r_z is derived as follows

$$
\begin{aligned}
&\mathbb{E}_{r_z}\left[\frac{1}{1+s^{-1}P_0^{-1}\beta(r_z)^{-1}\zeta(x)} | \mathrm{LoS}\right] \\
&= \int_0^{\infty}\left(\frac{1}{1+s^{-1}P_0^{-1}\beta(u)^{-1}\zeta(x)} f_{R_z}(u)\, du\right).
\end{aligned} \tag{111}
$$

By plugging (111) into (110), we can obtain (24).

APPENDIX C: PROOF OF LEMMA 5

By using the change of variable $\pi\lambda r^2 \to \widetilde{r}$, (45) can be rewritten as

$$\begin{aligned} & T_2^{\mathrm{NL}} \\ & = \int_{\pi\lambda d_1^2}^{\infty} \exp\left(-\frac{T\sigma^2}{P_0\left(\sqrt{\widetilde{r}(\pi\lambda)^{-1}}\right)^{\alpha^{\mathrm{NL}}(\epsilon-1)}}\right) \\ & \quad \times \mathscr{L}_{I_Z}\left(\frac{T}{P_0\left(\sqrt{\widetilde{r}(\pi\lambda)^{-1}}\right)^{\alpha^{\mathrm{NL}}(\epsilon-1)}}\right) e^{-\widetilde{r}} d\widetilde{r}. \end{aligned} \tag{112}$$

By using the change of variable $\widetilde{r} - \pi\lambda\left(d_1\right)^2 \to v$, (112) can be rewritten as

$$\begin{aligned} T_2^{\mathrm{NL}} &= \int_0^{\infty} \exp\left(-\frac{T\sigma^2}{P_0\left(\sqrt{\left[v+\pi\lambda(d_1)^2\right](\pi\lambda)^{-1}}\right)^{\alpha^{\mathrm{NL}}(\epsilon-1)}}\right) \\ &\times \mathscr{L}_{I_Z}\left(\frac{T}{P_0\left(\sqrt{\left[v+\pi\lambda(d_1)^2\right](\pi\lambda)^{-1}}\right)^{\alpha^{\mathrm{NL}}(\epsilon-1)}}\right) e^{-\pi\lambda(d_1)^2} e^{-v} dv. \end{aligned} \tag{113}$$

By using the method of Gauss-Laguerre quadrature as shown in (48), we complete the proof.

APPENDIX D: PROOF OF THEOREM 6

Based on (67) and conditioned on $\tilde{K} = \tilde{k}$, the probability of performing a DL transmission in subframe l ($l \in \{1, 2, \ldots, T\}$) can be calculated as

$$\begin{aligned} q_{l,\tilde{k}}^{\mathrm{D}} &= \Pr\left[Y_l = \text{'D'} \middle| \tilde{K} = \tilde{k}\right] \\ &\overset{(a)}{=} \Pr\left[N^{\mathrm{D}} \geq l\right] = 1 - F_{N^{\mathrm{D}}}\left(l-1\right), \end{aligned} \tag{114}$$

where Y_l denotes the link direction for the transmission on the l-th subframe, which takes a string value of 'D' and 'U' for the DL and the UL, respectively. Besides, the step (a) of (114) is due to the LTE TDD configuration structure shown in Fig. 9, and $F_{N^{\mathrm{D}}}\left(n^{\mathrm{D}}\right)$ is the cumulative mass function (CMF) of N^{D} in an active BS, which is written as

$$F_{N^{\mathrm{D}}}\left(n^{\mathrm{D}}\right) = \Pr\left[N^{\mathrm{D}} \leq n^{\mathrm{D}}\right] = \sum_{i=0}^{n^{\mathrm{D}}} f_{N^{\mathrm{D}}}\left(i\right). \tag{115}$$

Considering the dynamic allocation of subframe to the DL and the UL in dynamic TDD, the conditional probability of performing an UL transmission in subframe l is given by

$$q^{\mathrm{U}}_{l,\tilde{k}} = 1 - q^{\mathrm{D}}_{l,\tilde{k}} = F_{N^{\mathrm{D}}}\left(l-1\right). \tag{116}$$

Furthermore, the unconditional probabilities of performing a DL and UL transmissions on the l-th subframe, i.e., q^{D}_l and q^{U}_l, can be respectively derived by calculating the expected values of $q^{\mathrm{D}}_{l,\tilde{k}}$ and $q^{\mathrm{U}}_{l,\tilde{k}}$ over all the possible values of $\tilde{k}$ as shown in (69), which concludes our proof.

APPENDIX E: PROOF OF THEOREM 7

By examining the inter-cell inter-link interference for the l-th subframe ($l \in \{1,2,\ldots,T\}$) one by one, $\Pr^{\mathrm{D2U}}$ can be derived as

$$\begin{aligned}
\Pr^{\mathrm{D2U}} &= \Pr\left[Z = \text{'D'} \middle| S = \text{'U'}\right] \\
&= \sum_{l=1}^{T} \Pr\left[\left(Z = \text{'D'} \middle| L = l\right) \middle| S = \text{'U'}\right] \\
&\quad \times \Pr\left[L = l \,|S = \text{'U'}\right] \\
&\overset{(a)}{=} \sum_{l=1}^{T} q^{\mathrm{D}}_l \Pr\left[L = l \,|S = \text{'U'}\right] \\
&\overset{(b)}{=} \sum_{l=1}^{T} q^{\mathrm{D}}_l \frac{\Pr\left[S = \text{'U'} \middle| L = l\right] \Pr\left[L = l\right]}{\Pr\left[S = \text{'U'}\right]} \\
&\overset{(c)}{=} \sum_{l=1}^{T} q^{\mathrm{D}}_l \frac{q^{\mathrm{U}}_l \frac{1}{T}}{\frac{1}{T}\sum_{j=1}^{T} q^{\mathrm{U}}_j},
\end{aligned} \tag{117}$$

where (a) is obtained from

$$\Pr\left[\left(Z = \text{'D'} \middle| L = l\right) \middle| S = \text{'U'}\right] = \Pr\left[Z = \text{'D'} \middle| L = l\right] = q^{\mathrm{D}}_l,$$

due to the independence of the events $\left(Z = \text{'D'} \middle| L = l\right)$ and $\left(S = \text{'U'}\right)$; (b) is valid because of the Bayes' Theorem; and (c) comes from the calculation on the probability of the signal

being an UL one, which can be written by

$$\begin{aligned}\Pr\left[S=\text{'U'}\right] &= \sum_{j=1}^{T}\Pr\left[S=\text{'U'}\middle|\, L=j\right]\Pr\left[L=j\right] \\ &= \frac{1}{T}\sum_{j=1}^{T} q_j^{\mathrm{U}}. \end{aligned} \tag{118}$$

Similarly, it is easy to derive the results for $\Pr^{\mathrm{U2D}}$, which concludes our proof.

APPENDIX F: PROOF OF THEOREM 9

In static TDD, for a given UE number $\tilde{k}$ in an active BS, the probabilities that no UE requests any DL data and no UE requests any UL data can be calculated by $f_{M^{\mathrm{D}}}\left(0\right)$ from (64) and $f_{M^{\mathrm{U}}}\left(0\right)$ from (65), respectively. Even in such cases, static TDD still unwisely allocates N_0^{D} and N_0^{U} subframes for the DL and the UL, respectively, which causes resource waste. The probabilities of such resource waste for the DL and the UL are denoted by w^{D} and w^{U}, and they can be calculated as

$$\begin{cases} w^{\mathrm{D}} = \sum_{\tilde{k}=1}^{+\infty} f_{M^{\mathrm{D}}}\left(0\right) f_{\tilde{K}}\left(\tilde{k}\right) = \sum_{\tilde{k}=1}^{+\infty}\left(1-p^{\mathrm{D}}\right)^{\tilde{k}} f_{\tilde{K}}\left(\tilde{k}\right) \\ w^{\mathrm{U}} = \sum_{\tilde{k}=1}^{+\infty} f_{M^{\mathrm{U}}}\left(0\right) f_{\tilde{K}}\left(\tilde{k}\right) = \sum_{\tilde{k}=1}^{+\infty}\left(1-p^{\mathrm{U}}\right)^{\tilde{k}} f_{\tilde{K}}\left(\tilde{k}\right) \end{cases}. \tag{119}$$

Excluding such resource waste from N_0^{D} and N_0^{U}, we can obtain κ^{D} and κ^{U} for static TDD as

$$\begin{cases} \kappa^{\mathrm{D}} = \left(1-w^{\mathrm{D}}\right)\frac{N_0^{\mathrm{D}}}{T} \\ \kappa^{\mathrm{U}} = \left(1-w^{\mathrm{U}}\right)\frac{N_0^{\mathrm{U}}}{T} \end{cases}. \tag{120}$$

Our proof is thus completed by plugging (119), (64) and (65) into (120), followed by computing κ from (55).

APPENDIX G: PROOF OF THEOREM 11

The proof of $p^{\mathrm{cov},Link}(\lambda,\gamma)$, $f_{R,n}^{\mathrm{L}}(r)$ and $f_{R,n}^{\mathrm{NL}}(r)$ are given in our previous papers [6], [54]. Therefore we move on to evaluate $\Pr\left[\mathrm{SINR}^{Link}>\gamma\middle|\,\mathrm{LoS}\right]$ in (79) as

$$\begin{aligned}
&\Pr\left[\mathrm{SINR}^{Link}>\gamma\middle|\,\mathrm{LoS}\right]\\
&=\Pr\left[h>\frac{\gamma\left(I_{\mathrm{agg}}^{Link,\mathrm{D}}+I_{\mathrm{agg}}^{Link,\mathrm{U}}+P_{\mathrm{N}}^{Link}\right)}{P^{Link}\zeta_{b_o}^{\mathrm{B2U}}(r)}\middle|\,\mathrm{LoS}\right]\\
&=\mathbb{E}_{\left(I_{\mathrm{agg}}^{Link,\mathrm{D}}+I_{\mathrm{agg}}^{Link,\mathrm{U}}\right)}\left\{\exp\left(-\frac{\gamma\left(I_{\mathrm{agg}}^{Link,\mathrm{D}}+I_{\mathrm{agg}}^{Link,\mathrm{U}}+P_{\mathrm{N}}^{Link}\right)}{P^{Link}\zeta_{b_o}^{\mathrm{B2U}}(r)}\right)\right\}\\
&=\exp\left(-\frac{\gamma P_{\mathrm{N}}^{Link}}{P^{Link}\zeta_{b_o}^{\mathrm{B2U}}(r)}\right)\\
&\quad\times\mathbb{E}_{\left(I_{\mathrm{agg}}^{Link,\mathrm{D}}+I_{\mathrm{agg}}^{Link,\mathrm{U}}\right)}\left\{\exp\left(-\frac{\gamma\left(I_{\mathrm{agg}}^{Link,\mathrm{D}}+I_{\mathrm{agg}}^{Link,\mathrm{U}}\right)}{P^{Link}\zeta_{b_o}^{\mathrm{B2U}}(r)}\right)\right\}\\
&=\exp\left(-\frac{\gamma P_{\mathrm{N}}^{Link}}{P^{Link}\zeta_{b_o}^{\mathrm{B2U}}(r)}\right)\mathscr{L}_{I_{\mathrm{agg}}^{Link,\mathrm{D}}}\left(\frac{\gamma\left(I_{\mathrm{agg}}^{Link,\mathrm{D}}\right)}{P^{Link}\zeta_{b_o}^{\mathrm{B2U}}(r)}\right)\\
&\times\mathscr{L}_{I_{\mathrm{agg}}^{Link,\mathrm{U}}}\left(\frac{\gamma\left(I_{\mathrm{agg}}^{Link,\mathrm{U}}\right)}{P^{Link}\zeta_{b_o}^{\mathrm{B2U}}(r)}\right).
\end{aligned}\tag{121}$$

$\Pr\left[\mathrm{SINR}^{Link}>\gamma\middle|\,\mathrm{NLoS}\right]$ can be derived in a similar way.

APPENDIX H: DL RESULTS OF SUBCHAPTER IV-C3

For the DL, the coverage probability for the typical UE can be formulated as follows.

$T_1^{\mathrm{L,D}}$ *of DL*

Lemma 19. *The result of $T_1^{\mathrm{L,D}}$ is the DL coverage probability when the typical UE is associated with the typical BS with a LoS link of distance less than d_1. From Theorem 11, $T_1^{\mathrm{L,D}}$ can be derived as*

$$\begin{aligned}
T_1^{\mathrm{L,D}}&=\int_0^{d_1}\exp\left(-\frac{\gamma P_{\mathrm{N}}^{\mathrm{D}}}{P^{\mathrm{D}}\zeta_{b_o}^{\mathrm{B2U}}}\right)\mathscr{L}_{I_{\mathrm{agg}}^{\mathrm{D,D}}}\left(\frac{\gamma}{P^{\mathrm{D}}\zeta_{b_o}^{\mathrm{B2U,L}}}\right)\\
&\times\mathscr{L}_{I_{\mathrm{agg}}^{\mathrm{D,U}}}\left(\frac{\gamma}{P^{\mathrm{D}}\zeta_{b_o}^{\mathrm{B2U,L}}}\right)f_{R,1}^{\mathrm{L}}(r)dr.
\end{aligned}\tag{122}$$

The Laplace transform $\mathscr{L}_{I_{\mathrm{agg}}^{\mathrm{D,U}}}(s)$ of $I_{\mathrm{agg}}^{\mathrm{D,U}}$ evaluated at $s=\frac{\gamma}{P^{\mathrm{D}}\zeta_{b_o}^{\mathrm{B2U,L}}}$ can be computed as

$$\begin{aligned}
\mathscr{L}_{I_{\mathrm{agg}}^{\mathrm{D,U}}}(s)&=\exp\left(-2\pi p^{\mathrm{U}}\lambda\left(\int_{r_1}^{50}\left[\frac{1}{1+(sP^{\mathrm{U}}\zeta^{U2U,L})^{-1}}\right]xdx\right.\right.\\
&\left.\left.+\int_{50}^{\infty}\left[\frac{1}{1+(sP^{\mathrm{U}}\zeta^{U2U,NL})^{-1}}\right]xdx\right)\right).
\end{aligned}\tag{123}$$

$T_1^{\mathrm{NL,D}}$ *of DL*

Lemma 20. *The DL coverage probability when* $0 < r \leq d_1$ *and the signal is NLoS can be derived as*

$$\begin{aligned} T_1^{\mathrm{NL,D}} &= \int_0^{d_1} \exp\left(-\frac{\gamma P_{\mathrm{N}}^{\mathrm{D}}}{P^{\mathrm{D}}\zeta_{b_o}^{\mathrm{B2U}}}\right) \mathscr{L}_{I_{\mathrm{agg}}^{\mathrm{D,D}}}\left(\frac{\gamma}{P^{\mathrm{D}}\zeta_{b_o}^{\mathrm{B2U,NL}}}\right) \\ &\times \mathscr{L}_{I_{\mathrm{agg}}^{\mathrm{D,U}}}\left(\frac{\gamma}{P^{\mathrm{D}}\zeta_{b_o}^{\mathrm{B2U,NL}}}\right) f_{R,1}^{\mathrm{NL}}(r)dr, \end{aligned} \tag{124}$$

where the Laplace transform $\mathscr{L}_{I_{\mathrm{agg}}^{\mathrm{D,U}}}(s)$ *evaluated at* $s = \frac{\gamma}{P^{\mathrm{D}}\zeta_{b_o}^{\mathrm{B2U,NL}}}$ *can be derived as (123).*

$T_2^{\mathrm{L,D}}$ *of DL*

The result of $T_2^{\mathrm{L,D}}$ is the DL coverage probability when the typical UE is associated with the typical BS with a LoS link of distance larger than d_1. From Theorem 11, $T_2^{\mathrm{L,D}}$ can be derived as

$$T_2^{\mathrm{L,D}} = \int_{d_1}^{\infty} \Pr\left[\mathrm{SINR}^{Link} > \gamma \middle| r, \mathrm{LoS}\right] f_{R,2}^{\mathrm{L}}(r)dr. \tag{125}$$

Plugging $f_{R,2}^{\mathrm{L}}(r) = 0$ into (125), yields

$$T_2^{\mathrm{L,D}} = 0. \tag{126}$$

$T_2^{\mathrm{NL,D}}$ *of DL*

Lemma 21. *The DL coverage probability when* $r > d_1$ *and the signal is NLoS can be derived as*

$$\begin{aligned} T_2^{\mathrm{NL,D}} &= \int_{d_1}^{\infty} \exp\left(-\frac{\gamma P_{\mathrm{N}}^{\mathrm{D}}}{P^{\mathrm{D}}\zeta_{b_o}^{\mathrm{B2U}}}\right) \mathscr{L}_{I_{\mathrm{agg}}^{\mathrm{D,D}}}\left(\frac{\gamma}{P^{\mathrm{D}}\zeta_{b_o}^{\mathrm{B2U,NL}}}\right) \\ &\times \mathscr{L}_{I_{\mathrm{agg}}^{\mathrm{D,U}}}\left(\frac{\gamma}{P^{\mathrm{D}}\zeta_{b_o}^{\mathrm{B2U,NL}}}\right) f_{R,2}^{\mathrm{NL}}(r)dr, \end{aligned} \tag{127}$$

and the Laplace transform $\mathscr{L}_{I_{\mathrm{agg}}^{\mathrm{D,U}}}(s)$ *of* $I_{\mathrm{agg}}^{\mathrm{D,U}}$ *evaluated at* $s = \frac{\gamma}{P^{\mathrm{D}}\zeta_{b_o}^{\mathrm{B2U,NL}}}$ *can be computed as*

$$\mathscr{L}_{I_{\mathrm{agg}}^{\mathrm{D,U}}}(s) = \exp\left(-2\pi p^{\mathrm{U}}\lambda \int_r^{\infty} \left[\frac{1}{1+(sP^{\mathrm{U}}\zeta^{U2U,NL})^{-1}}\right] xdx\right). \tag{128}$$

APPENDIX I: UL RESULTS OF SUBCHAPTER IV-C3

For the UL, the coverage probability for the typical BS can be formulated as follows.

$T_1^{\mathrm{L,U}}$ *of UL*

Lemma 22. *The UL coverage probability when* $0 < r \leq d_1$ *and the signal is LoS can be derived as*

$$\begin{aligned} T_1^{\mathrm{L,U}} &= \int_0^{d_1} \exp\left(-\tfrac{\gamma P_{\mathrm{N}}^{\mathrm{U}}}{P^{\mathrm{D}}\zeta_{b_o}^{\mathrm{B2U}}}\right) \mathscr{L}_{I_{\mathrm{agg}}^{\mathrm{U,D}}}\left(\tfrac{\gamma}{P^{\mathrm{U}}\zeta_{b_o}^{\mathrm{B2U,L}}}\right) \\ &\times \mathscr{L}_{I_{\mathrm{agg}}^{\mathrm{U,U}}}\left(\tfrac{\gamma}{P^{\mathrm{U}}\zeta_{b_o}^{\mathrm{B2U,L}}}\right) f_{R,1}^{\mathrm{L}}(r)dr, \end{aligned} \tag{129}$$

and the Laplace transform $\mathscr{L}_{I_{\mathrm{agg}}^{\mathrm{U,D}}}(s)$ *of* $I_{\mathrm{agg}}^{\mathrm{U,D}}$ *evaluated at* $s = \frac{\gamma}{P^{\mathrm{U}}\zeta_{b_o}^{\mathrm{B2U,L}}}$ *can be computed as*

$$\begin{aligned} \mathscr{L}_{I_{\mathrm{agg}}^{\mathrm{U,D}}}(s) = \exp&\left(-2\pi p^{\mathrm{D}}\lambda \int_0^{d_1} \left[\tfrac{1}{1+(sP^{\mathrm{D}}\zeta^{B2B,L})^{-1}}\right]\left(1-\tfrac{x}{d_1}\right) x dx\right) \\ &\times \exp\left(-2\pi p^{\mathrm{D}}\lambda \int_0^{d_1} \left[\tfrac{1}{1+(sP^{\mathrm{D}}\zeta^{B2B,NL})^{-1}}\right]\left(\tfrac{x}{d_1}\right) x dx\right) \\ &\times \exp\left(-2\pi p^{\mathrm{D}}\lambda \int_{d_1}^{\infty} \left[\tfrac{1}{1+(sP^{\mathrm{D}}\zeta^{B2B,NL})^{-1}}\right] x dx\right). \end{aligned} \tag{130}$$

$T_1^{\mathrm{NL,U}}$ *of UL*

Lemma 23. *The UL coverage probability when* $0 < r \leq d_1$ *and the signal is NLoS can be derived as*

$$\begin{aligned} T_1^{\mathrm{NL,U}} &= \int_0^{d_1} \exp\left(-\tfrac{\gamma P_{\mathrm{N}}^{\mathrm{U}}}{P^{\mathrm{D}}\zeta_{b_o}^{\mathrm{B2U}}}\right) \mathscr{L}_{I_{\mathrm{agg}}^{\mathrm{U,D}}}\left(\tfrac{\gamma}{P^{\mathrm{U}}\zeta_{b_o}^{\mathrm{B2U,NL}}}\right) \\ &\times \mathscr{L}_{I_{\mathrm{agg}}^{\mathrm{U,U}}}\left(\tfrac{\gamma}{P^{\mathrm{U}}\zeta_{b_o}^{\mathrm{B2U,NL}}}\right) f_{R,1}^{\mathrm{NL}}(r)dr, \end{aligned} \tag{131}$$

where the Laplace transform $\mathscr{L}_{I_{\mathrm{agg}}^{\mathrm{U,D}}}(s)$ *evaluated at* $s = \frac{\gamma}{P^{\mathrm{U}}\zeta_{b_o}^{\mathrm{B2U,NL}}}$ *can be derived as (130).*

$T_2^{\mathrm{L,U}}$ *of UL*

The result of $T_2^{\mathrm{L,U}}$ is the UL coverage probability when the typical UE is associated with the typical BS with a LoS link of distance larger than d_1. The derivation of $T_2^{\mathrm{L,U}}$ is very similar to $T_2^{\mathrm{L,D}}$ and can be derived as

$$T_2^{\mathrm{L,U}} = 0. \tag{132}$$

$T_2^{\mathrm{NL,U}}$ *of UL*

Lemma 24. *The UL coverage probability when $r > d_1$ and the signal is NLoS can be derived as*

$$\begin{aligned} T_2^{\mathrm{NL,U}} &= \int_{d_1}^{\infty} \exp\left(-\tfrac{\gamma P_{\mathrm{N}}^{\mathrm{D}}}{P^{\mathrm{D}}\zeta_{b_o}^{\mathrm{B2U}}}\right) \mathscr{L}_{I_{\mathrm{agg}}^{\mathrm{U,D}}}\left(\tfrac{\gamma}{P^{\mathrm{U}}\zeta_{b_o}^{\mathrm{B2U,NL}}}\right) \\ &\times \mathscr{L}_{I_{\mathrm{agg}}^{\mathrm{U,U}}}\left(\tfrac{\gamma}{P^{\mathrm{U}}\zeta_{b_o}^{\mathrm{B2U,NL}}}\right) f_{R,2}^{\mathrm{NL}}(r) dr, \end{aligned} \tag{133}$$

where the Laplace transform $\mathscr{L}_{I_{\mathrm{agg}}^{\mathrm{U,D}}}(s)$ of $I_{\mathrm{agg}}^{\mathrm{U,D}}$ evaluated at $s = \frac{\gamma}{P^{\mathrm{U}}\zeta_{b_o}^{\mathrm{B2U,NL}}}$ can be computed as

$$\mathscr{L}_{I_{\mathrm{agg}}^{\mathrm{U,D}}}(s) = \exp\left(-2\pi p^{\mathrm{D}}\lambda \int_r^{\infty} \left[\tfrac{1}{1+(sP^{\mathrm{D}}\zeta^{B2B,NL})^{-1}}\right] x dx\right). \tag{134}$$

REFERENCES

[1] D. López-Pérez, M. Ding, H. Claussen, and A. H. Jafari, "Towards 1 Gbps/UE in Cellular Systems: Understanding Ultra-Dense Small Cell Deployments," *IEEE Communications Surveys Tutorials*, vol. 17, pp. 2078–2101, Fourthquarter 2015.

[2] 3GPP, "TR 36.872, Small cell enhancements for E-UTRA and E-UTRAN - Physical layer aspects," Dec. 2013.

[3] X. Ge, S. Tu, G. Mao, C. X. Wang, and T. Han, "5G Ultra-Dense Cellular Networks," *IEEE Wireless Communications*, vol. 23, pp. 72–79, February 2016.

[4] T. D. Novlan, H. S. Dhillon, and J. G. Andrews, "Analytical Modeling of Uplink Cellular Networks," *IEEE Transactions on Wireless Communications*, vol. 12, pp. 2669–2679, June 2013.

[5] X. Ge, S. Tu, T. Han, Q. Li, and G. Mao, "Energy efficiency of small cell backhaul networks based on gauss-markov mobile models," *IET Networks*, vol. 4, no. 2, pp. 158–167, 2015.

[6] M. Ding, P. Wang, D. López-Pérez, G. Mao, and Z. Lin, "Performance Impact of LoS and NLoS Transmissions in Dense Cellular Networks," *IEEE Transactions on Wireless Communications*, vol. 15, pp. 2365–2380, March 2016.

[7] T. Ding, M. Ding, G. Mao, Z. Lin, and D. López-Pérez, "Uplink performance analysis of dense cellular networks with LoS and NLoS transmissions," in *2016 IEEE International Conference on Communications (ICC)*, pp. 1–6, May 2016.

[8] 3GPP, "TR 36.828 (V11.0.0): Further enhancements to LTE Time Division Duplex (TDD) for Downlink-Uplink (DL-UL) interference management and traffic adaptation," June 2012.

[9] M. Ding, D. López-Pérez, R. Xue, A. V. Vasilakos, and W. Chen, "On dynamic time-division-duplex transmissions for small-cell networks," *IEEE Transactions on Vehicular Technology*, vol. 65, pp. 8933–8951, Nov 2016.

[10] S. Goyal, C. Galiotto, N. Marchetti, and S. Panwar, "Throughput and coverage for a mixed full and half duplex small cell network," in *2016 IEEE International Conference on Communications (ICC)*, pp. 1–7, May 2016.

[11] M. Ding, D. Lopez Perez, G. Mao, and Z. Lin, "What is the true value of dynamic tdd: A mac layer perspective," in *GLOBECOM 2017 - 2017 IEEE Global Communications Conference*, pp. 1–7, Dec 2017.

[12] J. G. Andrews, F. Baccelli, and R. K. Ganti, "A Tractable Approach to Coverage and Rate in Cellular Networks," *IEEE Transactions on Communications*, vol. 59, pp. 3122–3134, November 2011.

[13] X. Ge, K. Huang, C. X. Wang, X. Hong, and X. Yang, "Capacity Analysis of a Multi-Cell Multi-Antenna Cooperative Cellular Network with Co-Channel Interference," *IEEE Transactions on Wireless Communications*, vol. 10, pp. 3298–3309, October 2011.

[14] B. Yu, L. Yang, H. Ishii, and S. Mukherjee, "Dynamic TDD support in macrocell-assisted small cell architecture," *IEEE Journal on Selected Areas in Communications*, vol. 33, pp. 1201–1213, jun 2015.

[15] A. A. Kannan, B. Fidan, and G. Mao, "Robust distributed sensor network localization based on analysis of flip ambiguities," in *IEEE GLOBECOM 2008 - 2008 IEEE Global Telecommunications Conference*, pp. 1–6, Nov 2008.

[16] R. Mao and G. Mao, "Road traffic density estimation in vehicular networks," in *2013 IEEE Wireless Communications and Networking Conference (WCNC)*, pp. 4653–4658, April 2013.

[17] G. Mao and B. D. O. Anderson, "Graph theoretic models and tools for the analysis of dynamic wireless multihop networks," in *2009 IEEE Wireless Communications and Networking Conference*, pp. 1–6, April 2009.

[18] Y. Hu, Y. Hong, and J. Evans, "Uplink coverage and spatial blocking in Poisson cellular networks," in *2014 IEEE International Conference on Communications (ICC)*, pp. 5765–5770, June 2014.

[19] S. Singh, X. Zhang, and J. G. Andrews, "Uplink rate distribution in heterogeneous cellular networks with power control and load balancing," in *2015 IEEE International Conference on Communication Workshop (ICCW)*, pp. 1275–1280, June 2015.

[20] H. ElSawy and E. Hossain, "On Stochastic Geometry Modeling of Cellular Uplink Transmission With Truncated Channel Inversion Power Control," *IEEE Transactions on Wireless Communications*, vol. 13, pp. 4454–4469, Aug 2014.

[21] J. Arnau, I. Atzeni, and M. Kountouris, "Impact of LOS/NLOS propagation and path loss in ultra-dense cellular networks," in *2016 IEEE International Conference on Communications (ICC)*, pp. 1–6, May 2016.

[22] Y. Park, J. Heo, W. Chung, S. Weon, S. Choi, and D. Hong, "A new link adaptation method to mitigate sinr mismatch in ultra-dense small cell lte networks," *IEEE Transactions on Wireless Communications*, vol. 17, pp. 1109–1122, Feb 2018.

[23] A. H. Jafari, V. Venkateswaran, D. López-Pérez, and J. Zhang, "Diversity pulse shaped transmission in ultra-dense small cell networks," *IEEE Transactions on Vehicular Technology*, vol. 66, pp. 5866–5878, July 2017.

[24] B. Yang, G. Mao, M. Ding, X. Ge, and X. Tao, "Dense small cell networks: From noise-limited to dense interference-limited," *IEEE Transactions on Vehicular Technology*, vol. 67, pp. 4262–4277, May 2018.

[25] H. Zhang, L. Song, and Y. J. Zhang, "Load balancing for 5g ultra-dense networks using device-to-device communications," *IEEE Transactions on Wireless Communications*, vol. 17, pp. 4039–4050, June 2018.

[26] V. Fernández-López, K. I. Pedersen, B. Soret, J. Steiner, and P. Mogensen, "Improving dense network performance through centralized scheduling and interference coordination," *IEEE Transactions on Vehicular Technology*, vol. 66, pp. 4371–4382, May 2017.

[27] Y. Zhu, G. Zheng, L. Wang, K. Wong, and L. Zhao, "Content placement in cache-enabled sub-6 ghz and millimeter-wave multi-antenna dense small cell networks," *IEEE Transactions on Wireless Communications*, vol. 17, pp. 2843–2856, May 2018.

[28] L. Wang, K. Wong, R. W. Heath, and J. Yuan, "Wireless powered dense cellular networks: How many small cells do we need?," *IEEE Journal on Selected Areas in Communications*, vol. 35, pp. 2010–2024, Sept 2017.

[29] J. Liu, M. Sheng, and J. Li, "Improving network capacity scaling law in ultra-dense small cell networks," *IEEE Transactions on Wireless Communications*, vol. 17, pp. 6218–6230, Sept 2018.

[30] G. Yu, Z. Zhang, F. Qu, and G. Y. Li, "Ultra-dense heterogeneous networks with full-duplex small cell base stations," *IEEE Network*, vol. 31, pp. 108–114, November 2017.

[31] M. Ding and D. López-Pérez, "Performance impact of base station antenna heights in dense cellular networks," *IEEE Transactions on Wireless Communications*, vol. 16, pp. 8147–8161, Dec 2017.

[32] A. K. Gupta, M. N. Kulkarni, E. Visotsky, F. W. Vook, A. Ghosh, J. G. Andrews, and R. W. Heath, "Rate analysis and feasibility of dynamic tdd in 5g cellular systems," in *2016 IEEE International Conference on Communications (ICC)*, pp. 1–6, May 2016.

[33] H. Sun, M. Sheng, M. Wildemeersch, T. Q. S. Quek, and J. Li, "Traffic adaptation and energy efficiency for small

cell networks with dynamic TDD," *IEEE Journal on Selected Areas in Communications*, vol. 34, pp. 3234–3251, dec 2016.

[34] Y. Zhong, P. Cheng, N. Wang, and W. Zhang, "Dynamic tdd enhancement through distributed interference coordination," in *2015 IEEE International Conference on Communications (ICC)*, pp. 3509–3515, June 2015.

[35] M. N. Kulkarni, J. G. Andrews, and A. Ghosh, "Performance of dynamic and static TDD in self-backhauled mmwave cellular networks," *CoRR*, vol. abs/1701.07111, 2017.

[36] M. Ding, D. López-Pérez, A. V. Vasilakos, and W. Chen, "Analysis on the sinr performance of dynamic tdd in homogeneous small cell networks," in *2014 IEEE Global Communications Conference*, pp. 1552–1558, Dec 2014.

[37] H. H. Yang, G. Geraci, Y. Zhong, and T. Q. S. Quek, "Packet throughput analysis of static and dynamic tdd in small cell networks," *IEEE Wireless Communications Letters*, vol. 6, pp. 742–745, Dec 2017.

[38] H. Sun, M. Wildemeersch, M. Sheng, and T. Q. S. Quek, "D2d enhanced heterogeneous cellular networks with dynamic tdd," *IEEE Transactions on Wireless Communications*, vol. 14, pp. 4204–4218, Aug 2015.

[39] M. Zhou, H. Li, N. Zhao, S. Zhang, and F. R. Yu, "Feasibility analysis and clustering for interference alignment in full-duplex-based small cell networks," *IEEE Transactions on Communications*, vol. 67, pp. 807–819, Jan 2019.

[40] J. Liu, S. Han, W. Liu, and C. Yang, "The value of full-duplex for cellular networks: A hybrid duplex-based study," *IEEE Transactions on Communications*, vol. 65, pp. 5559–5573, Dec 2017.

[41] I. Atzeni and M. Kountouris, "Full-duplex mimo small-cell networks with interference cancellation," *IEEE Transactions on Wireless Communications*, vol. 16, pp. 8362–8376, Dec 2017.

[42] D. Korpi, J. Tamminen, M. Turunen, T. Huusari, Y. S. Choi, L. Anttila, S. Talwar, and M. Valkama, "Full-duplex mobile device: pushing the limits," *IEEE Communications Magazine*, vol. 54, pp. 80–87, September 2016.

[43] Spatial Channel Model AHG (Combined ad-hoc from 3GPP & 3GPP2), "Subsection 3.5.3, Spatial Channel Model Text Description V6.0," April 2003.

[44] C. Pozrikidis, *Numerical computation in science and engineering*, vol. 6. Oxford university press New York, 1998.

[45] G. Mao, B. D. O. Anderson, and B. Fidan, "Wsn06-4: Online calibration of path loss exponent in wireless sensor networks," in *IEEE Globecom 2006*, pp. 1–6, Nov 2006.

[46] M. Ding, D. López-Pérez, G. Mao, and Z. Lin, "Performance impact of idle mode capability on dense small cell networks," *IEEE Transactions on Vehicular Technology*, vol. 66, pp. 10446–10460, Nov 2017.

[47] S. Lee and K. Huang, "Coverage and economy of cellular networks with many base stations," *IEEE Communications Letters*, vol. 16, pp. 1038–1040, Jul. 2012.

[48] M. Ding, D. López-Pérez, G. Mao, and Z. Lin, "Study on the idle mode capability with LoS and NLoS transmissions," in *IEEE Globecom 2016*, pp. 1–6, Dec. 2016.

[49] M. Ding and D. López-Pérez, "On the performance of practical ultra-dense networks: The major and minor factors," in *2017 15th International Symposium on Modeling and Optimization in Mobile, Ad Hoc, and Wireless Networks (WiOpt)*, pp. 1–8, May 2017.

[50] J.-S. Ferenc and Z. Néda, "On the size distribution of poisson voronoi cells," *Physica A: Statistical Mechanics and its Applications*, vol. 385, pp. 518–526, Nov 2007.

[51] S. Singh, H. S. Dhillon, and J. G. Andrews, "Offloading in heterogeneous networks: Modeling, analysis, and design insights," *IEEE Transactions on Wireless Communications*, vol. 12, pp. 2484–2497, May 2013.

[52] I. Gradshteyn and I. Ryzhik, *Table of Integrals, Series, and Products (7th Ed.)*. Academic Press, 2007.

[53] M. Ding, D. López-Pérez, R. Xue, A. Vasilakos, and W. Chen, "On dynamic Time-Division-Duplex transmissions for small-cell networks," *IEEE Transactions on Vehicular Technology*, vol. 65, pp. 8933–8951, Nov. 2016.

[54] T. Ding, M. Ding, G. Mao, Z. Lin, D. López-Pérez, and A. Zomaya, "Uplink performance analysis of dense cellular networks with los and nlos transmissions," *IEEE Transactions on Wireless Communications*, vol. 16, no. 4, pp. 2601–2613, 2017.

[55] M. Ding, D. López-Pérez, and G. Mao, "A new capacity scaling law in ultra-dense networks," *arXiv:1704.00399 [cs.NI]*, Apr. 2017.